FABRICATION OF HELICAL POLYMERIC HOLLOW FIBER MEMBRANES AND CHARACTERIZATION OF THEIR FOULING BEHAVIOURS

A THESIS SUBMITTED TO
THE GRADUATE SCHOOL OF NATURAL AND APPLIED SCIENCES
OF
MIDDLE EAST TECHNICAL UNIVERSITY

BY

HAZAL YÜCEL

IN PARTIAL FULFILLMENT OF THE REQUIREMENTS
FOR
THE DEGREE OF MASTER OF SCIENCE
IN
CHEMICAL ENGINEERING

JUNE 2018

Approval of thesis:

FABRICATION OF HELICAL POLYMERIC HOLLOW FIBER MEMBRANES AND CHARACTERIZATION OF THEIR FOULING BEHAVIOURS

submitted by **HAZAL YÜCEL** in partial fulfillment of the requirements for the degree of **Master of Science in Chemical Engineering Department, Middle East Technical University** by,

Prof. Dr. Halil Kalıpçılar _____
Dean, Graduate School of **Natural and Applied Sciences**

Prof. Dr. Pınar Çalık _____
Head of Department, **Chemical Engineering**

Assoc. Prof. Dr. P. Zeynep Çulfaz Emecen _____
Supervisor, **Chemical Engineering Dept., METU**

Examining Committee Members:

Prof. Dr. Levent Yılmaz _____
Chemical Engineering Dept., METU

Assoc. Prof. Dr. P. Zeynep Çulfaz Emecen _____
Chemical Engineering Dept., METU

Prof. Dr. Yusuf Uludağ _____
Chemical Engineering Dept., METU

Prof. Dr. Göknur Bayram _____
Chemical Engineering Dept., METU

Asst. Prof. Dr. Enver Güler _____
Chemical Engineering and Applied Chemistry Dept.,
Atılım University

Date: 25.06.2018

I hereby declare that all information in this document has been obtained and presented in accordance with academic rules and ethical conduct. I also declare that, as required by these rules and conduct, I have fully cited and referenced all material and results that are not original to this work.

Name, Last name : Hazal YÜCEL

Signature :

ABSTRACT

FABRICATION OF HELICAL POLYMERIC HOLLOW FIBER MEMBRANES AND CHARACTERIZATION OF THEIR FOULING BEHAVIOURS

Yücel, Hazal
M. S. Department of Chemical Engineering
Supervisor: Assoc. Prof. Dr. P. Zeynep Çulfaz Emecen

June 2018, 107 pages

Membranes are used in many separation processes such as gas separation, microfiltration, ultrafiltration and hemodialysis. Hollow fiber membranes are advantageous since they have a high surface area per volume and are easily backwashed which is an advantage for fouling removal. The most important factors that affect the performance of filtration membranes are concentration polarization and fouling. They increase operational cost and reduce membrane lifetime and permeate flux. One approach that can reduce concentration polarization and fouling is modifying the hydrodynamics around the membrane surface by creating flow instabilities such as Dean vortices. Dean vortices are centrifugal instabilities formed in curved channels, such as spiraling tubes.

In this study, helical hollow fiber membranes are produced to investigate the effect of Dean vortices on the fouling behavior of the membranes. Four different solutions were used to produce membranes. PES is used as the membrane polymer for all of them, dimethylsulfoxide (DMSO) or N-methyl pyrrolidone (NMP) as solvents, polyethlylene glycol (PEG 400K), Triton 100x were hydrophilic pore forming agents

and water as non-solvent. Helical and straight hollow fiber membranes were produced by liquid rope coiling at 25°C (room temperature) and 50°C coagulation bath. Pure water permeances (PWP) and Bovine Serum Albumin (BSA, 66 kDa) rejections and fouling resistances with Baker's yeast (*Saccharomyces cerevisiae*) were measured.

Membrane geometry was seen to be affected by the air gap, polymer dope flow rate, bore liquid flow rate, ratio of polymer flow rate and bore liquid flow rate, bore liquid composition, coagulation bath temperature. For all solutions; increasing air gap turned membrane geometry straight to helical or irregular geometry. Increasing both polymer dope and bore liquid flow rate increased inner and outer diameter of the membranes. To observe effect of Dean vortices on fabricated membrane performance PWP and BSA rejections were measured for helical (H76) and straight (H77) membranes. For inside out process and outside-in process; helical membrane permeability during filtration decreased to 53% and 63% of the PWP, respectively. For inside out process and outside-in process; straight membrane permeability during filtration decreased to 33% and 36% of the PWP, respectively. BSA rejections of helical and straight membranes were 98% and 95%, respectively. Inside out results showing helical membranes fouling performance higher than straight membrane because of the Dean vortex. Outside in results showing fouling resistance of the straight fibers were more than helical ones. Helical membranes have improved hydrodynamics and less fouling compared to straight ones.

Keywords: Membrane, helical/twisted hollow fiber, liquid rope coiling, Dean vortices, membrane fouling.

ÖZ

KIVRIMLI KOVUKLU POLİMERİK ELYAF ÜRETİMİ VE KİRLENME DAVRANIŞLARININ İNCELENMESİ

Yücel, Hazal
Yüksek Lisans, Kimya Mühendisliği Bölümü
Tez Yöneticisi: Doç. Dr. P. Zeynep Çulfaz Emecen

Haziran 2018, 107 sayfa

Membranlar, gaz ayırma, mikrofiltrasyon, ultrafiltrasyon ve hemodiyaliz gibi birçok ayırma işleminde kullanılırlar. Kovuklu elyaf membranlar, kirlenmenin kaldırılmasında avantaj sağlayan hacim başına yüksek yüzey alanına sahip olma ve kolaylıkla geri yıkanabildikleri için avantajlıdırlar. Filtrasyon membranlarının performansını etkileyen en önemli etkenler, derişim kutuplaşması ve kirlenmedir. Bu etkenler operasyonel maliyeti artırır ve membran ömrünü ve geçirgenlik akışını azaltırlar. Dean vorteksler gibi akış düzensizlikleri oluşturarak membran yüzeyindeki hidrodinamiği değiştirmek derişim kutuplaşmasını ve kirlenmeyi azaltan yaklaşımlardan biridir. Dean vorteksler, spiral borular gibi kavisli kanallarda oluşan santrifüj düzensizlikleridir.

Bu çalışmada, Dean vortekslerin membranların kirlenme davranışları üzerindeki etkisini araştırmak için kıvrımlı kovuklu elyaf membranlar üretilmiştir. Membran üretimi için dört farklı çözelti kullanılmıştır. Membran polimeri olarak PES bütün çözeltilerde, çözücü olarak dimetil sülfoksit (DMSO) veya N-metil pirolidon (NMP), hidrofilik gözenek oluşturucu maddeler olarak polietilen glikol (PEG 400K) ve/veya Triton 100X, ve su çözmeyen olarak kullanılmıştır. Kıvrımlı ve düz kovuklu elyaf membranlar sıvı halat kıvrımlanması yöntemiyle 25°C (oda sıcaklığında) ve 50°C'lik

koagülasyon banyosunda üretilmiştir. Saf su geçirgenliği (PWP), Bovin Serum Albumin (BSA, 66 kDa) tutma oranları ve Baker mayası (Saccharomyces cerevisiae) ile kirlenme dirençleri ölçülmüştür.

Membran geometrisinin hava boşluğu, polimer çözeltisi akış hızı, kovuk sıvısı akış oranı, polimer akış hızı ve kovuk sıvısı akış oranı, kovuk sıvısı bileşimi, koagülasyon banyosu sıcaklığı tarafından etkilendiği görülmüştür. Tüm çözeltiler için; hava boşluğunu arttırmak, membranın düz geometrisini kıvrımlı veya düzensiz geometriye çevirmiştir. Hem polimer çözeltisi hem de kovuk sıvısı akış hızlarını arttırmak, membranların iç ve dış çaplarını arttırmıştır. Dean vortekslerin membran performansına etkilerini gözlemlemek için kıvrımlı (H76) ve düz (H77) membranların PWP ve BSA tutma oranları ölçülmüştür. Kıvrımlı membranda içten dışa ve dıştan içe deneylerde filtrasyon sırasındaki geçirgenlik sırasıyla PWP'nin %53 ve %63'üne düşmüştür. Düz membranda içten dışa ve dıştan içe deneylerde filtrasyon sırasındaki geçirgenlik sırasıyla PWP'nin %33 ve %36'üne düşmüştür. BSA tutma oranları kıvrımlı ve düz membranlar için sırasıyla %98 ve %95'dir. İçten dışa yapılan deneylerde kıvrımlı membranlarda kirlenme performansı Dean vortexten dolayı düz membranlara göre daha iyidir. Dıştan içe yapılan deneylerde düz membranlarda kirlenme direnci kıvrımlı membranlara göre daha yüksektir. Kıvrımlı membranlar düz olanlara kıyasla daha gelişmiş hidrodinamik ve daha az kirlenme göstermişlerdir.

Anahtar kelimeler: Membran, kıvrımlı/spiral kovuklu elyaf, sıvı halat kıvrımlanması, Dean vorteksler, membran kirlenmesi.

To Aydın, Mükafat, Tunç, Julio

ACKNOWLEDGEMENTS

Firstly I would like thank to my supervisor Assoc. Prof. Dr. P. Zeynep Çulfaz Emecen for her guidance, interest, and help through my thesis studies.

I also thank to my labmates who I spent 3-4 years in working hours. We shared a lot about life, not just about experiments that do not make any sense on their own. And thank you for listening my disastrous stories from every subject with patience. We have lots of memories but the most unforgettable ones for me are; lovely people furiously and jeolously entering the lab because we laugh so hard, days we teach Faqih, Serdar Ortaç songs and “truck back writing” and going to Cepa with singing Tüslemem and Papatü.

Finally I would like to express my deepest gratitude to my dear friend Fatma Çimen Atak and my family; Aydın, Mükafat, Tunç and Julio. Their endless support, love and patience are priceless and always with me throughout my life. I cannot imagine a life without them I feel very lucky and unique to have them in my life. Even these fancy words are very insufficient to express my feelings about them.

TABLE OF CONTENTS

LIST OF FIGURES

FIGURES

LIST OF TABLES

TABLES

NOMENCLATURE

HFMs	Hollow Fiber Membranes
A	Hollow Fiber Membrane Area, m^2
C_p	Permeate Concentration
C_f	Feed Concentration
J	Permeation Flux, L/h. m^2
R	Retention
R_{mem}	Membrane Resistance
R_{total}	Total Membrane Resistance
$R_{fouling}$	Membrane Fouling Resistance
PWP	Pure Water Permeance
TMP	Transmembrane Pressure
DMSO	Dimethly Sulfoxide
NMP	N-methyl Pyrrolidone
PEG400	Polyethylene Glycol
PES	Polyethersulfone
PS	Polysulfone
BSA	Bovine Serum Albumin
PBS	Phosphate Buffered Saline
SEM	Scanning Electron Microscopy
PDFR	Polymer Dope Flow Rate
BLFR	Bore Liquid Flow Rate
De	Dean Number
S	Straight
M	Meander
H	Helical
μ	Viscosity

CHAPTER 1

INTRODUCTION

Membranes are selectively permeable barriers between two phases; feed and permeate. In a membrane separation process feed is a mixture of desired and undesired components. When feed is sent to the membrane it is separated into two streams; retentate and permeate. Retentate is the unfiltered or pass over side of the feed. Permeate is the passing through side of the feed stream. Figure 1.1 schematically shows the membrane separation process.

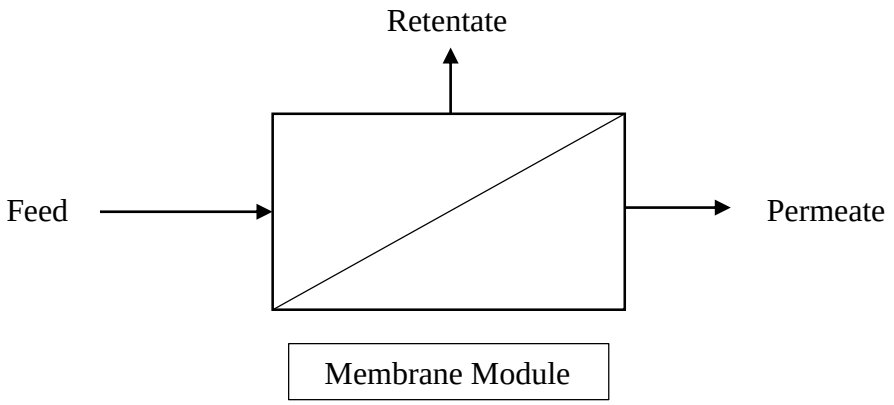

Figure 1.1. Schematic of membrane filtration process.

Membranes can be used in different separation processes such as gas separation, microfiltration, ultrafiltration and hemodialysis. Figure 1.2 shows pressure-driven membrane processes that use membranes with different pore diameter range so that their application in separation processes change [1].

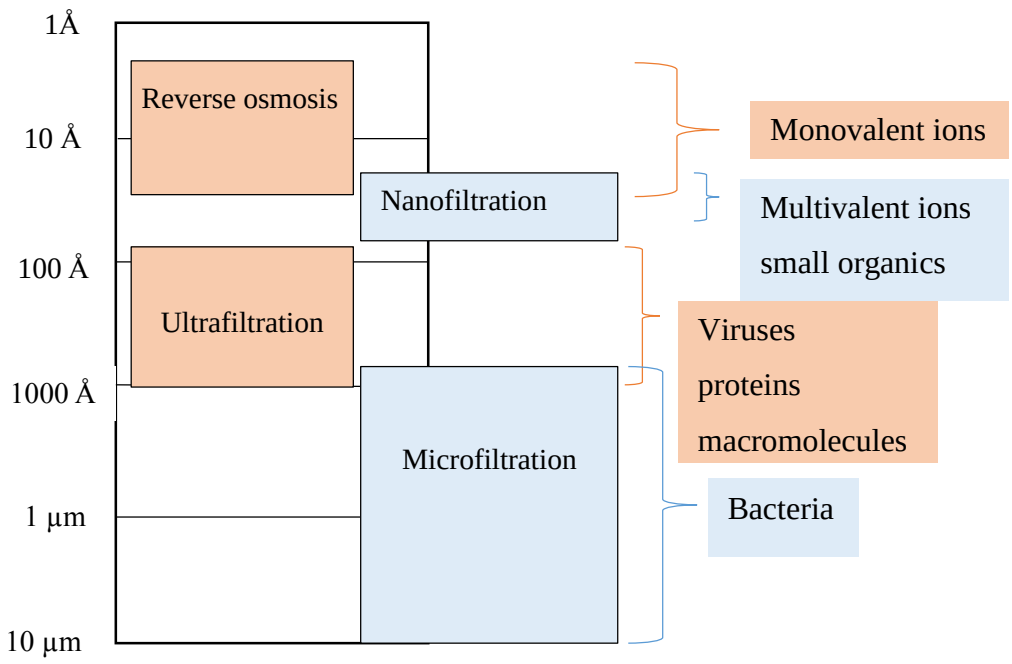

Figure 1.2. The relative size of different solutes removed by each class of membrane [1].

1.1. Pressure-Driven Membranes

Separation through porous pressure-driven membranes like microfiltration, ultrafiltration membranes depend on their pore sizes, and the size of feed components namely by molecular sieving. Nanofiltration membranes are also porous membranes and their separation mechanisms are both by molecular sieving and by charge exclusion.

1.1.1. Microfiltration Membranes

Microfiltration membranes can be produced using different materials such as polymeric or ceramic materials. They can be produced by sintering, stretching, track-etching or phase inversion technique. Their structure may be both asymmetric and symmetric. Their pore size is in the range between 0.1 and 10 µm, can be seen Figure 1.2. In industry they are used in sterilization of food or pharmaceuticals, waste water treatment [2].

1.1.2. Ultrafiltration Membranes

Ultrafiltration membranes can be produced using different materials such as polymeric or ceramic materials like microfiltration membranes. Compared to microfiltration membranes their pore sizes smaller. Their pore size is in between 1-100 nm. Phase inversion is mostly used for producing ultrafiltration membranes so that they usually have an asymmetric structure. They are used in food industry, pharmaceutical industry, waste water treatment [1, 2].

1.1.3. Nanofiltration and Reverse Osmosis Membranes

Nanofiltration membranes have pore sizes under 1 nanometer [3]. Their separation performance is in between ultrafiltration and reverse osmosis membranes since all ions are rejected by reverse osmosis membranes, but nanofiltration membranes reject multi-valent ions and allow monovalent ions to permeate [4]. Nowadays they are both produced by interfacial polymerization. They have both composite structures and can be both used in water treatment [1, 2].

1.2. Membrane Fabrication via Phase Inversion Technique

Phase inversion is a common technique for polymeric membrane fabrication since both asymmetric and symmetric membrane structures can be obtained. This technique simply turns homogenous polymer solution to a membrane with the help of non-solvent. Another known name of this technique is the Loeb-Sourirajan technique.

Phase inversion procedure is; firstly casting the polymer solution then precipitating it in a nonsolvent, e.g. water. With this technique both symmetric (isotropic) and asymmetric (anisotropic) membranes can be fabricated. Isotropic membranes structural properties like porosity and pore size remain the same with the membrane' cross section. On the other hand anisotropic membranes structural properties change across the cross section.

As shown in Figure 1.3 membrane fabrication via phase inversion technique starts with the initial casting solution. Polymer, solvent (and possibly additives) are both in liquid phase at the initial state, A. When solution is immersed in the non-solvent (water) the overall composition moves towards the two-phase region and phase separation starts after passing through the binodal or the spinodal curve. One phase precipitates which is the polymer-rich phase, and forms the membrane matrix, one phase is the polymer-lean phase which forms the membrane pores. During path A to C, the viscosity of the polymer-rich phase increase and it solidifies. After a certain time final membrane is produced at that point C where two phases are in equilibrium.

Precipitation rate is also important, since it affects the produced membrane pore structure. With phase inversion technique membranes can be fabricated as flat membranes and hollow fiber membranes [1, 2, 5-7].

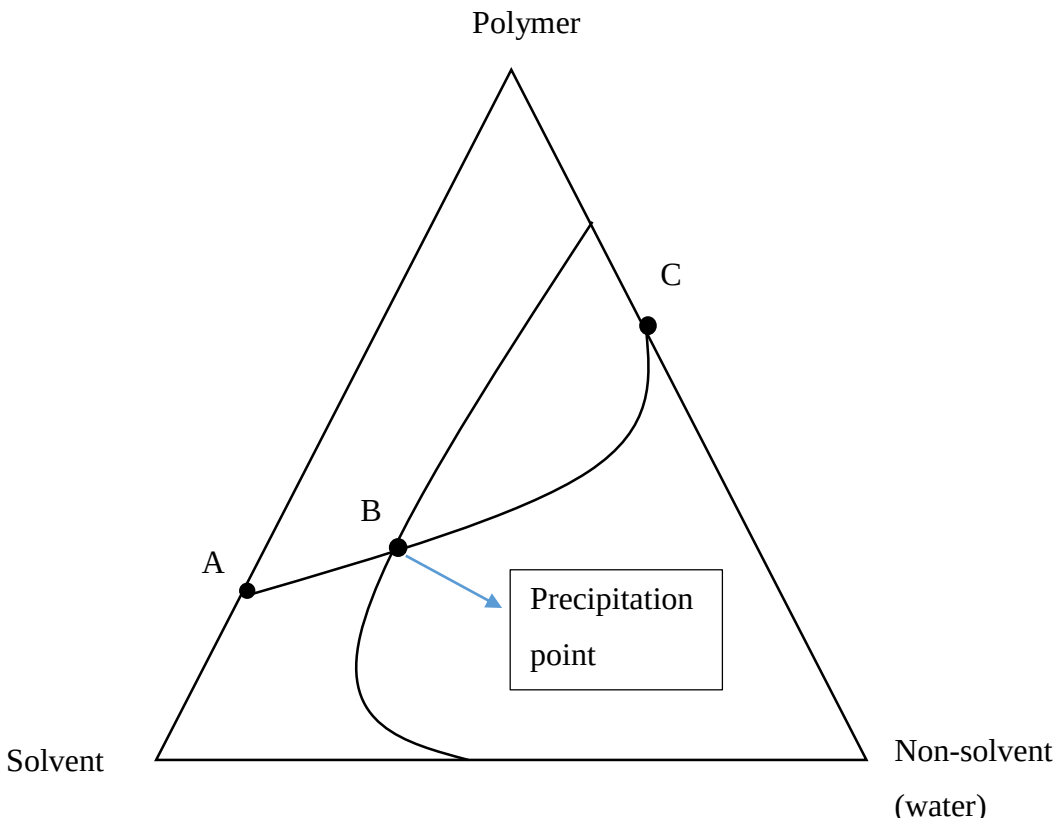

Figure 1.3. Membrane formation via phase separation [1, 6].

1.3. Hollow Fiber Membranes

Hollow fiber membranes are more advantageous than flat membranes because they have high surface area per volume, pressure resistance and they can easily be cleaned by backwashing [5, 8, 9]. Dry or wet spinning process are generally used to produce hollow fiber membranes [12]. To form fiber membranes a device called spinneret is used. Spinneret picture and its schematic shown in Figures 1.4 and 1.5.

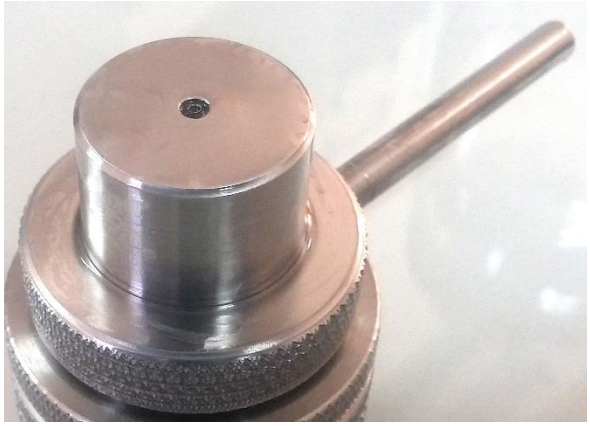

Figure 1.4. Spinneret.

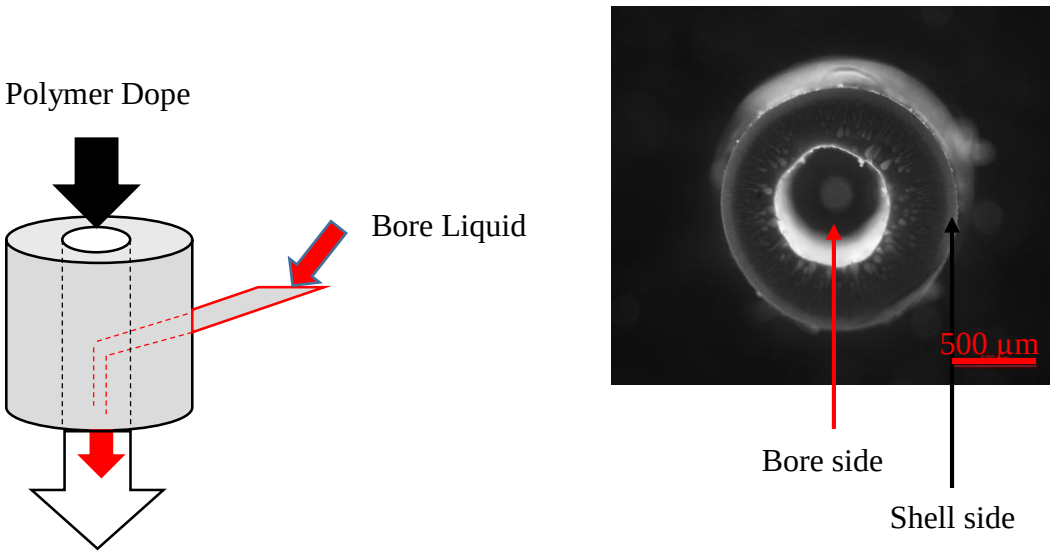

Figure 1.5. Schematic of spinneret and microscope image of hollow fiber.

There are two ways to produce hollow fiber membranes which are wet spinning and dry-wet spinning. In wet spinning after extrusion through spinneret polymer solution directly enters coagulation bath which is filled with the non-solvent. On the other hand in dry-wet spinning after fiber exit the spinneret there is an air gap after which the fiber enters the liquid coagulation bath [13].

To fabricate high performance hollow fiber membranes selection of membrane material is also important since chemical, mechanical and permeation need of the separation system is important too [1, 2]. Polyethersulfone (PES) and polysulfone (PS) as membrane matrix former are commonly used in especially microfiltration and ultrafiltration processes since they have advantageous properties such as durability at wide temperature limits until 75°C to 125°C, wide pH tolerances from 1 to 13, very good resistance to chlorine until 200 ppm and resistance to chemicals like aliphatic hydrocarbons, alcohols, acids [9].

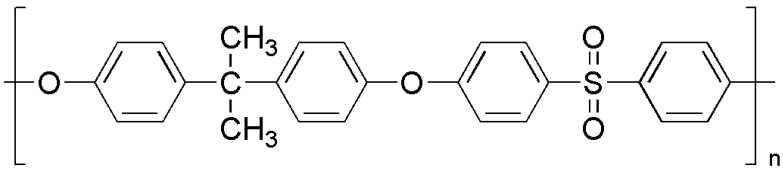

Figure 1.6. Chemical structure of Polyethersulfone.

1.4. Concentration Polarization and Fouling

During a membrane separation process some substances (colloids, macromolecules) in the feed cannot pass through the membrane and the concentration of these retained solutes increase near the membrane-solution interface. This phenomenon is called concentration polarization [9]. After concentration polarization occurs retained materials' deposition may start on the membrane surface which is called fouling.

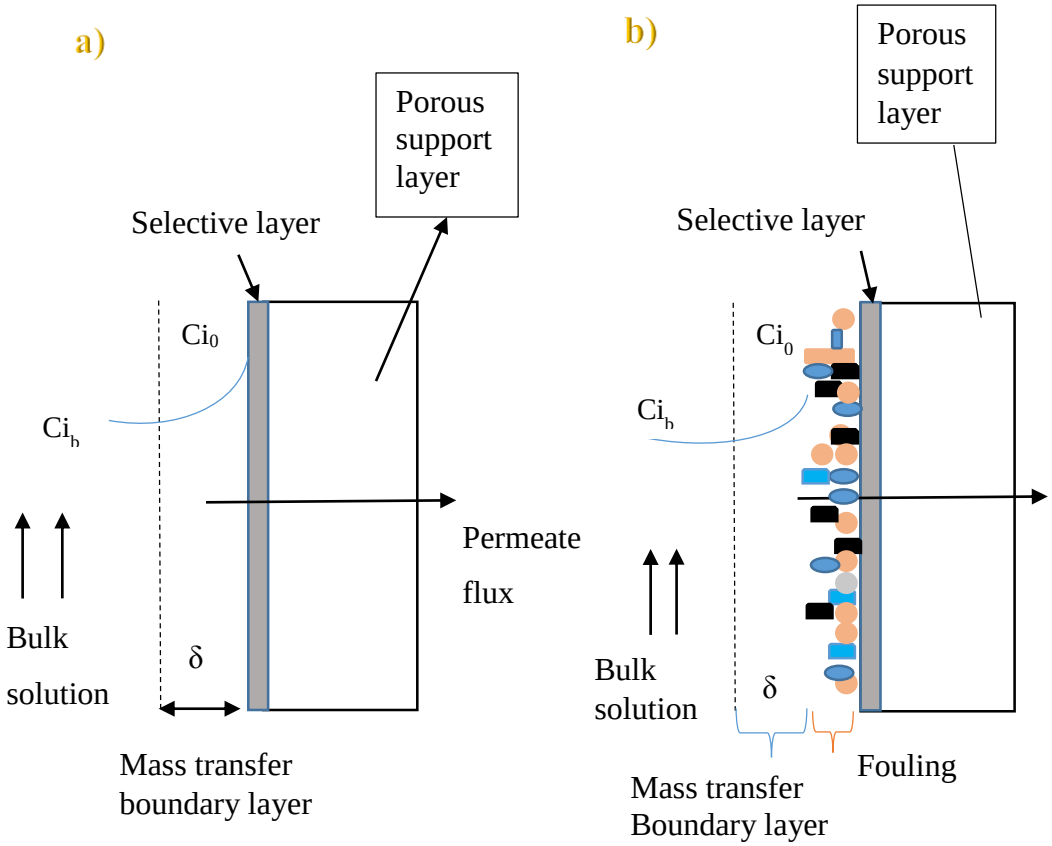

Figure 1.7. Concentration polarization (a) and fouling (b) mechanism from left to the right [1, 14].

Concentration polarization and fouling both decrease the permeate flux or increase transmembrane pressure required to sustain a certain flux during filtration, decrease membrane lifetime and increase energy consumption. Additionally they change membranes' retention of solutes [1, 11, 14-18]. Figure 1.7 shows the concentration polarization and fouling separately. There are several ways to prevent these phenomena which will be covered in literature survey.

1.5. Methods to Prevent Concentration Polarization and Fouling

1.5.1. Filtration Methods

To prevent concentration polarization and fouling filtration method selection is important. In earlier times dead-end filtration was the only filtration method for membrane separation processes. In this filtration feed solution pass through the membrane perpendicularly. As time passes flux always decreases because retained particles are deposited on the membrane surface and produce a cake layer which will increase until the process stopped. In cross-flow filtration, feed solution passes parallel to the membrane surface and the main advantage of this filtration is the possibility of preventing fouling since particles deposited on the membrane surface can be dragged with the tangential flow [14, 16, 22]. Both dead-end and cross-flow filtrations are shown in Figure 1.8 schematically.

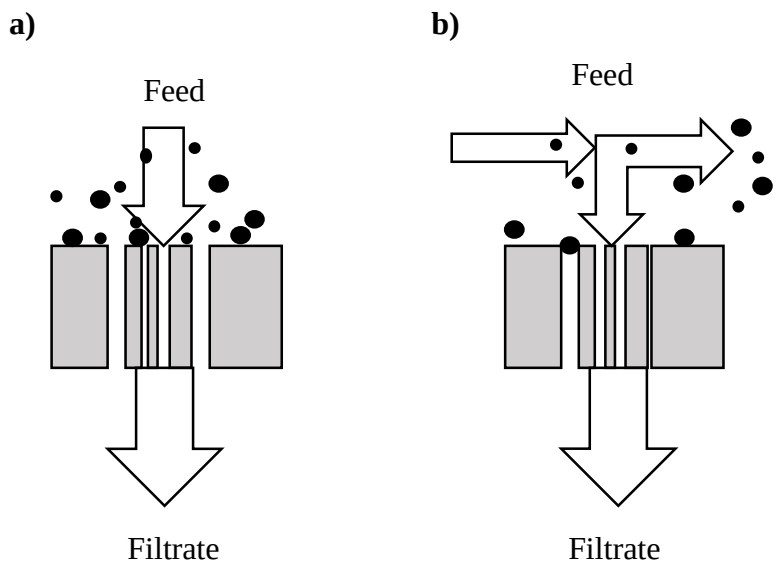

Figure 1.8. Schematic representation of Dead-end filtration (a) and Cross-flow filtration (b).

1.5.2. Physical, Hydrodynamic and Chemical Methods

Other ways to reduce concentration polarization and fouling are shown in Figure 1.9. Methods can be classified into three, as chemical, hydrodynamic and physical methods.

Chemical methods include surface modifications. They generally have little effect of decreasing concentration polarization and fouling since after cake layer formation their effect reduces. Physical methods include paddle or static mixer and mechanical scouring where scale-up is not very easy. Hydrodynamic methods include creating turbulent flow, instabilities and adding inserts.

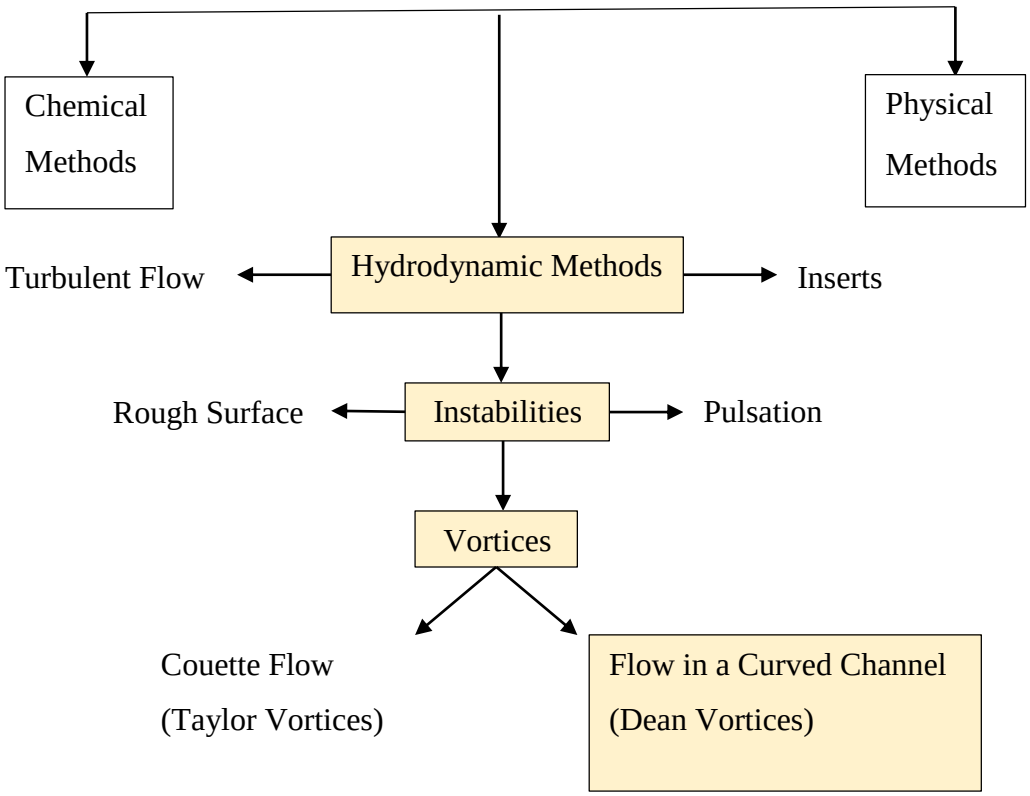

Figure 1.9. Methods to prevent fouling and concentration polarization [8, 18].

Hydrodynamic Improvements

To reduce concentration polarization and fouling hydrodynamic methods which include turbulent flow, instabilities and inserts are used. Placing inserts within the flow channel can be done by setting up inserts a specified distance away from the membrane surface. It is a process which is hard to scale-up. Using turbulent flow by changing the Reynolds Number during the whole process is not economic, another point for this method is it increases the pressure drop of the system. On the other hand instabilities as a result of unstable flows can be observed by placing corrugations on the membrane surface or giving pulsations which is making oscillating flow near the membrane. Placing protuberances or making corrugations on the membrane surface induce secondary flow on the membrane surface. Pulsations result in solute movement away from membrane surface to the bulk and increase the mass transfer rate by reducing the concentration polarization and fouling so membrane performance increase but they also increase the energy consumption of the system. Another way to produce instabilities is creating vortices which are called Dean and Taylor vortices. Taylor vortices occur as a result of the Couette flow and Dean vortices occur as a result of flow in a curved channel. To create Taylor vortices rotating devices are used. To rotate devices there is an extra energy consumption needed. Also to replace or repair these devices are not easy. On the other hand to create Dean vortices there is no need for any other device or material. Dean vortices are fluid instabilities that occur as a result of curved channels such as flow in helical hollow fibers (Fig 1.10). An efficient way to reduce concentration polarization and fouling can be to create Dean vortices in a hollow fiber membrane [8, 9,15, 18-20].

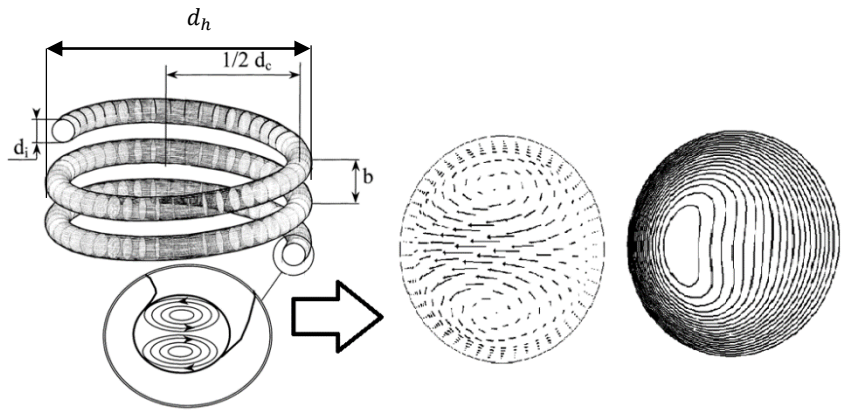

Figure 1.10. Dean vortices in curved channels [28,21]

The extent of Dean vortices can be related to Dean number; De which is a dimensionless number. Dean number can be expressed as follows depending on the fiber geometry;

$$De = Re\sqrt{\frac{d_i}{d_c}} \tag{1}$$

Re is the Reynolds number, d_i is the inside diameter of the fibers and d_c is the effective coil diameter, expressed as following;

$$d_c = d_h\left[1 + \left(\frac{b}{\pi d_h}\right)^2\right] \tag{2}$$

d_h is the helix diameter and b is the pitch as shown in Figure 1.10.
Following literature survey includes helical, meander or different geometry modules which were made by twisting the produced straight fibers.

Chung et al. investigated effect of Dean vortices on concentration polarization in spiral curved channels. They used numerical methods and 3-D diffusion equations to quantitatively measure the Dean flow and its effect on the curved channel inside and outside. They compared the flat membrane channel and spiral membrane channel results under the same parameters. Also they investigated how fast concentration

build-up in these channels and growth of concentration polarization layer in axial direction. As a result they revealed that concentration build-up is very slow with axial distance for spiral channel compared to the flat channel because of the Dean vortices. Also the outer wall concentration polarization is lower than the inner wall because of the vortex strength of the outer wall is higher than the inner wall [18].

Another study about comparing Dean vortices effect was made by Winzeler and Belfort. To compare Dean vortices effect on filtration performance of Baker's yeast broth and dairy whey; they use tubular and flat channel modules from microfiltration membranes. They placed spiral half tube onto a flat membrane which can be seen schematically in Figure 1.10. For both feeds they found permeation fluxes are five times higher with the tubular modules which include the Dean vortices because of the curved geometry [8].

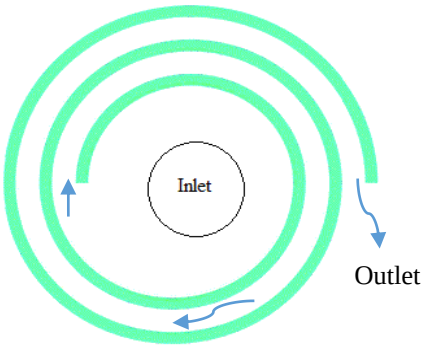

Figure 1.11. Spiral half tube onto a flat membrane

Teoh and co-workers studied on membrane distillation and investigated different hollow fiber module designs like inserting baffles, spacers or both of them at the same time or just by changing the geometry of the membrane. They found that hollow fibers that have spiral geometry like helical or braided configuration, increase the permeate flux by 36% which is because of the Dean vortices occuring on the membrane surface. Also helical hollow fiber membranes have a higher membrane effective area than straight ones because in helical modules fibers do not touch each other surface. They revealed a summary of different configurations and flux enhancement which showed

that the most effective geometry was the helical geometry with 49% flux enhancement [23].

Mallubhotla et al. studied microfiltration with yeast broth suspensions by using spiral membrane modules to observe the self-cleaning effect of this configuration. They observed 60% flux improvement with respect to the case without Dean vortices with the high yeast concentrations (0.15-0.25 %). With low yeast concentrations (0.013 %) flux improvement was 300% [24].

Kaufhold and co-workers studied on increasing the membrane contactors oxygen transfer rates by using Dean vortices in different membrane geometries. They found that for the curved membranes there is a linear relation between Dean number and oxygen transfer rate enhancement factor. Also they revealed that preparation of helical fiber modules increased cost and hard to do but the meander shape ones are more feasible for large scale processes [25].

Ghogomu et al. produced cellulose acetate straight hollow fiber membranes. To compare their performance they convert these straight membrane to different designs; helical, meander-shaped and helically coiled. They measured that in curved modules limiting flux is higher than the straight ones, which implies less fouling. To obtain same limiting flux values for straight modules, Reynolds number must be higher than curved modules which means straight modules energy consumption is higher. They found that Dean vortices effect on mass transfer is only noticeable when De reaches a critical value of around 20. Also they calculate that for a certain permeate flow rate curved modules energy consumption is lower than straight modules [26].

Moulin et al. investigated Dean vortex flux enhancement in coiled and straight hollow fiber ultrafiltration membranes by using bentonite suspension and dextran solution. They revealed that there is a critical Dean number which explain the point of changing the flow pattern and vortex observed or the point that mass transfer enhancement occur. For different process affected by Dean number, general observation is to observe Dean vortex effect Dean number must be at least 20. Also they calculated that

Dean vortices increased flux at least 2 times compare to the straight ones. When coil diameter decrease, flux can increase up to 2 times [27].

Liu et al. did another study about increasing mass transfer with the help of hollow fiber geometry. To investigate mass transfer they used nitrogen to strip dissolved oxygen from water. They found that coiled module mass transfer rate was two times higher than mass transfer in straight module. Also they reported that to get higher mass transfer coefficients fiber diameter must be smaller [28].

Chung and Lee compared helical and straight microfiltration membrane modules. At the same pressure they found that helical modules' (with Dean vortex) permeation flux 57% higher than straight module. They used two different feed solutions for filtration with kaolin and bentonite. For kaolin filtration membrane fouling reduced more effectively with vortex flow in helical modules than bentonite filtration. Also the flux enhancement revealed for kaolin and bentonite was 47% and 73% respectively [19].

1.6. Liquid Rope Coiling

Barnes et al. firstly studied on a viscous liquid stream and observed periodic buckling which occurs when a thin stream of viscous fluid is poured onto a surface from a certain height as seen in Figure 1.12 and they called this phenomenon "liquid rope coiling effect" [29]. Buckling instability helps helical geometry to occur. Because of axial pressure and liquid rope buckling competing with each other, liquid rope coiling occurs. This phenomenon is affected by liquid density, viscosity, gravity, flow rate, rope size and height. Because of the viscosity of liquid, liquid rope does not break due to the gravity and inertial stretching.

Figure 1.12. Liquid rope coil effect forming large coils on the PES solution.

Jia et al. fabricated helical cellulose fibers via liquid rope coiling. They observed helical structure when cellulose-cuprammonium solution is poured into a movable coagulation bath due to buckling instability of the liquid jet. To obtain continuous flow during the process they determined a certain range for polymer solution flow rate which is greater than 6 mL/min. Frequency of coiling increased with increasing spinning height. On the other hand they observe liquid rope can break after a certain height or can be very thin. The size of helical fibers was strongly related with air gap and flow rate. Increased air gap and decreased flow rate were shown to decrease the fiber diameter [30].

Luelf and his colleagues have recently prepared PES hollow fibers via rope coiling. With changing bore liquid and polymer solution composition a wide variety of geometries were obtained like meander, curly, figure of eight and w-pattern. They revealed that when higher falling speed was observed because of the fluid densities also higher velocity difference was observed and that improves the effect of rope coiling. Also they observed that if the solution is viscous, phase separation can hinder the rope coiling because solidification occurs. As a process parameter increasing spinning height increased the rope coil effect. Another process parameter is pulling wheel speed. When it is too high from the free fall speed of the fiber in the coagulation bath, it also hinders the rope coiling and fibers can only be produced in straight geometry [10].

2.1.Aim of the Study

In this study our aim was to fabricate helical hollow fiber membranes via liquid rope coiling and compare their fouling behavior to straight fibers. We use PES as membrane polymer. After producing desired helical fibers by changing the parameters straight hollow fibers produced with same solutions, their characterization and performance tests made by measuring pure water permeances, BSA retention and fouling during yeast filtration.

CHAPTER 2

EXPERIMENTAL METHODS

2.1. Materials

Polyether sulfone (PES, Ultrason E6020P) was provided from BASF which was used as the membrane polymer in this project. Solvents for preparing different solutions; N-Methyl-2-pyrrolidone (NMP) and dimethyl sulfoxide (DMSO) were purchased from Merck and Sigma-Aldrich, respectively. Additives Triton X100 and polyethylene glycol (PEG400) were purchased from Sigma-Aldrich and Merck, respectively. As a non-solvent in solutions and all feed solutions, ultrapure water (0.055 µS/cm) was used, and it was taken from Human UP 900 device. Tap water was used for coagulation of the hollow fiber membranes.

Produced UF membranes characterization experiments are done with several materials; for rejection tests bovine serum albumin solution (BSA, 66kDa) in phosphate buffered saline (PBS, pH=7.4) was used and they were both purchased from Sigma-Aldrich. For fouling experiments Baker's yeast, Saccharomyces cerevisiae (dry active yeast of Dr. Oetker) which is dyed with Brilliant Blue R and acetic acid (purchased from Sigma-Aldrich) and isopropanol (purchased from Merck), were used. To make these characterization experiments modules were prepared by using epoxy solution which includes REN HY 5160 and RENLAM CY 219 both were purchased from RenShape Solutions.

2.2. Membrane Preparation

2.2.1. Flat Membranes

Before hollow fiber membrane production, as a preliminary study flat membranes were fabricated. Firstly solutions were prepared then poured onto the straight glass surface. As soon as solution poured onto the glass, stainless steel casting bar was used to cast the solution at 250 µm thickness (Figure 2.1).

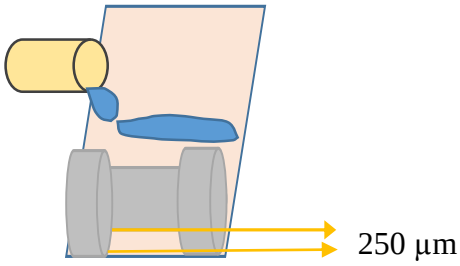

Figure 2.1. Schematic of the flat sheet membranes casting.

Direct liquid-induced phase separation (LIPS) and LIPS followed by vapor induced phase separation (VIPS) was used for coagulation. Humid air production done by using aquarium pump and vapor exposure time was 10 minutes [33].

2.2.2. Fabrication of Fibers

As seen in Figure 2.2 spinning system contains polymer dope tank, bore liquid tank, polymer dope pump, bore liquid pump, spinneret and coagulation tank, an electric panel to control pumps flow rates. All tanks were made in METU Chemical Engineering Department Workshop. Spinneret was made by FAYMER Makina at Ostim, Ankara. Polymer liquid pump and bore liquid pump were purchased from Mahr.

Before the solution preparation, PES was dried at 80°C in oven overnight. Solutions were mixed with magnetic stirrer or on roller mixer. Table 2.1 shows solutions which are used in spinning.

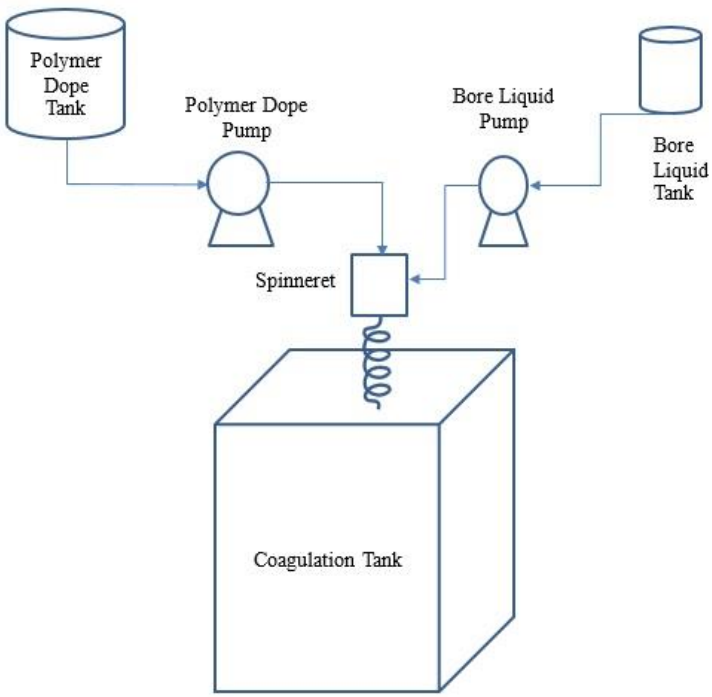

Figure 2.2. Schematic of spinning system.

After homogenous solution was obtained it was filtered with 250 mesh screen, by using nitrogen gas pressure (0-2 bar). Then filtered solution was put into the polymer tank and kept overnight for degassing before the spinning process. At the spinning day, coagulation tank was filled with tap water. Bore liquid was prepared and filled up bore liquid tank. Spinneret was placed into the system. After pumps start to work, polymer dope and bore liquid met as soon as they out of the spinneret and poured into the coagulation bath. Bore liquid forms hollow bore of the fibers and polymer dope forms the membrane matrix. In this system several parameters affect on fabricated membranes morphology and performance like polymer dope flow rate, bore liquid flow rate, polymer dope and bore liquid flow rate ratio, air gap (distance between spinneret exit and coagulation bath level), coagulation bath temperature.

Produced membranes were taken out of the coagulation bath and put into the tap water, washed several times for one day. Then membranes were put into another solution for 24 hours, which contains 10% glycerol and 90% water to prevent their pores collapsing after they dried.

Table 2.1. Polymer Dope Compositions

Solution Code	PES (wt.%)	PEG400 (wt.%)	Triton100X (wt.%)	NMP (wt.%)	DMSO (wt.%)	Upwater (wt.%)
D	20	40	-	-	40	-
M	15.3	-	5.1	72.3	-	7.3
N	15	-	5	70.7	-	9.3
O	15	20	5	52.4	-	7.6

Solution M: 75% of coagulation value

Solution N: 95% of coagulation value

Solution O: 95% of coagulation value

To characterize fabricated membranes firstly membrane modules were prepared by using epoxy solution which contains REN HY 5160 and RENLAM CY 219 as 1:2 weight ratio respectively. Each module has one fiber and approximately 5 cm length.

2.3. Characterization of Membranes

All characterization tests were made with the same cross-flow system which shown in Figure 2.3.

2.3.1. Pure Water Permeance

Pure water permeances were measured at two different pressures at 1 and 2 bar. When pressure was constant, permeate was collected and measured every 30 minutes, this data divided by the membrane effective area (A, m^2) and called permeate flux (J, $L/h.m^2$).

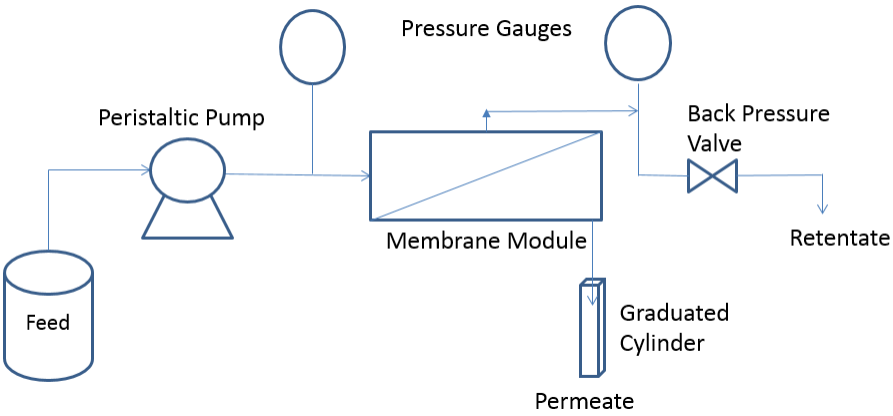

Figure 2.3. Schematic of performance tests cross-flow system.

Figure 2.4. Picture of performance tests cross-flow system.

When the measured data were fixed which means membrane permeation was at steady state. At that transmembrane pressure (TMP) and the data gave membrane pure water permeance (PWP, L/h.m^2.bar). PWP of the membranes were calculated with using following equation;

$$\mathrm{PWP} = \frac{\mathrm{J}}{\mathrm{TMP}} \tag{2.1}$$

2.3.2. Retention Test

Membrane retention tests were made by using 1 g/L BSA solution at 1 and 2 bar, and Reynolds number was at 500. To prepare BSA feed solution, firstly 1 tablet of PBS was dissolved in 200 mL ultrapure water, then 0.2 gram BSA was added and mixed with this solution. Before the filtration test sample was taken from the prepared feed solution. During filtration permeate and retentate samples were taken with respect to time and their concentration were determined by using UV/visible spectroscopy instrument Schimadzu UV-1601 at 278 nm. Retention of the membranes were calculated by following equation;

$$\text{Retention } \% = \left[1 - \frac{C_P}{\left(\frac{C_F + C_R}{2}\right)}\right] \times 100 \qquad (2.2)$$

Where;

C_P= Permeate concentration (g/L)

C_F= Feed concentration (g/L)

C_R= Retentate concentration (g/L)

2.3.3. Membrane Fouling

After pure water permeances are calculated fouling experiments were done with the same module. Fouling tests were made by using dyed-yeast (0.025% dye) at 2 bar and Reynolds number 400 in a cross-flow mode.

To prepare dyed-yeast firstly 1 gram Dr. Oetker yeast was dissolved in 250 mL ultrapure water, centrifuged three times at 2500 rpm for 10 minutes and supernatant was discarded each time. Precipitated yeast were dried, then mixed for 3 hours with 0.15 gr Brilliant Blue R dye, 25 mL acetic acid, 62.5 mL isopropanol and 161.5 mL ultrapure water. After mixing, solution was centrifuged as yeast preparation method; three times at 2500 rpm for 10 minutes and supernatant was discarded. Final precipitate was dried in fume hood. For filtration test 0.05 gr dyed-yeast was dissolved in 200 mL ultrapure water. Remained dyed-yeast was stored in desiccator [31].

During filtration, dyed-yeast solution were always on the mixer and permeance data were taken every 2 mL for 1 hour. Membrane resistances (R_m, m^{-1}) and fouling resistances (R_f, m^{-1}) of the membranes were calculated by using following equations;

$$R = \frac{TMP}{\eta . j} \tag{2.3}$$

$$R = R_M + R_f \tag{2.4}$$

Where;

R = Total resistance, m^{-1}

η= viscosity of permeate, Pa.s

j= flux during filtration, $L/h.m^2.bar$

2.3.4. Membrane Morphology Analysis by SEM

Membranes' cross-sections and surface morphology were observed by scanning electron microscopy (SEM, FEI Nanosem 430) in METU Metallurgical and Materials Engineering Department. To observe cross-section of the membranes they were broken with liquid nitrogen and, to observe inner surface of the membranes they were cut off tangentially by lancet, to observe outer surface of the membrane any pretreatment were not needed and they were put onto sample holders with conductive tape. After that they stored in vacuum for two days. Just before the analysis samples sputter-coated with gold-palladium under vacuum. Images were taken from 100x to 100 000x.

2.4. Characterization of the Polymer Dopes

2.4.1. Viscosity

Solution viscosities were measured by using rotational viscometer (TA Instruments ARES rheometer) at METU Central Laboratory. The viscometer type was coaxial cylinders and measurements were done at 25 ±1 °C.

2.4.2. Cloud point Measurements

Cloud point was used to determine binodal composition of new solutions since it was observed when solution is reached phase separation. To determine cloud point of the solution M, titration method was used. Cloud point of solution N was determined by Gülçin Kaltalı [32]. Lastly cloud point of solution O was determined by preparing solutions with different amount of water and after stirring their turbidity observed.

In titration method firstly, solutions were prepared and mixed homogenously. After the homogenous solution was obtained 25% solvent 75% non-solvent mixture were added to the solution mixture drop by drop. Every drop was made solution partly turbid, to prevent this after every drop solution mixed again until became homogenous again at a constant temperature. After a point solution became completely turbid since it reached the phase separation, that point was the cloud point of this solution at that composition and it defined as following;

$$\text{Coagulation value} = \frac{\text{H}_2\text{O (in solution)}}{\text{H}_2\text{O (at cloud point)}} \tag{2.5}$$

CHAPTER 3

RESULTS AND DISCUSSION

3.1. Cloud Point Experiments

Every polymer-solvent-non solvent system has its own, unique ternary phase diagram. First, PES-DMSO-water ternary system phase diagram was determined by cloud point experiments as a preliminary study. Cloud point determination was made by six different PES compositions which started from 5% to 30%. Figure 3.1. shows ternary phase diagram of the DMSO system. Also Figure 3.2. shows NMP-water system ternary phase diagram that was also used to produce hollow fiber membranes which was determined by Gülçin Kaltalı [32].

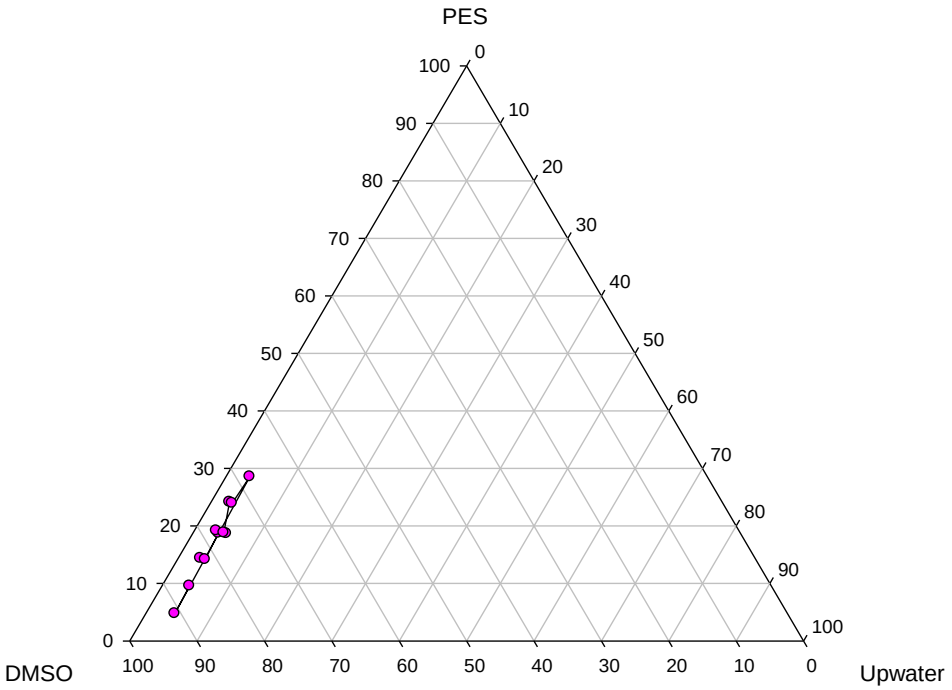

Figure 3.1. Ternary plot for DMSO-PES-water system.

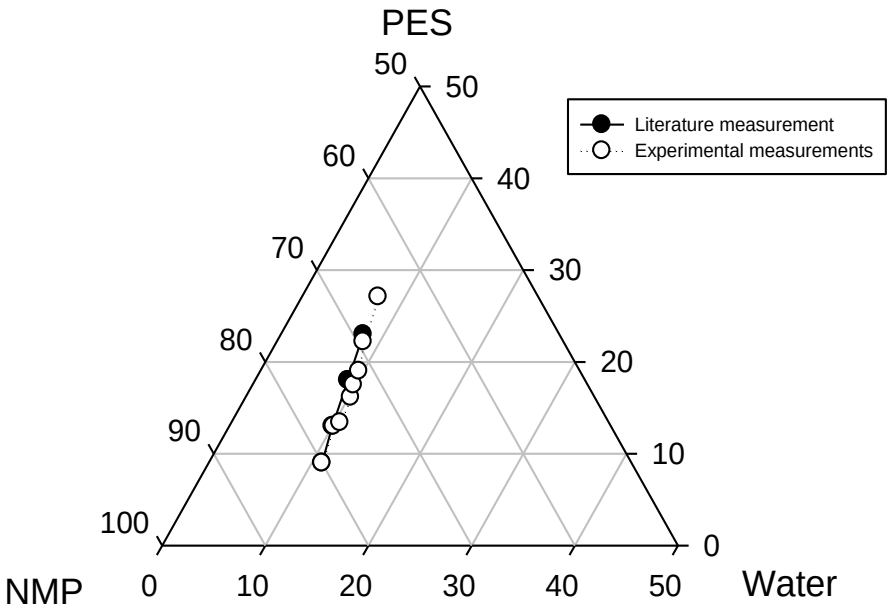

Figure 3.2. Ternary plot for NMP-PES-water system.

As seen in the figures, solutions with DMSO were reached cloud point combination with less water content compared to NMP solutions.

3.2. Flat Membranes

As a preliminary study flat membranes were produced before the hollow fiber membrane production. Flat membranes were fabricated by using five different solutions. All have DMSO as a solvent and some of them have PEG400 as a pore forming agent. Combinations of them given as following;

Solution A: 20 wt. % PES, 80 wt. % DMSO
Solution B: 20 wt. % PES, 78 wt. % DMSO, 2 wt. % Up water
Solution C: 20 wt. % PES, 20 wt. % PEG400, 60 wt. % DMSO
Solution D: 20 wt. % PES, 40 wt. % PEG400, 40 wt. % DMSO
Solution E: 20 wt. % PES, 60 wt. % PEG400, 20 wt. % DMSO

By looking at the membranes' characterization tests because of having high permeability of water, solution C, D and E were considered to produce hollow fiber membranes. Solution E was not selected because of having high viscosity so solution D was selected for producing hollow fiber membranes (Table 3.1). After that, produced flat membranes from solution D both coagulated in water and in humid air were investigated by using SEM (Figure 3.3). Observations showed that both membranes have nodular structure at both air side and support side. Selective layer was formed on the air side for both.

Table 3.1. Pure water permeances of flat membranes produced in humid air and water.

Solutions	**A**	**B**	**C**	**D**	**E**
PWP* (L/h.m^2.bar)	<1	2	71±18	79±35	42±7
PWP (L/h.m^2.bar)**	36±9	125±17	55±22	31±8	42±17

*Coagulated in humid air

**Coagulated in water

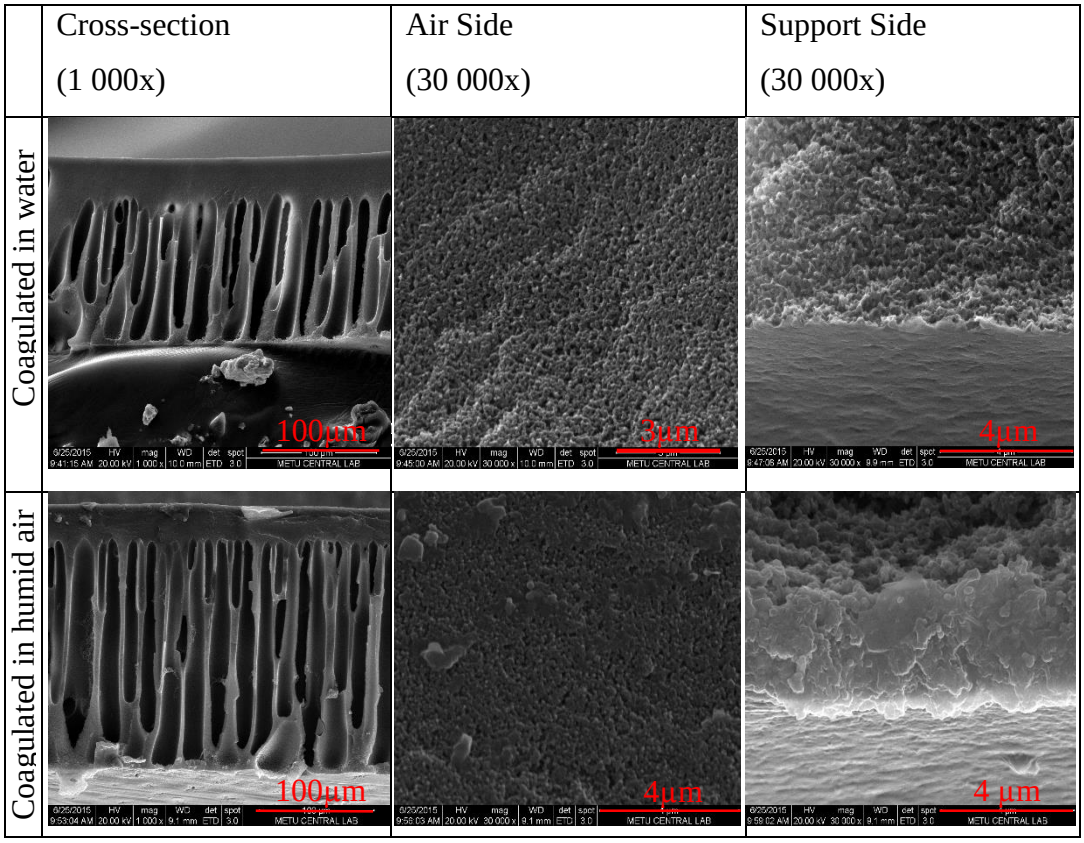

Figure 3.3. SEM images of flat membranes produced from solution D.

3.3. Hollow Fiber Membranes

Hollow fiber membranes (HFMs) were fabricated by using four different solutions. Combinations of them given as following;

Solution D: 20 wt. % PES, 40 wt. % PEG400, 40 wt. % DMSO
Solution M: 15.3 %PES, 5.1 %Triton 100X, 72.3%NMP, 7.3 %Upwater (75% of coagulation value)
Solution N: 15 %PES, 5 %Triton 100X, 70.7 %NMP, 9.3 %Upwater (95% of coagulation value)
Solution O: 15% PES, 5% Triton 100X, 20% PEG400, 52.4% NMP, 7.6% Upwater (95% of coagulation value)

Viscosity measurements were done for these four solutions. Solution D much more viscous than other solutions M, N and O which can be seen in Table 3.2.

Table 3.2. Solution viscosities at shear rate 1 s^{-1}.

Solution	**Viscosity at shear rate 1 s^{-1} (Pa.s)**
D	28.770
M	1.793
N	2.480
O	5.486

When producing HFMs their geometry were influenced by several parameters; polymer dope flow rate (PDFR), bore liquid flow rate (BLFR), ratio of polymer dope and bore liquid flow rates, non-solvent composition of bore liquid, coagulation bath temperature and air gap. In our study most of the parameters were observed with using different solutions as a polymer dope. HFMs were fabricated at two different coagulation bath temperatures; at 25°C (at room temperature) and at 50°C.

3.3.1. Solution D

3.3.1.1. Effect of spinning parameters on fiber geometry

For solution D investigated parameters were; air gap, coagulation bath temperature, coagulation value, polymer dope flow rate and bore liquid flow rate. During these experiments polymer dope flow rate (PDFR) and bore liquid flow rate (BLFR) ratio was always 3:1. And non-solvent (water) and solvent (DMSO) ratio of bore liquid was always at 1:9.

Fiber geometries are straight (S), helical (H) and meander (M). When the geometry does not change throughout the spinning are called regular. If the geometry change throughout the spinning it is called irregular (Irr.).

<u>Relation Between Air Gap and Polymer Dope Flow Rate and Bore Liquid Flow Rates</u>

Table 3.3 shows how geometry of the produced fibers change with increasing air gap and decreasing PDFR-BLFR with coagulation bath temperature at room temperature. (When coagulation bath temperature at 50°C fibers could be produced only in a straight geometry with the parameters tested.) Also Table 3.4 shows the inner and outer diameters of the membranes, can be followed by using membrane codes in Table 3.3.

Table 3.3. Relation between air gap and PDFR-BLFR for solution D membranes produced 25±2°C.

Air gap → / PDFR ↓	7 cm	8.5 cm	9.5 cm	10 cm	10.5 cm
11.48 mL/min	S (1SolD6)	-	Irr. H (3SolD4)	-	Irr. H/M (1SolD3)
8.61 mL/min	Irr. S (1SolD7)	Irr. H/M (1SolD4)	M (3SolD2)	Irr. H (3SolD5)	Irr. H (1SolD2)
5.74 mL/min	-	S (2SolD3)	-	-	Irr. H (1SolD1)
2.87 mL/min	-	S (2SolD2)	Irr. H/M (3SolD6)	-	-

When PDFR was 11.48 mL/min and BLFR was 3.45 mL/min and coagulation bath temperature was at room temperature; increasing air gap turns HFMs geometry from straight (S) to irregular helical (Irr. H) form, can be seen in Figure 3.4. At this parameters when air gap at 7 cm; decreasing both polymer dope flow rate and bore liquid flow rate changed HFMs geometry regular straight to irregular straight (Fig 3.4, Fig 3.5) Also how the measurement was done of inner and outer diameter of the membrane shown in Fig 3.4 (a). When air gap at 9.5 cm geometry changed from irregular meander and helical form to regular meander to irregular helical form with increasing PDFR and BLFR (Fig 3.4, Fig 3.5, Fig 3.7). When air gap at 10.5 cm and other parameters were the same geometry changed from irregular helical to irregular helical and meander with increasing PDFR and BLFR (Fig 3.4, Fig 3.5, Fig 3.6).

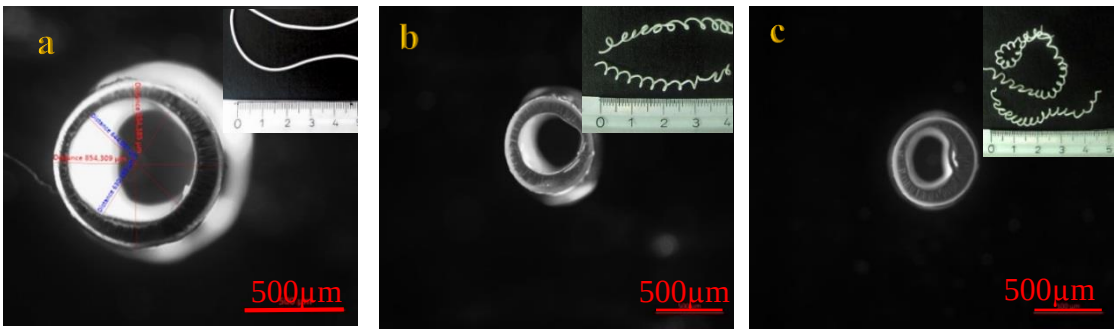

Figure 3.4. Microscope images of membranes 1SolD6 (a), 3SolD4 (b) and 1SolD3 (c).

When PDFR was 8.61 mL/min and BLFR was 2.59 mL/min and coagulation bath temperature was at room temperature; increasing air gap turns HFMs geometry from irregular straight to irregular helical and meander then irregular helical form, can be seen in Figure 3.5. When air gap at 8.5 cm and other parameters were the same geometry changed from straight to irregular helical and meander to regular meander with increasing PDFR and BLFR (Figures 3.4-3.8).

When PDFR was 5.74 mL/min and BLFR was 1.73 mL/min and coagulation bath temperature was at room temperature; increasing air gap turns HFMs geometry from straight to irregular helical form, can be seen in Figure 3.6.

When PDFR was 2.87 mL/min and BLFR was 0.86 mL/min and coagulation bath temperature was at room temperature; increasing air gap turns HFMs geometry from straight to irregular helical and meander form, can be seen in Figure 3.7. Observation of geometry change from straight to helical form by increasing air gap also incoherence with the literature (10, 30).

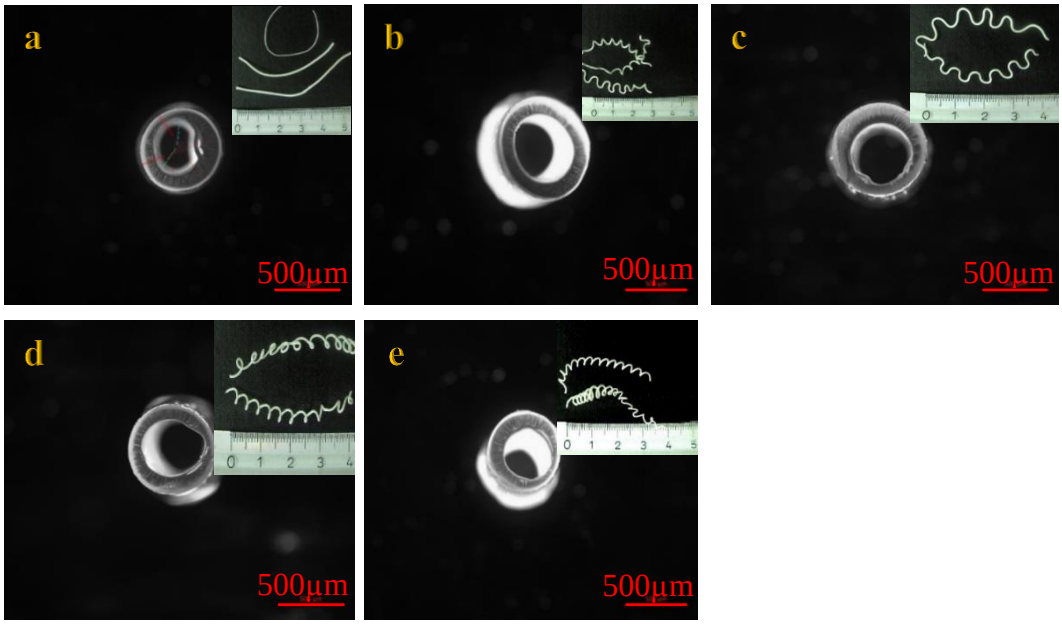

Figure 3.5. Microscope images of membranes 1SolD7 (a), 1SolD4 (b), 3SolD2 (c), 3SolD5 (d) and 1SolD2 (e).

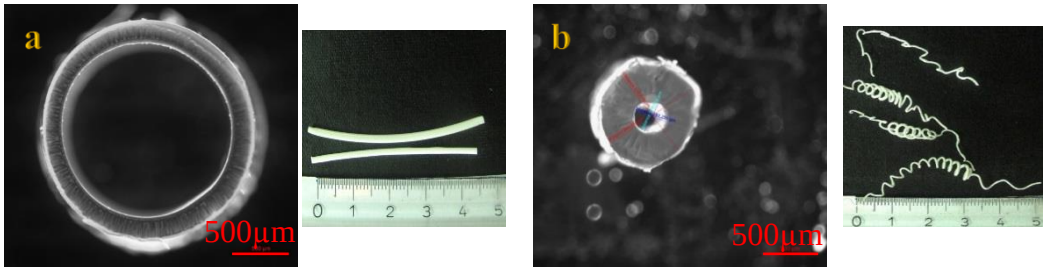

Figure 3.6. Microscope images of the membranes 2SolD3 (a) and 1SolD1 (b).

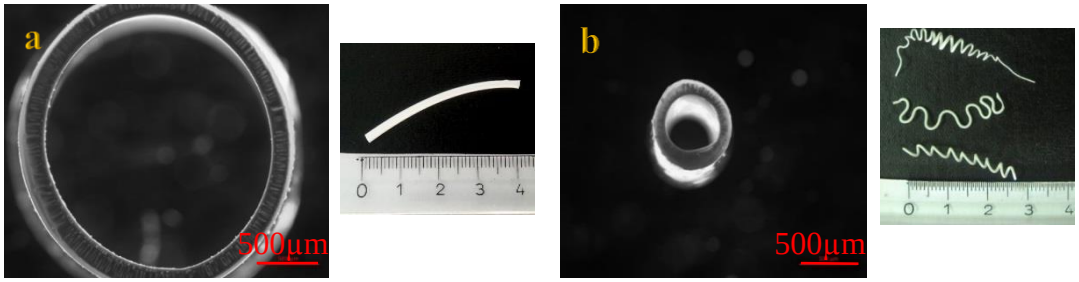

Figure 3.7. Microscope images of the membranes 2SolD2 (a) and 3SolD6 (b).

Table 3.4. Inner and outer diameters of the produced membranes from solution D at coagulation bath temperature at room temperature.

Membrane Code	Inner Diameter (µm)	Outer Diameter (µm)
1SolD1	276	840
1SolD2	392	610
1SolD3	392	610
1SolD4	493	717
1SolD6	637	854
1SolD7	393	610
2SolD2	1934	2293
2SolD3	1482	1888
3SolD2	450	695
3SolD4	421	657
3SolD5	421	657
3SolD6	454	685

At constant PDFR changing the air gap effect on membranes' inner and outer diameter can be seen in Table 3.4. When PDFR was constant increasing air gap result in decrease both inner and outer diameter of the fibers. Another comparison can be done when the air gap was constant and PDFR was changing. Decreasing PDFR at a constant air gap result in decrease both inner and outer diameter of the fibers.

Coagulation Value

Solution D were prepared with different coagulation values 95% and 50%. All fibers produced from these solutions at coagulation bath temperature at 50°C. Fabricated HFMs were observed by optical microscope. As a result, the new membranes became thicker both inside and as an outside diameter but have thinner wall thickness. Only straight geometry was observed for all combinations of all parameters. It was because of the increased amount of non-solvent (water) in the polymer solution that coagulated immediately and hindered the formation of helical or meander geometry. Microscope images of solution D and coagulation value 95% and 50% of the solution can be shown in Figure 3.8 and parameters in Table 3.5.

Table 3.5. Parameters of the produced fibers from different coagulation value solutions of D.

Memb. Code	Coa. Value	PDFR (mL/min)	BLFR (mL/min)	Air Gap (cm)	Geo.	Inner Diameter (µm)	Outer Diameter (µm)
D1	0	5.74	1.73	8	S	815	2033
G1	50			8.5	S	1153	2115
F4	95			8.5	S	1240	2129

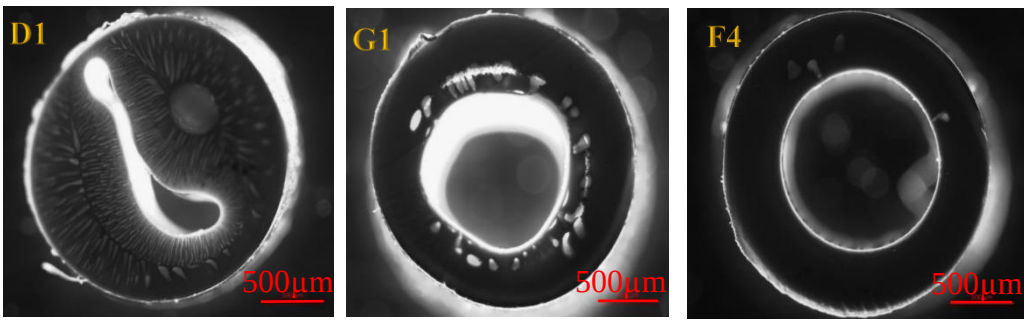

Figure 3.8. Optical microscope images of the membranes fabricated from different coagulation values of D.

Coagulation Bath Temperature

Spinnings were done with solution D at two different coagulation bath temperatures at 25°C and at 50°C. Changing the coagulation bath temperature from 25°C to 50°C, a higher value, was changed the membrane geometry and structure (pore size) since vapor induced phase separation in air gap. When coagulation bath temperature was at 50°C air gap contains more vapor than when coagulation bath temperature was at 24°C. Air in the air gap has a higher relative humidity so that phase inversion starts earlier. For producing HFMs from solution D when all other parameters were fixed changing the bath temperature from 24°C to 50°C was changed helical membranes to straight ones. Straight membranes at 24°C remained the same geometry at 50°C (Table 3.6, Figure 3.9), however they were much thicker at 50°C.

Table 3.6. Effect of coagulation bath temperature to the solution D membranes geometry.

Membrane Code	**PDFR (mL/min)**	**BLFR (mL/min)**	**Air Gap (cm)**	**T (°C)**	**Geo.**	**Inner Diameter (µm)**	**Outer Diameter (µm)**
1SolD3	11.48	3.45	10.5	24	Irr. H/M	392	610
D5			11.5	50	S	835	1904
1SolD2	8.61	2.59	10.5	24	Irr.H	392	610
D3			10.5	50	S	1174	2271

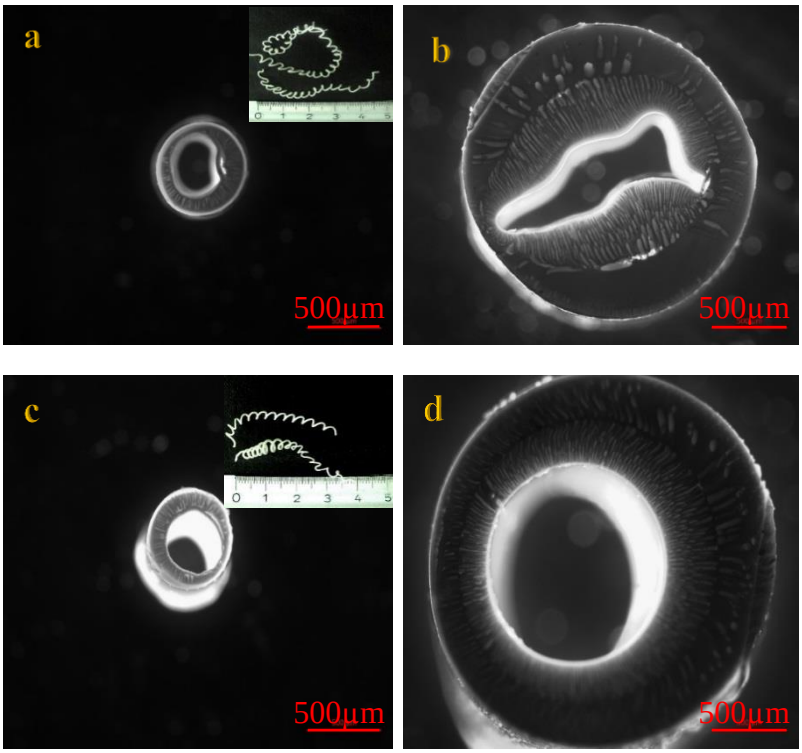

Figure 3.9. Microscope images of the membranes 1SolD3 (a), D5 (b), 1SolD2 (c) and D2 (d).

3.3.1.2 Morphology of the membranes from solution D

Figure 3.10 shows SEM images of produced fibers that have regular straight, helical and meander geometry at the coagulation bath temperature was at room temperature. Their production parameters were given at Table 3.7. SEM analysis shown that all the membranes have macrovoids and nodular structure. They all have selective layer at the shell side of the fiber.

Figure 3.11 shows another SEM analysis which was done with helical membranes, produced in coagulation bath temperature was at room temperature and 50°C. When coagulation bath temperature was at 50°C produced membrane have more macrovoids than membranes produced when coagulation bath temperature was at room temperature. On the other hand they both have selective skin layer at shell side of the membranes.

Table 3.7. Parameters of regular produced fibers from solution D at coagulation bath temperature was at room temperature.

Membrane Code	PDFR (mL/min)	BLFR (mL/min)	Air Gap (cm)	Geometry
1SolD6	11.48	3.45	7	S
3SolD2	8.61	2.59	9.5	M
1SolD2	8.61	2.59	10.5	H

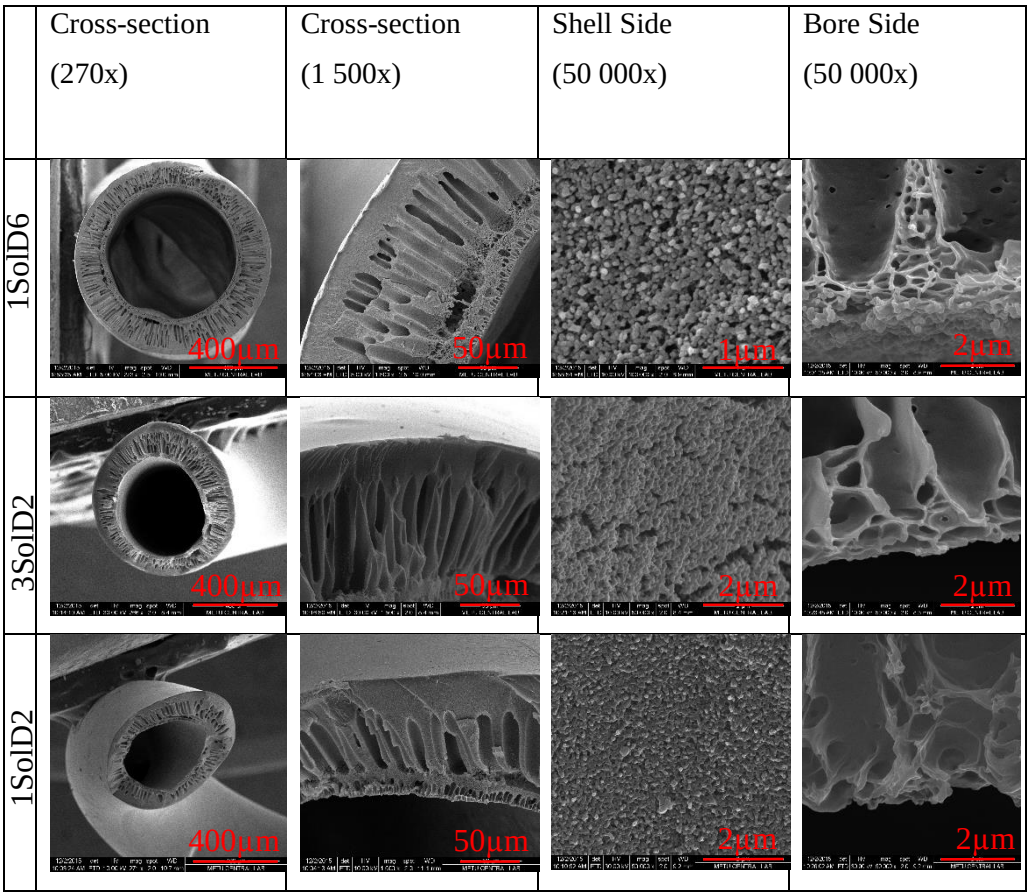

Figure 3.10. SEM images of the membranes from solution D at coagulation bath temperature was at room temperature.

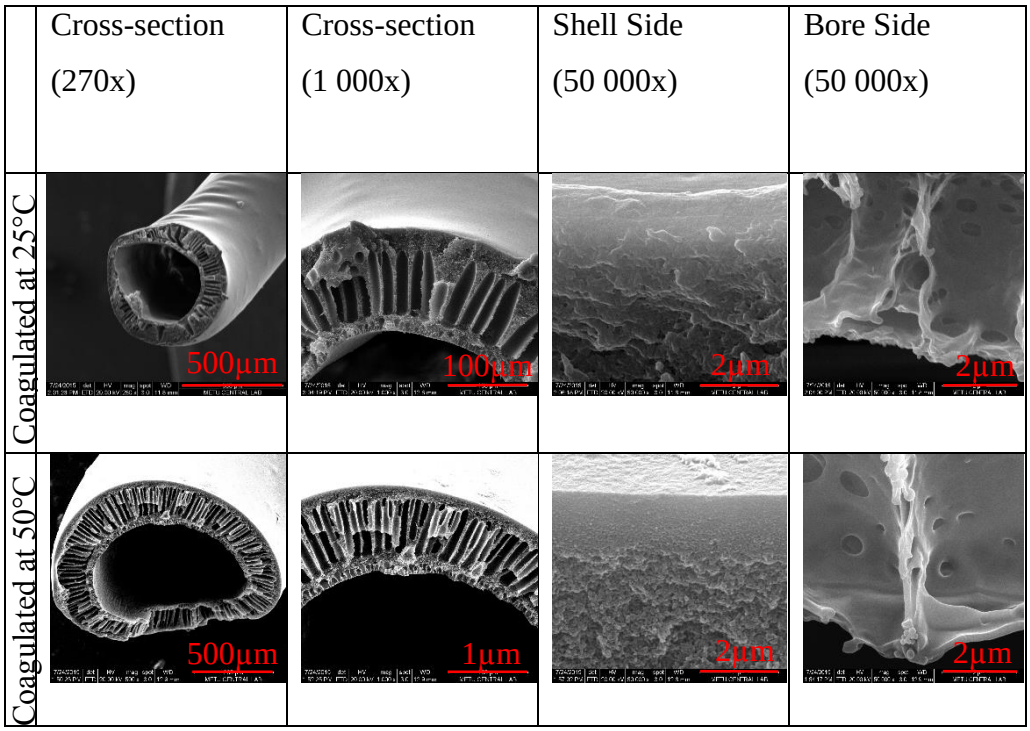

Figure 3.11. SEM images of the membranes from solution D at coagulation bath temperature was at room temperature and 50°C.

3.3.2. Solution M

DMSO were reached cloud point combination with less water content compared to NMP solutions as seen in Figures 3.1 and 3.2. This information tells us before the membrane coagulate and geometry was straight, VIPS may be seen. So we investigate solutions with NMP.

<u>Relation Between Air Gap and Polymer Dope Flow Rate and Bore Liquid Flow Rates</u>

Table 3.8 shows how geometry of the produced fibers change with increasing air gap and decreasing PDFR-BLFR at coagulation bath temperature at 25±2°C with solution M. Also Table 3.10 shows the inner and outer diameters of the membranes, can be followed by using membrane codes in Table 3.8.

Table 3.8. Relation between air gap and PDFR-BLFR for solution M membranes produced at 25±2°C.

Air gap → / PDFR ↓	4 cm	6 cm	8 cm
17.23 mL/min	S (H74)	-	-
11.48 mL/min	S (H73)	S (H72)	H (H71)
8.61 mL/min	S (H77)	H (H76)	H (H75)
2.87 mL/min	Disc. (H78)	-	-

When PDFR was 17.23 mL/min and BLFR was 5.18 mL/min and coagulation bath temperature was at room temperature, air gap was at 4 cm (Fig 3.12); decreasing PDFR and BLFR by using their pumps did not change the membrane regular straight geometry but at the lowest flow rates membrane could not produce because of the discontinuous flow of the polymer dope.

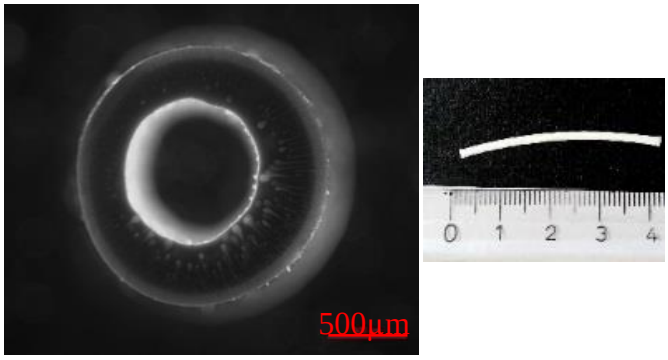

Figure 3.12. Microscope image of the membrane H74.

When PDFR was 11.48 mL/min and BLFR was 3.45 mL/min and coagulation bath temperature was at room temperature, increasing air gap turns HFMs geometry from regular straight to regular helical form, can be seen in Figure 3.13. When air gap at 6 cm increasing PDFR and BLFR change geometry from regular helical structure to regular straight form. When air gap at 8 cm increasing PDFR and BLFR did not change the HFMs regular straight geometry within the tested range.

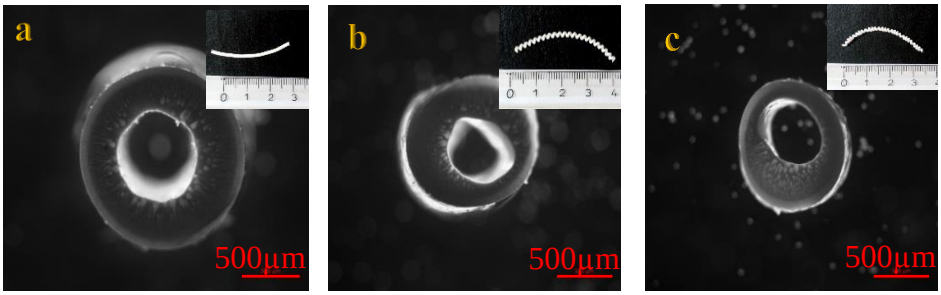

Figure 3.13. Microscope images of the membranes H73 (a), H72 (b) and H71 (c).

When PDFR was 8.61 mL/min and BLFR was 2.59 mL/min and coagulation bath temperature was at room temperature, increasing air gap turns HFMs geometry from regular straight to regular helical form, can be seen in Figure 3.14.

Table 3.9 shows how geometry of the produced fibers change with increasing air gap and decreasing PDFR-BLFR at coagulation bath temperature at 50±2°C. Also Table 3.10 shows the inner and outer diameters of the membranes, can be followed by using membrane codes in Table 3.9.

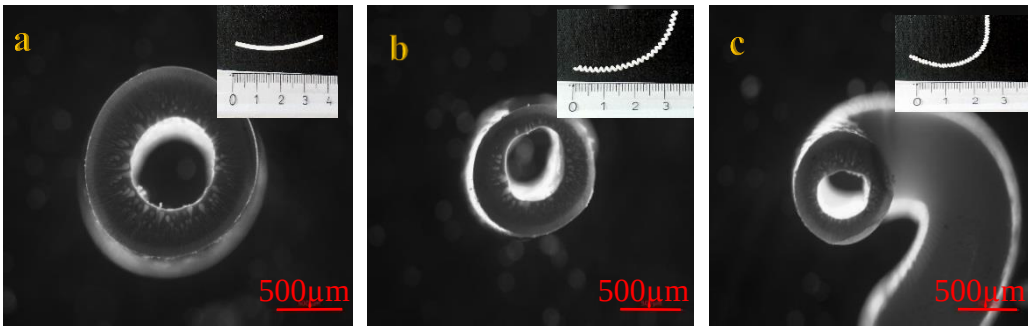

Figure 3.14. Microscope images of the membranes H77 (a), H76 (b) and H75 (c).

By looking at Table 3.9; when PDFR was 17.23 mL/min and BLFR was 5.17 mL/min and coagulation bath temperature was at 50°C, increasing air gap turns HFMs geometry from straight to helical form then at the highest air gap geometry became irregular again, HFMs can be seen in Figure 3.16. When air gap was at 6 cm decreasing both PDFR and BLFR changed the geometry of the HFMs firstly regular straight to irregular then lowest flow rates geometry was turn regular straight form again. At 8 cm; decreasing flow rates change the geometry from irregular helical form then irregular helical and straight form at the lowest flow rates geometry became irregular helical again. At 8.5 cm decreasing the flow rates change geometry from regular

straight then irregular helical form. From another point, as the air gap increased the geometry of the membranes turned from straight to helical. Also irregular helical fibers and partly meandering were observed. But there is no regular meander shape membrane was produced. It may be because of the low viscosity of the solution M.

When PDFR was 14.35 mL/min and BLFR was 4.31 mL/min and coagulation bath temperature was at 50°C, air gap was at 7 cm (Fig 3.15); decreasing PDFR and BLFR change the HFMs geometry from regular straight to irregular straight and helical form.

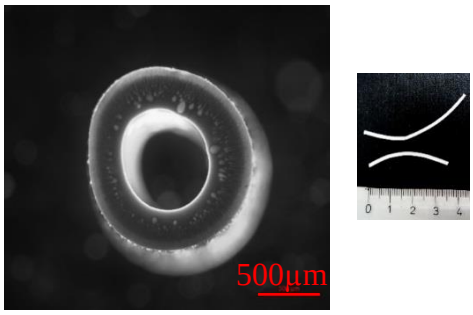

Figure 3.15. Microscope image of the membrane H96.

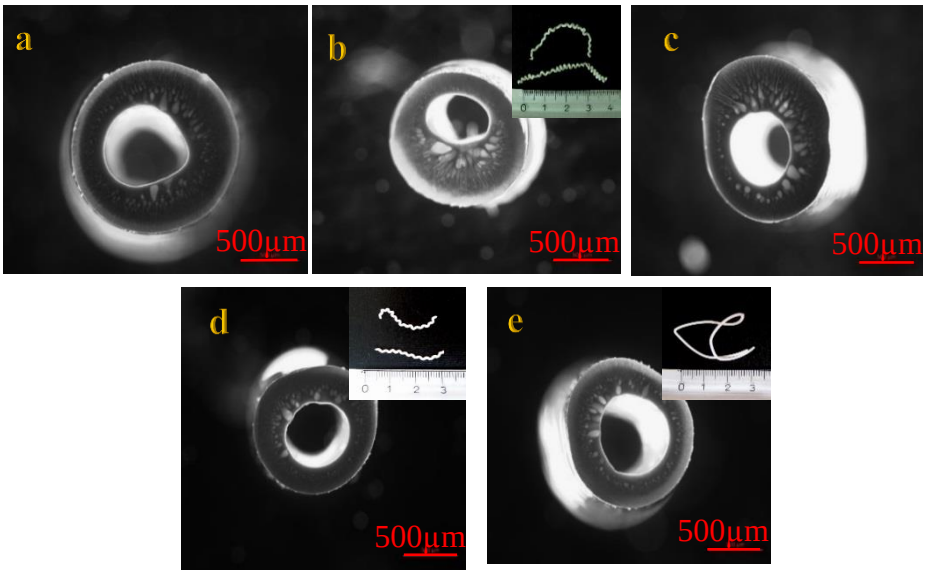

Figure 3.16. Microscope images of the membranes H94 (a), H6 (b), H19 (c), H32 (d) and H115 (e).

When coagulation bath temperature was at 50°C, at different constant PDFRs increasing air gap changed geometry from regular straight form to irregular helical or

straight forms. Only at the highest PDFR at 17.23 ml/min increasing air gap result in the change regular straight geometry to regular helical form at 12 cm. When fibers were produced at PDFR was 8.61 mL/min and BLFR was 2.59 mL/min; with the increasing air gap geometry turns from straight to irregular straight and helical form then there was no significant regular geometry was observed. At 4 cm; decreasing PDFR and BLFR were not change the HFMs regular straight geometry (Figure 3.18). As we can see at the lowest air gaps geometry of the fibers stable and the highest air gaps geometry of the fibers unstable it is related to the solution viscosity which is nearly equal to the water viscosity.

When PDFR was 5.74 mL/min and BLFR was 1.72 mL/min and coagulation bath temperature was at 50°C, increasing air gap did not change HFMs straight geometry, can be seen in Figure 3.19.

Table 3.9. Relation between air gap and PDFR-BLFR for solution M membranes produced at 50±2°C.

PDFR → / Air gap ↓	17.23 mL/min	14.35 mL/min	11.48 mL/min	8.61 mL/min	5.74 mL/min
2 cm	-	-	S (H105)	-	-
2.5 cm	-	-	S (H83)	-	Disc. (H7)
4 cm	-	-	-	S (H91)	S (H92)
4.2 cm	-	-	S (H38)	-	-
5.5 cm	-	-	-	Irr.S/H/M (H12)	-
6 cm	S (H94)	-	Irr. S (H85)	S (H90)	S (H93)
6.7 cm	-	-	S (H103)	-	S (H102)
7 cm	-	S (H96)	Irr. S/H (H95)	Irr. H/S (H98)	-
7.5 cm	-	-	Irr. H (H5)	Irr. H (H23)	-
8 cm	Irr. H (H6)	-	Irr. H/S (H86)	Irr. H (H22)	-
8.5 cm	S (H19)	-	-	Irr. H (H17)	-
9 cm	-	-	S (H100)	Irr. H/S (H99)	-
11 cm	-	-	Irr. H/S (H87)	Irr. H (H88)	-
12 cm	H (H32)	-	-	-	-
16 cm	Irr. S (H115)	-	-	-	-

Table 3.10. Inner and outer diameters of the produced membranes from solution M.

Membrane Code	Inner Diameter (µm)	Outer Diameter (µm)	Membrane Code	Inner Diameter (µm)	Outer Diameter (µm)
H5	462	1038	H85	702	1309
H6	465	1091	H86	704	1195
H7	-	-	H87	683	1260
H12	951	1343	H88	428	853
H17	673	1036	H90	566	1184
H19	573	1260	H91	417	979
H22	343	637	H92	518	1316
H23	480	876	H93	436	964
H32	553	1082	H94	663	1431
H38	646	1337	H95	686	1280
H71	514	996	H96	713	1341
H72	561	1088	H98	604	994
H73	689	1402	H99	628	1247
H74	870	1617	H100	683	1260
H75	383	778	H102	775	1160
H76	519	948	H103	543	1240
H77	635	1307	H105	646	1350
H83	840	1355	H115	654	1182

Similar comparison between solution D and solution M membranes can be done about inner and outer diameter by looking at Table 3.11. When PDFR was constant increasing air gap result in decrease both inner and outer diameter of the fibers like solution D membranes. Another comparison can be done when the air gap was constant and PDFR was changing. Decreasing PDFR at a constant air gap result in decrease both inner and outer diameter of the fibers.

Another comparison for the diameters of solution M membranes can be done by looking at coagulation bath temperature. At the same air gap and PDFR inner and outer diameter of the membranes which coagulation bath temperature was room temperature was smaller than which coagulation bath temperature was at 50°C.

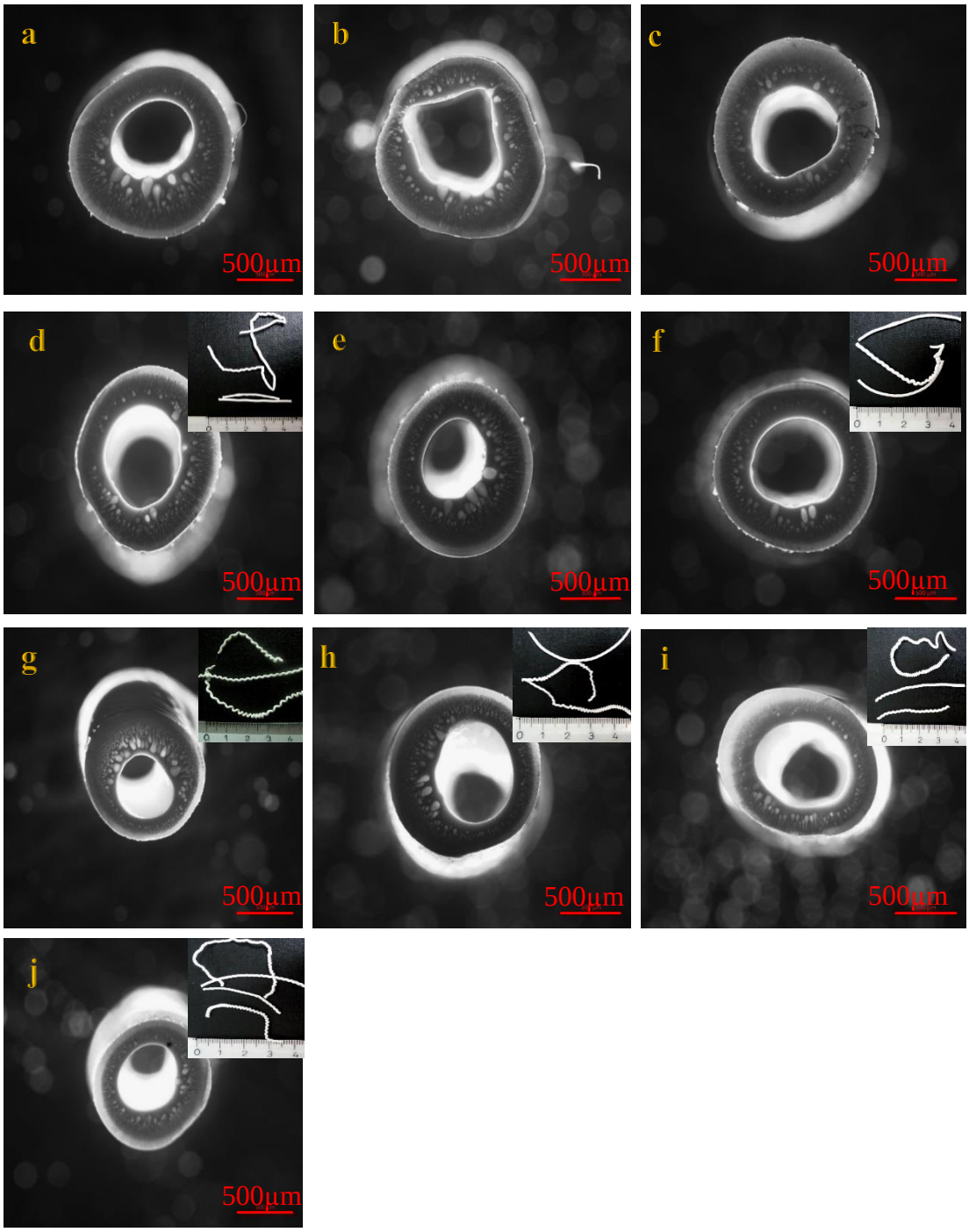

Figure 3.17. Microscope images of membranes H105 (a), H83 (b), H38 (c) H85 (d), H103 (e), H95 (f), H5 (g), H100 (h), H86 (i) and H87 (j).

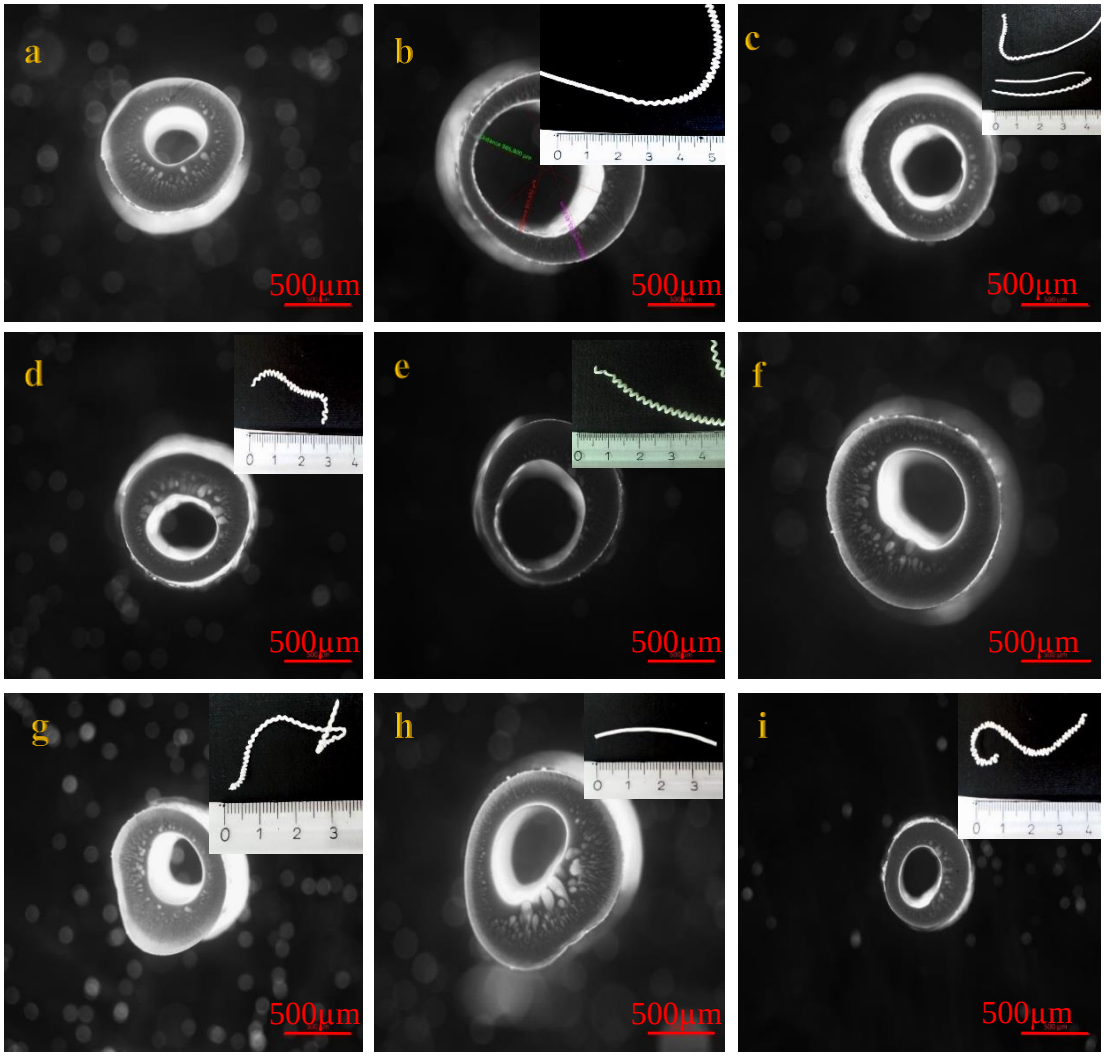

Figure 3.18. Microscope images of the membranes H91 (a), H12 (b), H98 (c), H23 (d), H17 (e), H99 (f), H88 (g), H90 (h) and H22 (i).

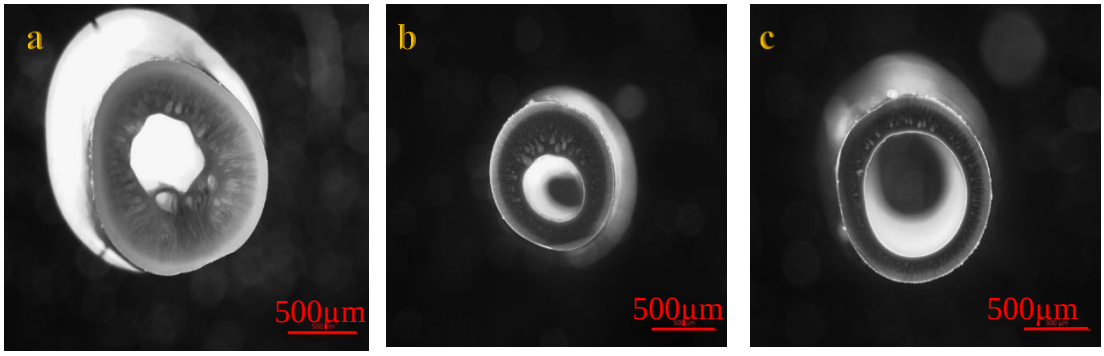

Figure 3.19. Microscope images of the membranes H92 (a), H93 (b) and H102 (c).

Polymer Dope Flow Rate and Bore Liquid Flow Rate Ratio

When fabricating HFMs from solution M except from the general PDFR/BLFR ratio 3:1; different PDFR-BLFR ratios were examined.

When bore liquid combination was 70 wt. %NMP and 30 wt. %Upwater and polymer dope flow rate was at 18.18 mL/min changing PDFR-BLFR ratio by changing BLFR result different geometries at different air gaps. At air gap 6 cm increasing PDFR-BLFR ratio did not change the straight geometry (Table 3.11, Fig 3.20).

Table 3.11. Different polymer dope and bore liquid flow rate ratios at 6 cm.

Memb. Code	PDFR (mL/min)	BLFR (mL/min)	Geo.	PDFR/BLFR ratio	Inner Diameter (µm)	Outer Diameter (µm)
H150	18.18	0.86	S	19:1	110	1400
H151	18.18	1.73	S	9.5:1	460	1445
H152	18.18	3.45	S	4.75:1	681	1479

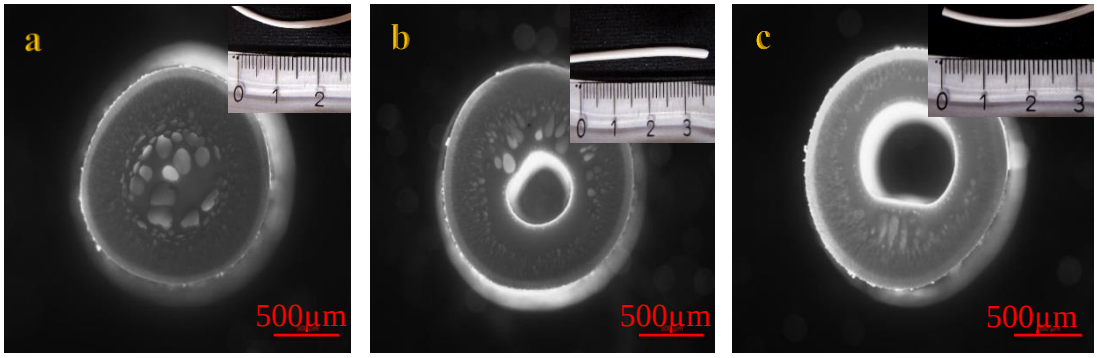

Figure 3.20. Microscope images of the membranes H150 (a), H151 (b) and H152 (c).

When air gap was 7 cm increasing PDFR-BLFR ratio changed membrane geometry from regular straight to irregular straight form (Table 3.12, Fig 3.21). When bore liquid combination was 70 wt. %NMP and 30 wt. %Upwater and air gap at 8 cm increasing PDFR-BLFR ratio changed the geometry from irregular helical meander form to regular helical form (Table 3.13, Fig 3.22). When bore liquid combination was 70 wt. %NMP and 30 wt. %Upwater and air gap at 10 cm increasing PDFR-BLFR ratio did not change the helical fiber geometry (Table 3.14, Fig 3.23).

Table 3.12. Different polymer dope and bore liquid flow rate ratios at 7 cm.

Memb. Code	PDFR (mL/min)	BLFR (mL/min)	Geo.	PDFR/BLFR ratio	Inner Diameter (µm)	Outer Diameter (µm)
H135	18.18	0.86	S	19:1	265	1303
H142	18.18	1.73	S	9.5:1	441	1300

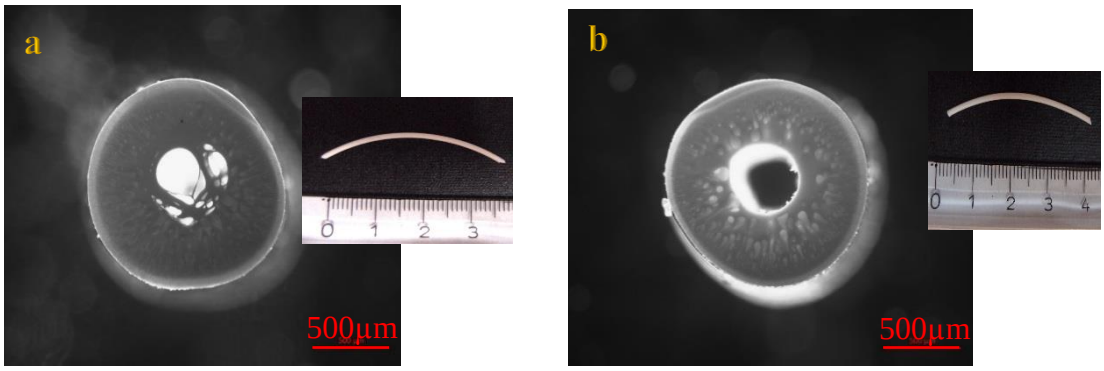

Figure 3.21. Microscope images of the membranes H135 (a) and H142 (b).

Table 3.13. Different polymer dope and bore liquid flow rate ratios at 8 cm.

Memb. Code	PDFR (mL/min)	BLFR (mL/min)	Geo.	PDFR/BLFR ratio	Inner Diameter (µm)	Outer Diameter (µm)
H143	18.18	0.86	Irr. H	19:1	281	1215
H145	18.18	3.45	Irr. M/H	4.75:1	580	1252
H146	18.18	5.17	Irr. H	3.17:1	618	1285

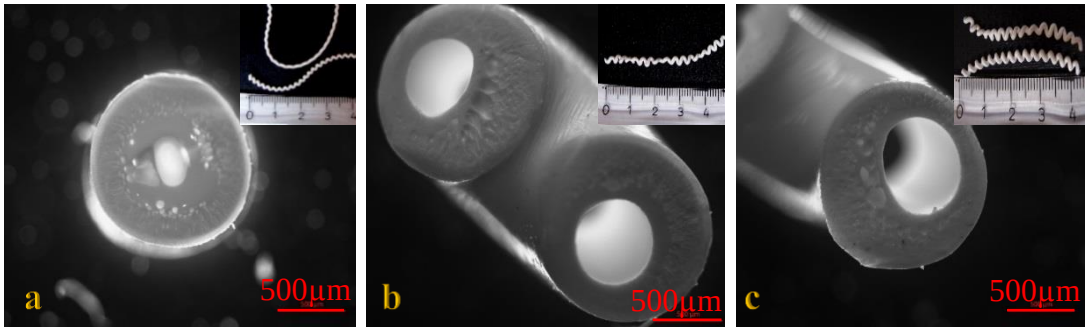

Figure 3.22. Microscope images of the membranes H143 (a), H145 (b) and H146 (c).

Table 3.14. Different polymer dope and bore liquid flow rate ratios at 10 cm.

Memb. Code	PDFR (mL/min)	BLFR (mL/min)	Geo.	PDFR/BLFR ratio	D_i (µm)	D_o (µm)	D_{helix} (mm)	Pitch (mm)
H157	18.18	0.86	H	19:1	270	1155	1.5	2.1
H158	18.18	1.73	Irr. S	9.5:1	318	1434	-	-
H159	18.18	3.45	H	4.75:1	427	1180	1.9	2.5
H161	18.18	5.17	H	3.17:1	585	1218	2.0	2.6

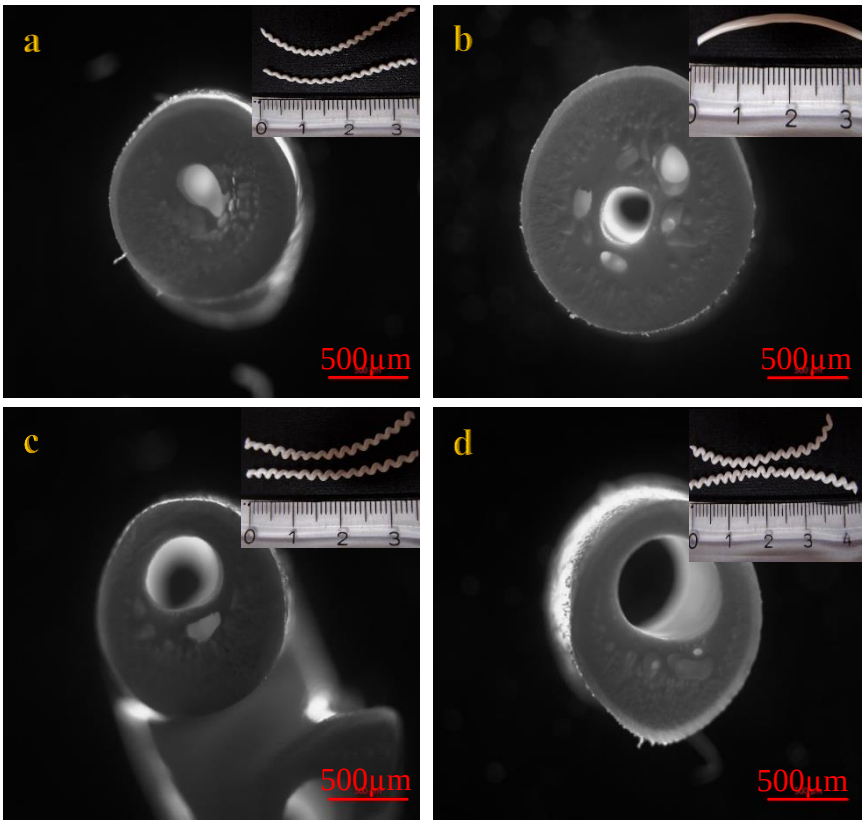

Figure 3.23. Microscope images of the membranes H157 (a), H158 (b), H159 (c) and H161 (d).

When air gap was 14 cm increasing PDFR-BLFR ratio changed the geometry from irregular straight to mostly straight form (Table 3.15, Fig 3.24). When air gap was 16 cm increasing PDFR-BLFR ratio changed the irregular straight geometry to straight geometry (Table 3.16, Fig 3.25). But produced straight membrane was fiber with no hollow because of the BLFR was very low.

Table 3.15. Different polymer dope and bore liquid flow rate ratios at 14 cm.

Memb. Code	PDFR (mL/min)	BLFR (mL/min)	Geo.	PDFR/ BLFR ratio	Inner Diameter (µm)	Outer Diameter (µm)
H119	18.18	0.86	Mostly S	19:1	494	1065
H120	18.18	1.73	Mostly S	9.5:1	304	1096
H113	18.18	5.18	Irr. S	3.17:1	607	1213

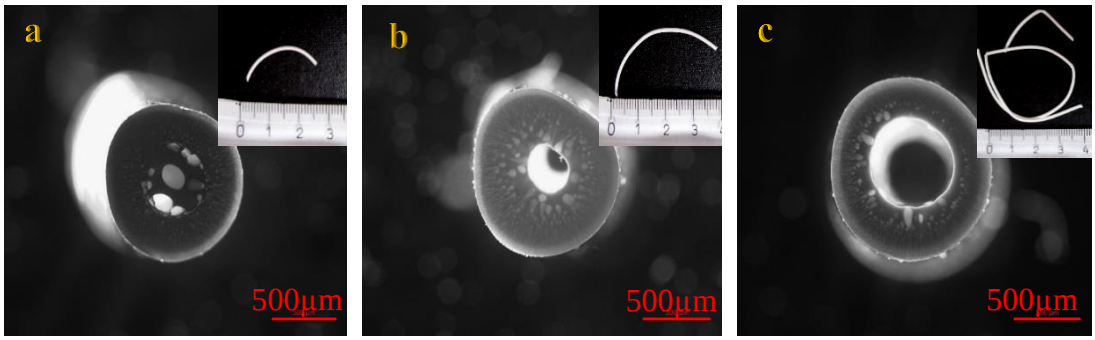

Figure 3.24. Microscope images of the membranes H119 (a), H120 (b) and H113 (c).

Table 3.16. Different polymer dope and bore liquid flow rate ratios at 16 cm.

Memb. Codes	PDFR (mL/min)	BLFR (mL/min)	Geo.	PDFR/BLFR ratio	Inner Diameter (µm)	Outer Diameter (µm)
H118	18.18	0.86	S	19:1	-	950
H117	18.18	1.73	S	9.5:1	343	1030
H116	18.18	3.45	S	4.75:1	525	1117
H114	18.18	5.17	Irr. S	3.17:1	538	1119

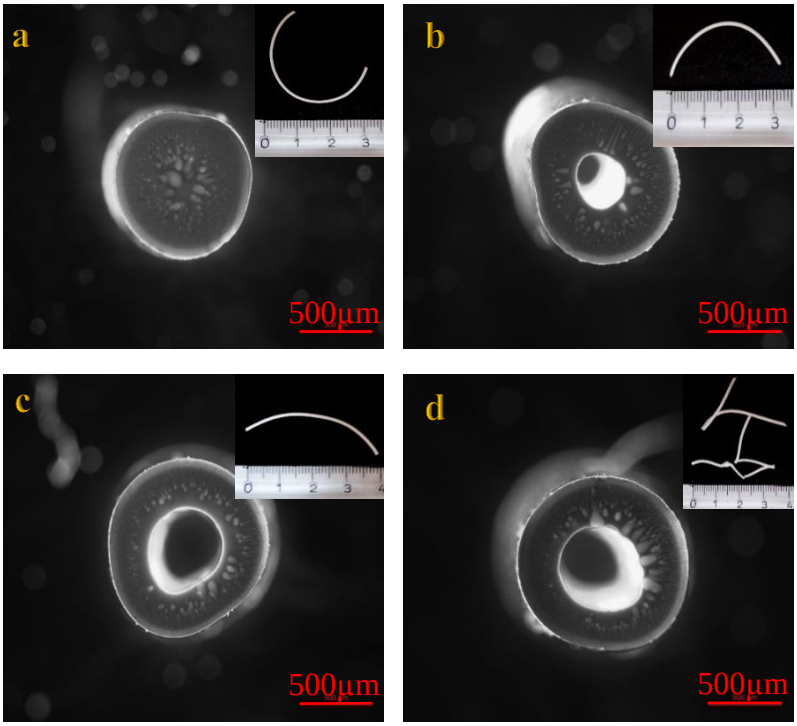

Figure 3.25. Microscope images of the membranes H118 (a), H117 (b), H116 (c) and H114 (d).

When polymer dope flow rate was 8.61 mL/min changing PDFR-BLFR ratio by changing BLFR result different geometries at different air gaps. At air gap 4 cm increasing PDFR-BLFR ratio did not change the straight geometry (Table 3.17, Fig 3.26).

Table 3.17. Different polymer dope and bore liquid flow rate ratios at 4 cm.

Memb. Code	PDFR (mL/min)	BLFR (mL/min)	Geo.	PDFR/BLFR ratio	Inner Diameter (µm)	Outer Diameter (µm)
H125	8.61	0.86	S	10:1	161	1046
H124	8.61	1.73	S	5:1	385	1119
H123	8.61	2.59	S	3.3:1	607	1170

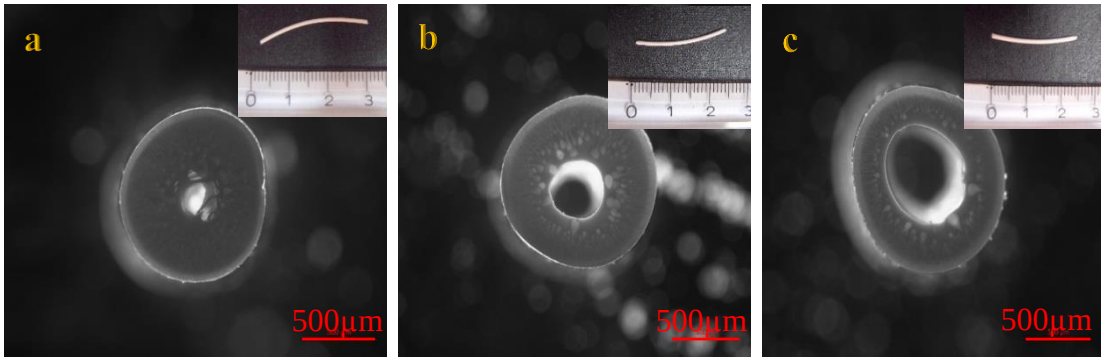

Figure 3.26. Microscope images of the membranes H125 (a), H124 (b) and H123 (c).

When air gap was 6 cm increasing PDFR-BLFR ratio changed the geometry from regular straight to irregular meander or helical form (Table 3.18, Fig 3.27). When air gap was 7 cm increasing PDFR-BLFR ratio changed the regular straight geometry to irregular meander or helical geometry (Table 3.19, Fig 3.28). When air gap was 8 cm increasing PDFR-BLFR ratio did not change the irregular helical and straight geometry (Table 3.20, Fig 3.29).

Table 3.18. Different polymer dope and bore liquid flow rate ratios at 6 cm.

Memb. Code	PDFR (mL/min)	BLFR (mL/min)	Geo.	PDFR/ BLFR ratio	Inner Diameter (µm)	Outer Diameter (µm)
H128	8.61	0.86	Irr. M/H	10:1	193	1027
H127	8.61	1.73	Irr. H/S	5:1	375	1099
H126	8.61	2.59	S	3.3:1	589	1172

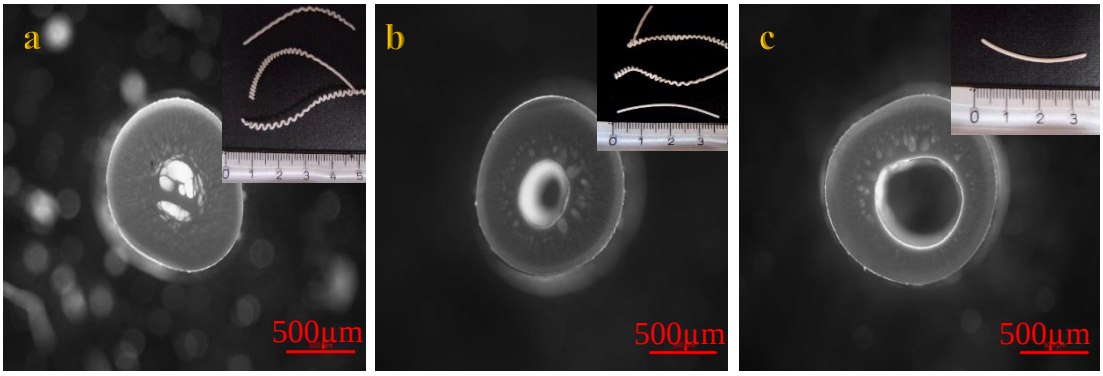

Figure 3.27. Microscope images of the membranes H128 (a), H127 (b) and H126 (c).

Table 3.19. Different polymer dope and bore liquid flow rate ratios at 7 cm.

Memb. Code	PDFR (mL/min)	BLFR (mL/min)	Geo.	PDFR/ BLFR ratio	Inner Diameter (µm)	Outer Diameter (µm)
H129	8.61	0.86	Irr. M/H	10:1	88	867
H130	8.61	1.73	Irr. H/S	5:1	417	995
H98	8.61	2.59	Irr. H/S	3.3:1	604	994
H97	8.61	4.31	S	2:1	801	1260

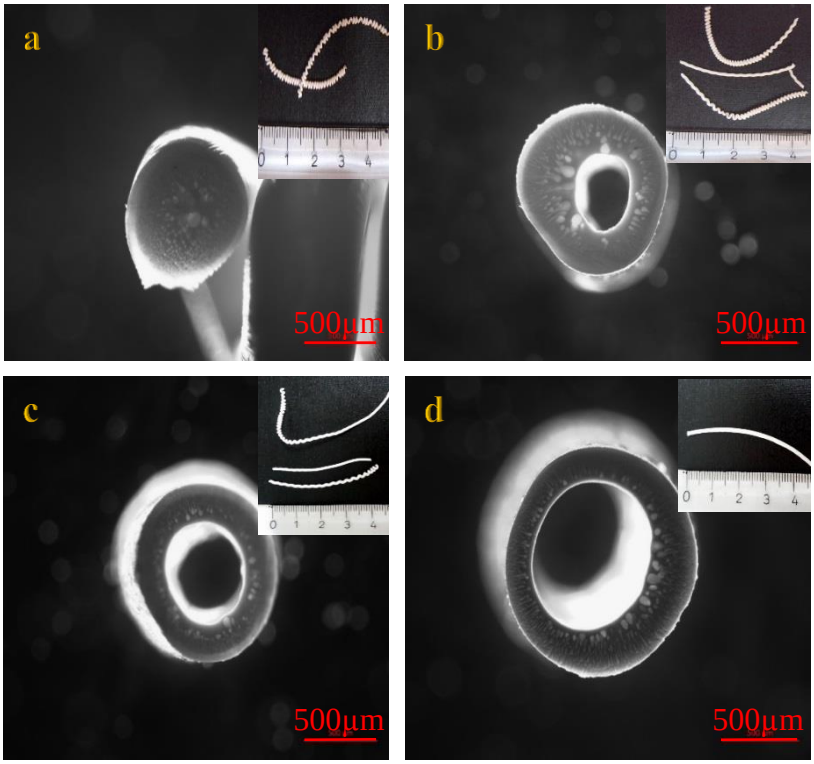

Figure 3.28. Microscope images of the membranes H129 (a), H130 (b), H98 (c) and H97 (d).

Table 3.20. Different polymer dope and bore liquid flow rate ratios at 8 cm.

Memb. Code	PDFR (mL/min)	BLFR (mL/min)	Geo.	PDFR/ BLFR ratio	Inner Diameter (µm)	Outer Diameter (µm)
H133	8.61	0.86	Irr. H	10:1	58	707
H132	8.61	1.73	Irr. H/S	5:1	437	1031
H131	8.61	2.59	Irr. H/S	3.3:1	514	1081

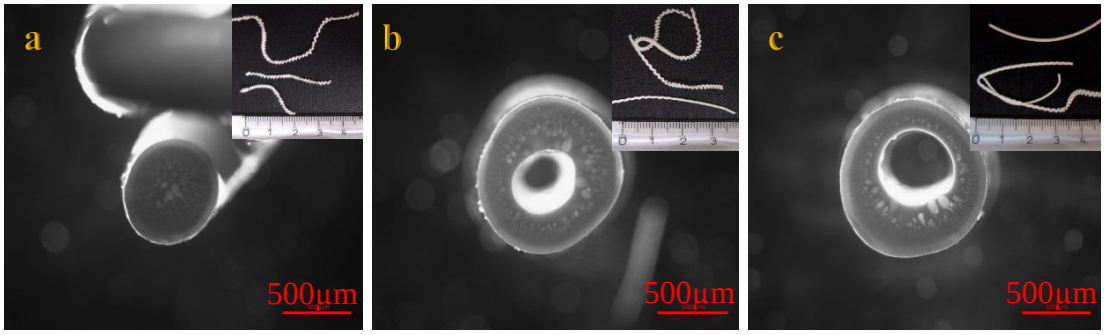

Figure 3.29. Microscope images of the membranes H133 (a), H132 (b) and H131 (c).

Non-solvent and solvent ratio of Bore Liquid

Spinning was done for solution M with two different bore liquid combination, two different non-solvent (water) and solvent (NMP) ratio when coagulation bath temperature was always at 50°C. First one was solvent and non-solvent composition at 80% NMP and 20% up water (Non-solvent and solvent ratio was 1:4), second one was 70% NMP and 30% up water (Non-solvent and solvent ratio was 3:7).

When PDFR and BLFR were 17.23 mL/min and 5.18 mL/min, respectively and air gap at 8 cm changing the non-solvent and solvent ratio did not change the fibers irregular helical geometry but that can be observed inner and outer diameters of the fibers quite different (Table 3.21, Fig 3.30).

Table 3.21. Parameters when PDFR and BLFR 17.23 mL/min and 5.18 mL/min, respectively and the air gap at 8 cm.

Memb. Code	wt. % Water	wt. % NMP	Geo.	Inner Diameter (µm)	Outer Diameter (µm)
H148	30	70	Irr. H	721	1409
H6	20	80	Irr. H	465	1091

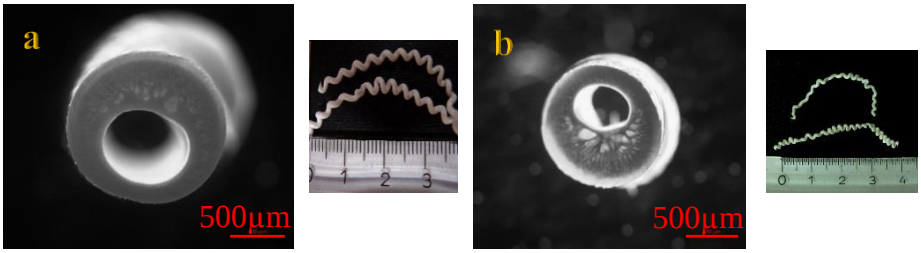

Figure 3.30. Microscope images of the membranes H148 (a) and H6 (b).

When PDFR and BLFR were 11.48 mL/min and 3.45 mL/min, respectively and air gap at 8 cm changing the non-solvent and solvent ratio resulted discontinuous flow of the fiber at the highest non-solvent amount (Table 3.22).

Table 3.22. Parameters when PDFR and BLFR 11.48 mL/min and 3.45 mL/min, respectively and the air gap at 8 cm.

Memb. Code	wt. % Water	wt. % NMP	Geometry	Inner Diameter (µm)	Outer Diameter (µm)
H155	30	70	Disc.	-	-
H86	20	80	Irr. H/S	704	1195

When PDFR and BLFR were 8.61 mL/min and 2.59 mL/min, respectively and air gap at 8 cm changing the non-solvent and solvent ratio resulted discontinuous flow of the fiber at the highest non-solvent amount like previous parameters (Table 3.23). Water is a strong coagulant because of that membrane produced and broken off before entering the coagulation bath at both PDFR 11.48 mL/min and 8.61 mL/min. When PDFR was higher, 17.23 mL/min, membrane could reach the coagulation bath before the break off.

Table 3.23. Parameters when PDFR and BLFR 8.61 mL/min and 2.59 mL/min, respectively and the air gap at 8 cm.

Memb. Code	wt. % Water	wt. % NMP	Geo.	Inner Diameter (µm)	Outer Diameter (µm)
H149	30	70	Disc.	-	-
H131	20	80	Irr. H/S	514	1081

Coagulation Bath Temperature

Spinnings were done with solution M at two different coagulation bath temperatures at 27°C and at 50°C. Changing the coagulation bath temperature from 27°C to 50°C changed the membrane geometry and structure (pore size) since vapor induced phase separation occured in air gap.

When PDFR and BLFR were 17.23 mL/min and 5.18 mL/min, respectively at air gap 8 cm changing the coagulation bath temperature from 27°C to 50°C resulted in geometry change from regular straight to irregular helical form (Table 3.24). Their microscope images can be found in Figures 3.12 and 3.30.

Table 3.24. Effect of coagulation bath temperature to membrane geometry from solution M when PDFR and BLFR were 17.23 mL/min and 5.18 mL/min.

Memb. Code	**PDFR (mL/min)**	**BLFR (mL/min)**	**Air Gap (cm)**	**T (^{0}C)**	**Geo.**	**Inner Diameter (µm)**	**Outer Diameter (µm)**
H74	17.23	5.18	8	27	S	870	1617
H6				50	Irr. H	465	1091

When PDFR and BLFR were 11.48 mL/min and 3.45 mL/min, respectively at air gap 6 cm changing the coagulation bath temperature from 27°C to 50°C resulted in geometry change from regular helical to irregular straight form. When the other parameters were fixed and air gap at 8cm, changing the coagulation bath temperature from 27°C to 50°C was result in geometry change from regular helical to irregular helical and straight form (Table 3.25). Their microscope images can be found in Figures 3.13 and 3.17.

When PDFR and BLFR were 8.61 mL/min and 2.59 mL/min, respectively at air gap 4 cm changing the coagulation bath temperature from 27°C to 50°C did not change regular straight geometry of the fibers. When the other parameters were fixed and air gap was at 6 cm, changing the coagulation bath temperature from 27°C to 50°C resulted in geometry change from regular helical to regular straight form (Table 3.26).

When air gap was at 8 cm changing the coagulation bath temperature from 27°C to 50°C resulted in geometry change from regular helical to irregular helical form. Their microscope images can be found in Figures 3.14 and 3.18.

Table 3.25. Effect of coagulation bath temperature to membrane geometry from solution M when PDFR and BLFR were 11.48 mL/min and 3.45 mL/min.

Membr. Code	PDFR (mL/min)	BLFR (mL/min)	Air Gap (cm)	T (^{0}C)	Geo.	D_i (µm)	D_o (µm)	D_{helix} (mm)	Pitch (mm)
H72	11.48	3.45	6	27	H	561	1088	2.0	2.0
H85				50	Irr.S	702	1309	-	-
H71			8	27	H	514	996	2.0	1.4
H86				50	Irr.S/H	704	1195	-	-

Table 3.26. Effect of coagulation bath temperature to membrane geometry from solution M when PDFR and BLFR were 8.61 mL/min and 2.59 mL/min.

Membr. Code	PDFR (mL/min)	BLFR (mL/min)	Air Gap (cm)	T (^{0}C)	Geo.	D_i (µm)	D_o (µm)	D_{helix} (mm)	Pitch (mm)
H77	8.61	2.59	4	27	S	635	1307	-	-
H91				50	S	417	979	-	-
H76			6	27	H	519	948	2.0	1.9
H90				50	S	566	1184	-	-
H75			8	27	H	383	778	1.6	1.2
H89				50	Irr.H	561	1048	-	-

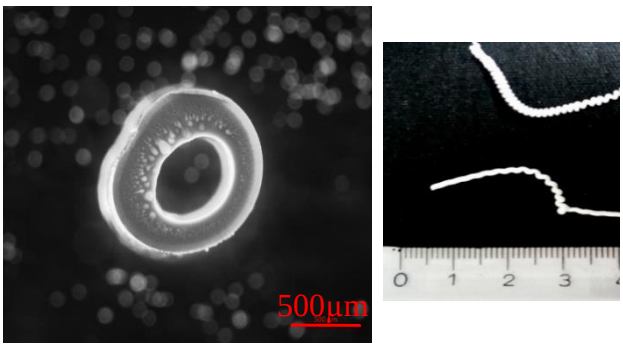

Figure 3.31. Microscope image of the membrane H89.

3.2.2.1. Morphology of the membranes from solution M

Figure 3.32 shows SEM images of produced fibers that have regular straight and helical geometry at the coagulation bath temperature was at 27°C and 50°C. Their production parameters were given at Table 3.27. SEM analysis showed that both of the membranes have macrovoids. For H76 macrovoids more close to the bore side of the membrane than H126. They both have selective layer at the shell side of the fiber.

Table 3.27. Parameters of regular produced fibers from solution M at different coagulation bath temperatures.

Membrane Code	PDFR (mL/min)	BLFR (mL/min)	Air Gap (cm)	T (^{0}C)	Geometry
H76	8.61	2.59	6	27	H
H126				50	S

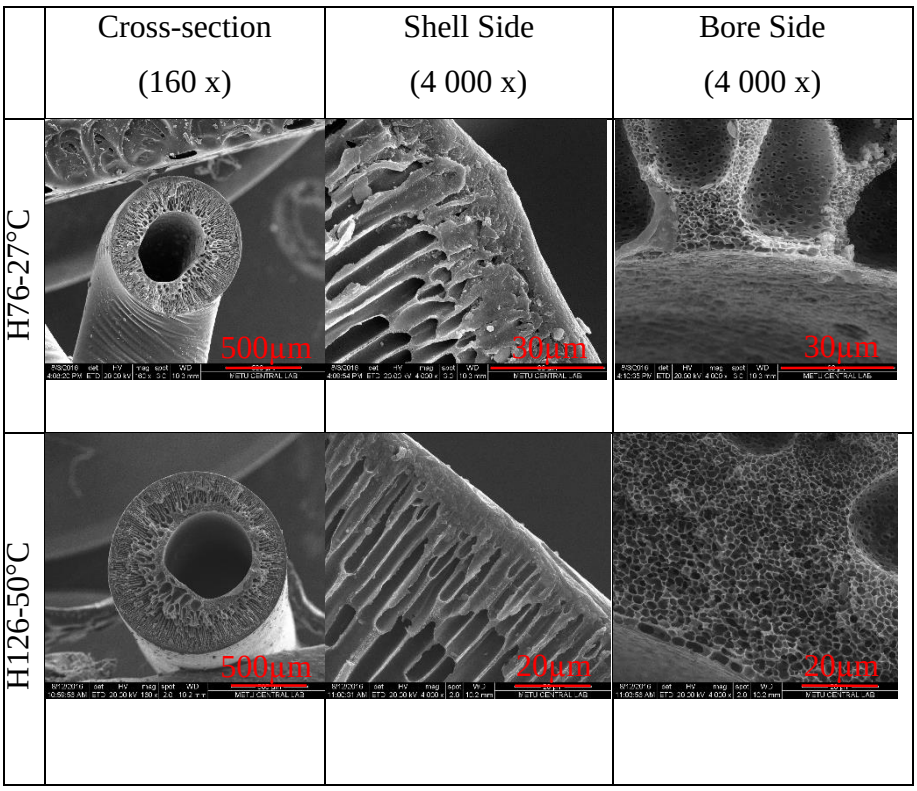

Figure 3.32. SEM images of the membranes from solution M produced from different coagulation bath temperatures.

Another example for changing the coagulation bath temperature from 27°C and 50°C can be seen in Figure 3.33. For these membranes air gap was also changing and these result in changing the produced membranes geometry (Table 3.28). They both have macrovoids and selective skin layer on the shell side of the membranes. Also H86 which was produced at coagulation bath temperature was 50°C has pores that are smaller than macrovoids closer to the shell side of the membrane.

Table 3.28. Parameters of produced fibers from solution M at different coagulation bath temperatures.

Membrane Code	PDFR (mL/min)	BLFR (mL/min)	Air Gap (cm)	Geometry
H72	11.48	3.45	6	S
H86			8	Irr. S/H

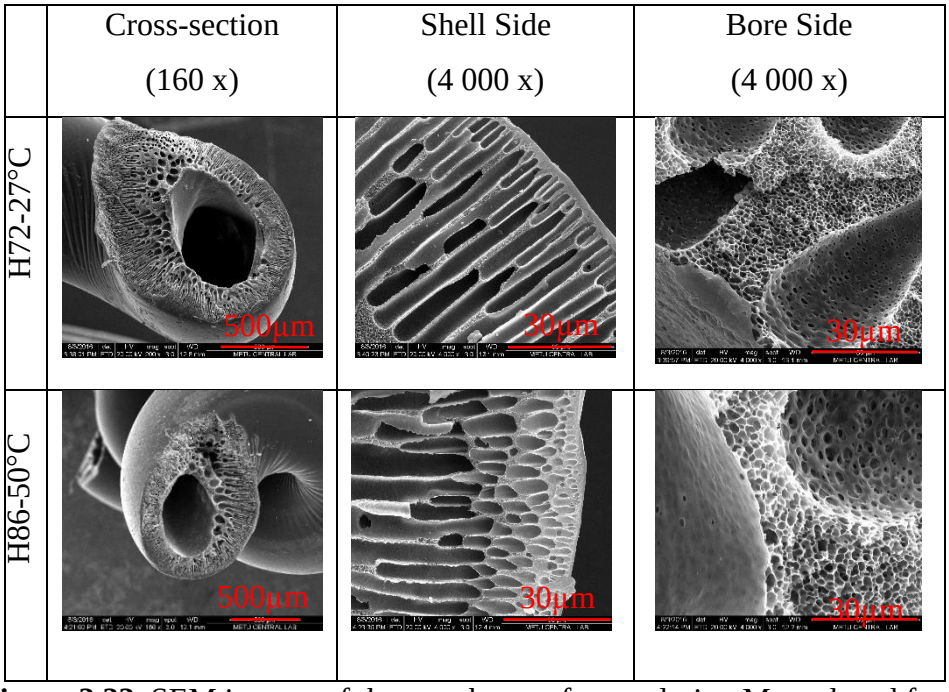

Figure 3.33. SEM images of the membranes from solution M produced from different coagulation bath temperature.

Figure 3.34 shows another SEM analysis which was done with regular straight and helical membranes, produced in coagulation bath temperature was at room temperature. When all parameters were fixed (Table 3.29), changing the PDFR and

BLFR effect were investigated. They both have macrovoids and selective skin layer on shell side of the membranes. When looking at the crossections membrane H75 have more macrovoids closer to the bore side than membrane H74.

Table 3.29. Parameters of regular produced fibers from solution M at different PDFR and BLFR.

Membrane Code	PDFR (mL/min)	BLFR (mL/min)	Air Gap (cm)	Geometry
H74	17.23	5.18	8	S
H75	8.61	2.59	8	H

	Cross-section (160 x)	Shell Side (4 000 x)	Bore Side (4 000 x)
H74-27°C	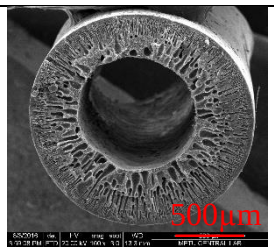	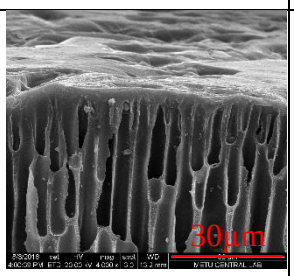	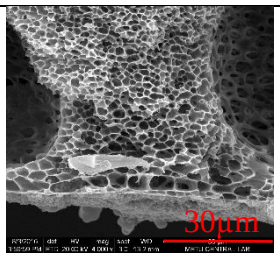
H75-27°C	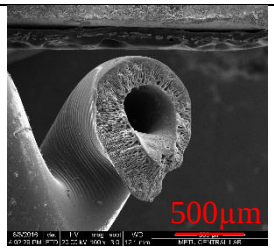	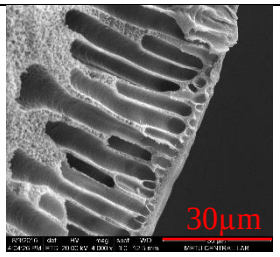	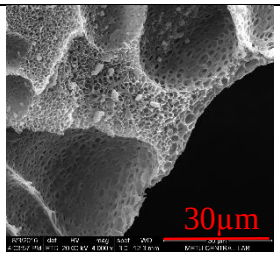

Figure 3.34. SEM images of the membranes from solution M produced from different PDFR and BLFR.

Figure 3.35 shows another SEM analysis which was done with regular helical membranes, produced in coagulation bath temperature was at 50°C. When all parameters were fixed except from air gap (Table 3.30), changing the PDFR and BLFR effect were investigated. They both have large cellular pores at the bore side and selective skin layer at the shell side of the membranes. When looking at the bore

diameter of the membranes H143, which has very low BLFR, have very small bore diameter and slightly smaller pores than membrane H159.

Table 3.30. Parameters of regular produced fibers from solution M at different PDFR and BLFR ratio.

Membrane Code	PDFR (mL/min)	BLFR (mL/min)	Air Gap (cm)	Geometry
H143	18.18	0.86	8	H
H159	18.18	3.45	10	H

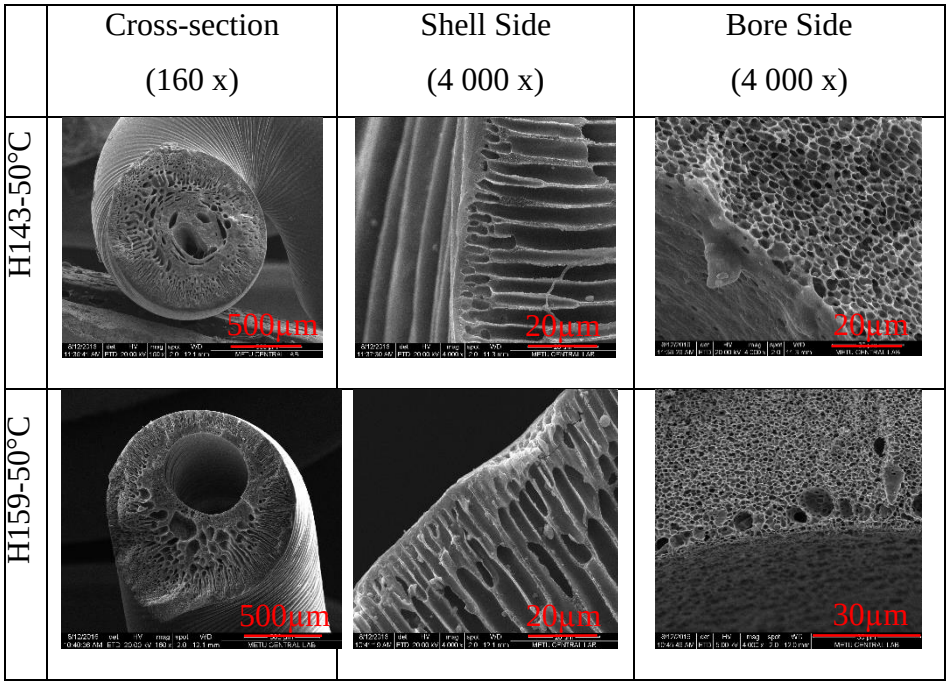

Figure 3.35. SEM images of the membranes from solution M produced from different PDFR and BLFR ratio.

3.3.3. Solution N

Solution N has 9.3% water which is at 95% of its coagulation value for the 15% PES, 5% Triton in NMP solution. Spinning done for solution N with solvent and non-solvent composition was 80% NMP and 20% up water (Non-solvent and solvent ratio was 1:4). Coagulation bath temperature was always at 50^0C.

Relation Between Air Gap and Polymer Dope Flow Rate and Bore Liquid Flow Rates

Table 3.31 shows how geometry of the produced fibers change with increasing air gap and decreasing PDFR-BLFR at coagulation bath temperature at 50°C. Also Table 3.32 shows the inner and outer diameters of the membranes, can be followed by using membrane codes in Table 3.31.

Table 3.31. Relation between air gap and PDFR-BLFR for solution N membranes produced at 50±2°C.

Air gap → / PDFR ↓	4 cm	6 cm	7 cm	8 cm	10 cm
11.48 mL/min	Irr. S (H165)	Irr. S (H164)	-	Disc. (H163)	Disc. (H162)
8.61 mL/min	S (H166)	Irr. S (H167)	Irr. S/M (H168)	Irr. M (H169)	-

Table 3.32. Inner and outer diameters of the produced membranes from solution N at coagulation bath temperature at 50±2°C.

Membrane Code	**Inner Diameter (µm)**	**Outer Diameter (µm)**
H162	477	837
H163	502	1040
H164	716	1269
H165	769	1335
H166	545	1173
H167	539	1005
H168	557	1036
H169	448	828

When PDFR was 11.48 mL/min and BLFR was 3.45 mL/min and coagulation bath temperature was at 51°C, increasing air gap results discontinuous flow from irregular straight HFMs geometry, can be seen in Figure 3.36. When air gap was 4 cm increasing both polymer dope flow rate and bore liquid flow rate changed HFMs geometry from regular straight to irregular straight. When air gap was 6 cm increasing both polymer

dope flow rate and bore liquid flow rate did not change HFMs irregular straight geometry. At 8 cm; increasing both polymer dope flow rate and bore liquid flow rate changed HFMs irregular meander geometry to discontinuous flow (Fig 3.36, Fig 3.37). When PDFR was 8.61 mL/min and BLFR was 2.59 mL/min and coagulation bath temperature was at 51°C, increasing air gap changed the geometry from straight to irregular straight then irregular meander form, can be seen in Figure 3.38.

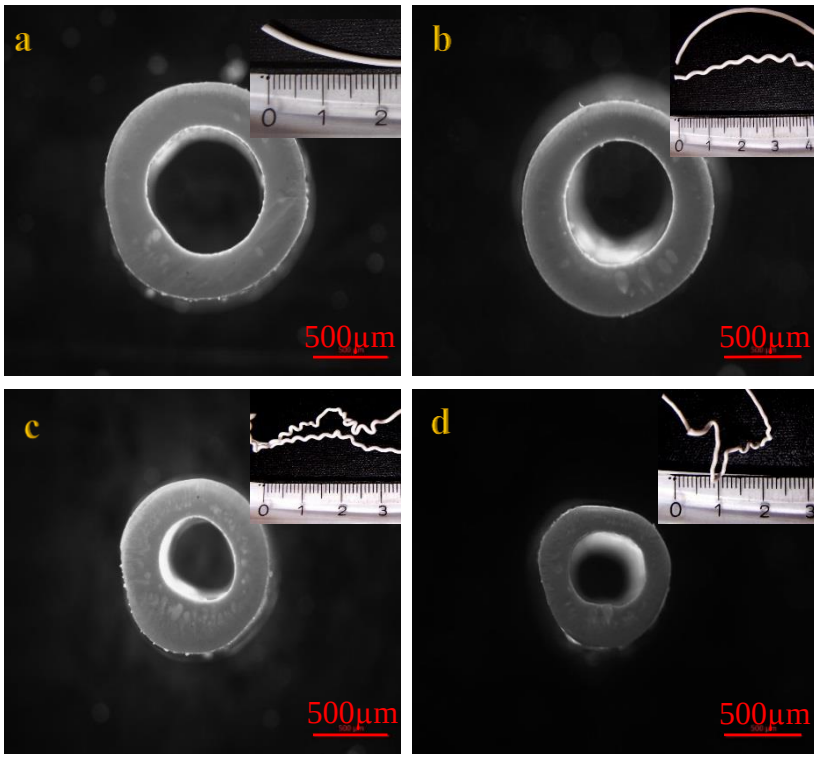

Figure 3.36. Microscope images of the membranes H165 (a), H164 (b), H163 (c) and H162 (d).

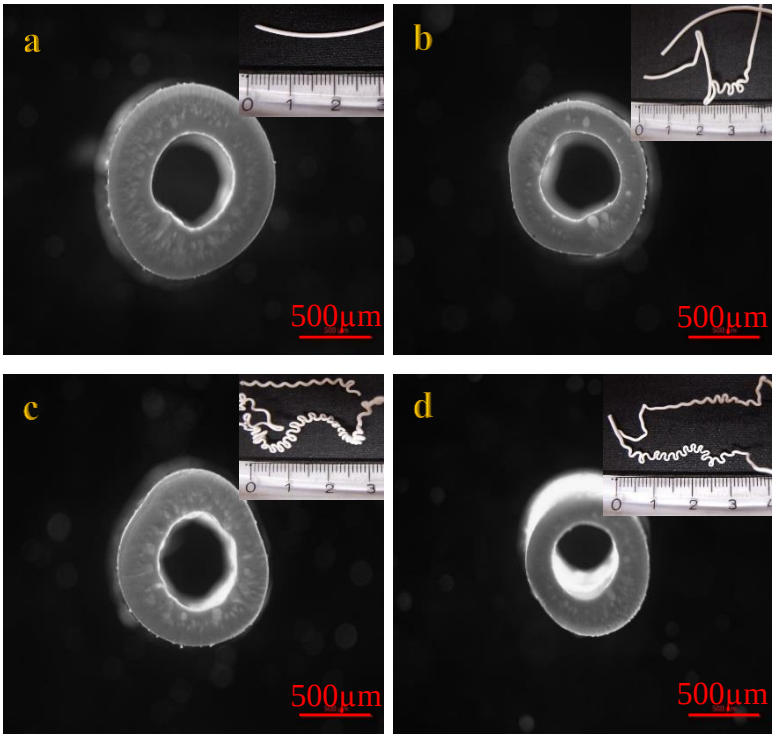

Figure 3.37. Microscope images of the membranes H166 (a), H167 (b), H168 (c) and H169 (d).

Polymer dope Flow Rate and Bore Liquid Flow Rate Ratio

At a certain air gap and high flow rates irregular helical geometry was observed and by increasing the PDFR/BLFR ratio regular helical geometry achieved (Table 3.33). Also in Figure 3.38 microscope pictures show that increasing flow rate ratio decreases the membrane bore diameter.

Table 3.33. Spinning parameters at 10 cm.

Memb. Code	PDFR (mL/min)	BLFR (mL/min)	Geo.	PDFR/BLFR ratio	D_i (µm)	D_o (µm)	D_{helix} (mm)	Pitch (mm)
H172	18.18	3.45	H	4.7:1	440	1053	1.9	2.0
H171	18.18	5.18	Irr. H	3.2:1	750	1195	-	-

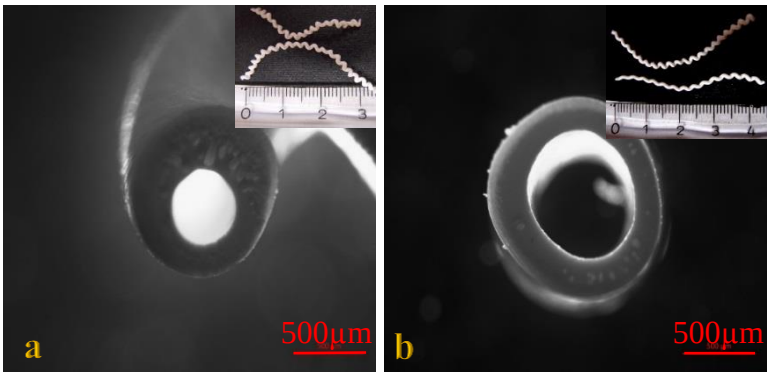

Figure 3.38. Microscope images of the membranes H172 (a) and H171 (b).

3.2.3.1. Morphology of the membranes from solution N

Figure 3.39 shows SEM images of produced fibers that have regular straight and helical geometry at the coagulation bath temperature of 50°C. Their production parameters were given at Table 3.34. SEM analysis shown that all the membranes have macrovoids near the membrane shell side. They all have selective layer at the shell side of the fiber. Inner side of the fibers observed in SEM by cutting of the fibers with the help of lancet. They both have closed cellular pores on bore side.

Table 3.34. Parameters of regular produced fibers from solution N at coagulation bath temperature was at 50°C.

Membrane Code	PDFR (mL/min)	BLFR (mL/min)	Air Gap (cm)	Geometry
H166	8.61	2.59	4	S
H170	18.18	5.18	8	H

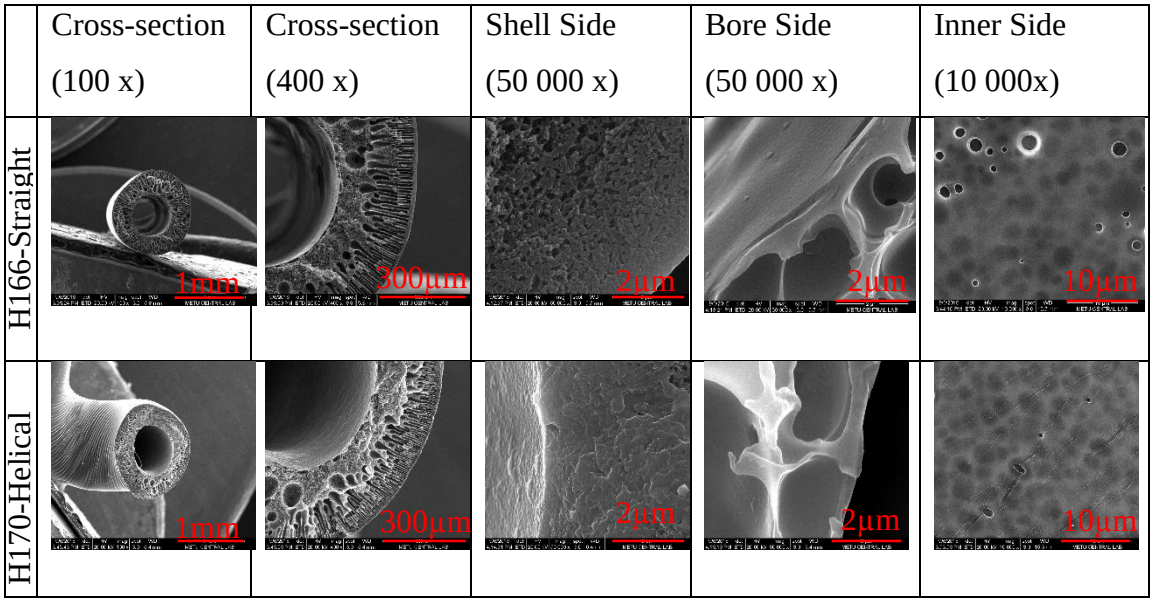

Figure 3.39. SEM images of the straight and helical membranes from solution N

3.3.4. Solution O

Solution O has 7.6% up water which is at 95% coagulation value for 15% PES, 20% PEG400, 5% Triton in NMP solution. 80% NMP and 20% up water was used as a bore liquid solvent and non-solvent composition in this spinning process. Coagulation bath temperature was at 50^0C.

<u>Relation Between Air Gap and Polymer Dope Flow Rate and Bore Liquid Flow Rates</u>

Table 3.35 shows how geometry of the produced fibers change with increasing air gap and decreasing PDFR-BLFR at coagulation bath temperature at 50°C. Also Table 3.36 shows the inner and outer diameters of the membranes, can be followed by using membrane codes in Table 3.35.

Table 3.35. Relation between air gap and PDFR-BLFR for solution O membranes produced at 50±2°C.

Air gap → / PDFR ↓	4 cm	6 cm	8 cm	10 cm	12 cm
17.23 mL/min	-	-	H (mostly) (H176)	H (mostly) (H185)	H (H187)
11.48 mL/min	S (H178)	Irr. H (H174)	Irr. H (H175)	H (mostly) (H184)	-
14.36 mL/min	-	-	Irr. H (H183)	H (H186)	-
8.61 mL/min	S (H179)	-	-	-	-
5.74 mL/min	Disc. (H181)	-	-	-	-

When PDFR was 17.23 mL/min and BLFR was 5.18 mL/min and coagulation bath temperature was at 49°C, increasing air gap changes the geometry from mostly regular helical to regular helical form, can be seen in Figure 3.40. When air gap at 8 cm and the other parameters were fixed, increasing both polymer dope flow rate and bore liquid flow rate changed HFMs geometry from irregular helical to mostly helical. At 10 cm; increasing both polymer dope flow rate and bore liquid flow rate did not change HFMs mostly helical geometry significantly (Figures 3.40-3.42).

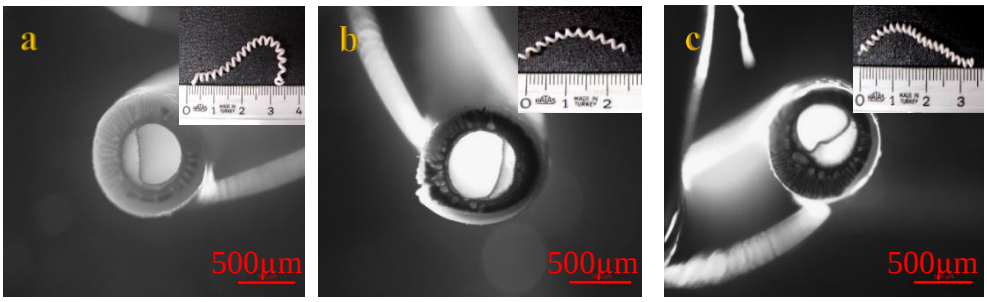

Figure 3.40. Microscope images of the membranes H176 (a), H185(b) and H187 (c).

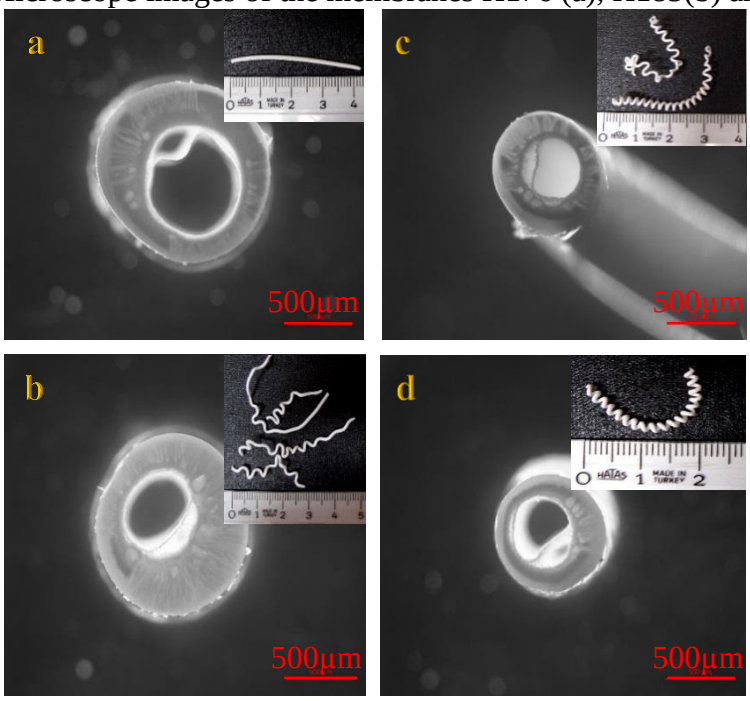

Figure 3.41. Microscope images of the membranes H178 (a), H174 (b), H175 (c) and H184 (d).

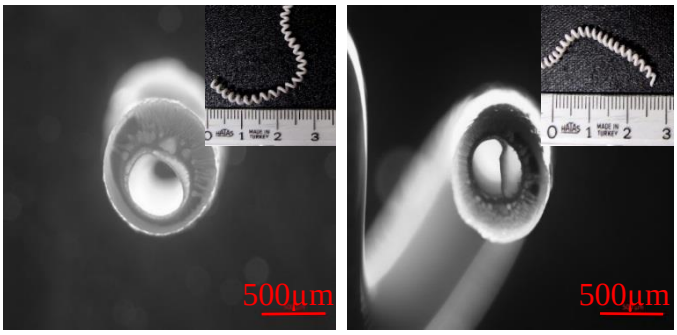

Figure 3.42. Microscope images of the membranes H183 (a) and H186 (b).

At the same coagulation bath temperature when PDFR was 11.48 mL/min and BLFR was 3.45 mL/min, increasing air gap changed the geometry from regular straight to

irregular helical then mostly helical form, can be seen in Figure 3.41. When air gap was at 4 cm; increasing both polymer dope flow rate and bore liquid flow rate changed HFMs geometry discontinuous flow to regular straight (Fig 3.41, Fig 3.43).

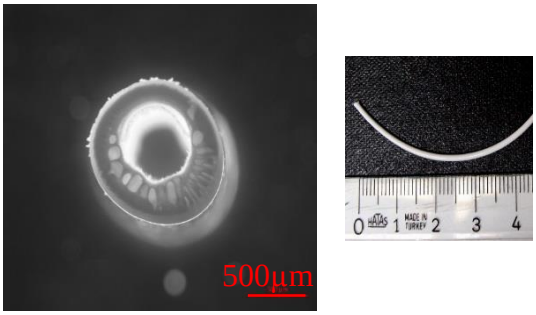

Figure 3.43. Microscope image of the membrane H179.

When PDFR was 14.36 mL/min and BLFR was 4.31 mL/min, increasing air gap changes the geometry from irregular helical to regular helical form, can be seen in Figure 3.42.

Table 3.36. Inner and outer diameters of the produced membranes from solution O at coagulation bath temperature at 50±2°C.

Membrane Code	Inner Diameter (µm)	Outer Diameter (µm)
H174	465	1159
H175	397	805
H176	499	994
H178	644	1229
H179	560	1075
H181	-	-
H183	418	894
H184	365	780
H185	514	908
H186	406	813
H187	419	900

By looking at Tables 3.35 and 3.36 together like the previous solutions (D, M) at the same PDFR increasing air gap decrease the membrane both inner and outer diameter. At low flow rates like PDFR was 5.74 mL/min and BLFR was 1.73 mL/min (H181) continuous membranes could not be produced.

Polymer Dope Flow Rate and Bore Liquid Flow Rate Ratio

When air gap at 4 cm increasing PDFR:BLFR ratio did not change the regular straight geometry of the fibers (Table 3.37, Fig 3.44). When air gap was 8 cm increasing ratio changed the irregular helical geometry to regular helical geometry (Table 3.38, Fig 3.45).

Table 3.37. Different polymer dope and bore liquid flow rate ratios at 4 cm.

Memb. Code	PDFR (mL/min)	BLFR (mL/min)	Geo.	PDFR/ BLFR ratio	Inner Diameter (µm)	Outer Diameter (µm)
H180	11.48	2.59	S	4.4:1	596	1187
H178	11.48	3.45	S	3.3:1	644	1229

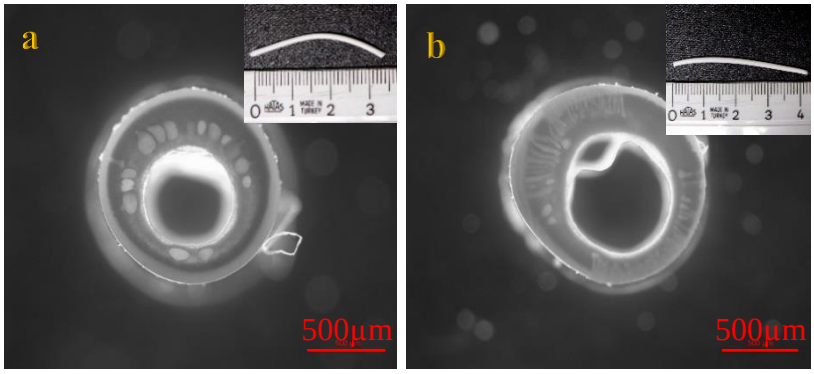

Figure 3.44. Microscope images of the membranes H180 (a) and H178 (b).

Table 3.38. Different polymer dope and bore liquid flow rate ratios at 8 cm.

Memb. Code	PDFR (mL/min)	BLFR (mL/min)	Geo.	PDFR/ BLFR ratio	Inner Diameter (µm)	Outer Diameter (µm)
H177	17.23	3.45	H	5:1	444	968
H176	17.23	5.18	H (mostly)	3.3:1	499	994

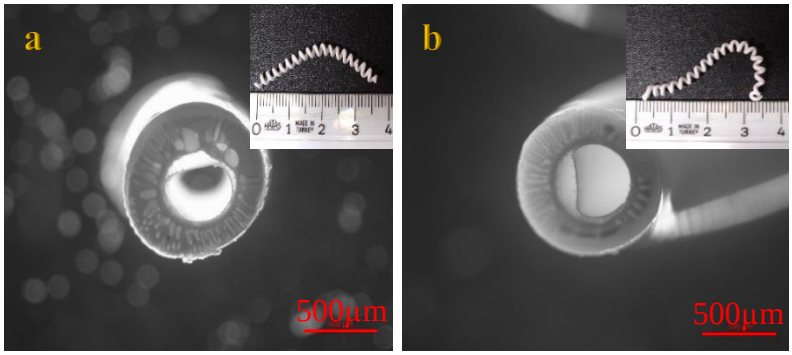

Figure 3.45. Microscope images of the membranes H177 (a) and H176 (b).

3.3.5. Comparison of Solution M versus N

Solution M and N different from each other by coagulation values. As a PES-NMP-Triton-water system there is one phase diagram. Adding water (non-solvent) in the solutions make them closer to the binodal curve. Solution N has higher water content than solution M; 9.5% and 7.3% respectively.

Table 3.39. Coagulation value effect of produced membranes.

Membrane Code	PDFR (mL/min)	BLFR (mL/min)	Air Gap (cm)	Geometry	Inner Diameter (µm)	Outer Diameter (µm)
H166 (Sol N)	8.61	2.59	4	S	545	1173
H123 (Sol M)	8.61	2.59	4	S	607	1170
H172 (Sol N)	18.18	3.45	10.2	H	440	1053
H160 (Sol M)	18.18	3.45	10	H	447	1160

Because of having high water content solution N was closer to the binodal curve than solution M. As a result of that produced membranes have different properties at the same spinning parameters. Table 3.39 shows that at the same air gap, same flow rates and same coagulation bath temperature (50°C) produced membranes geometry could be the same but membrane diameters were changed. For the membranes which were produced from solution M both inside and outside diameters were higher than the membranes from solution N (Fig 3.46).

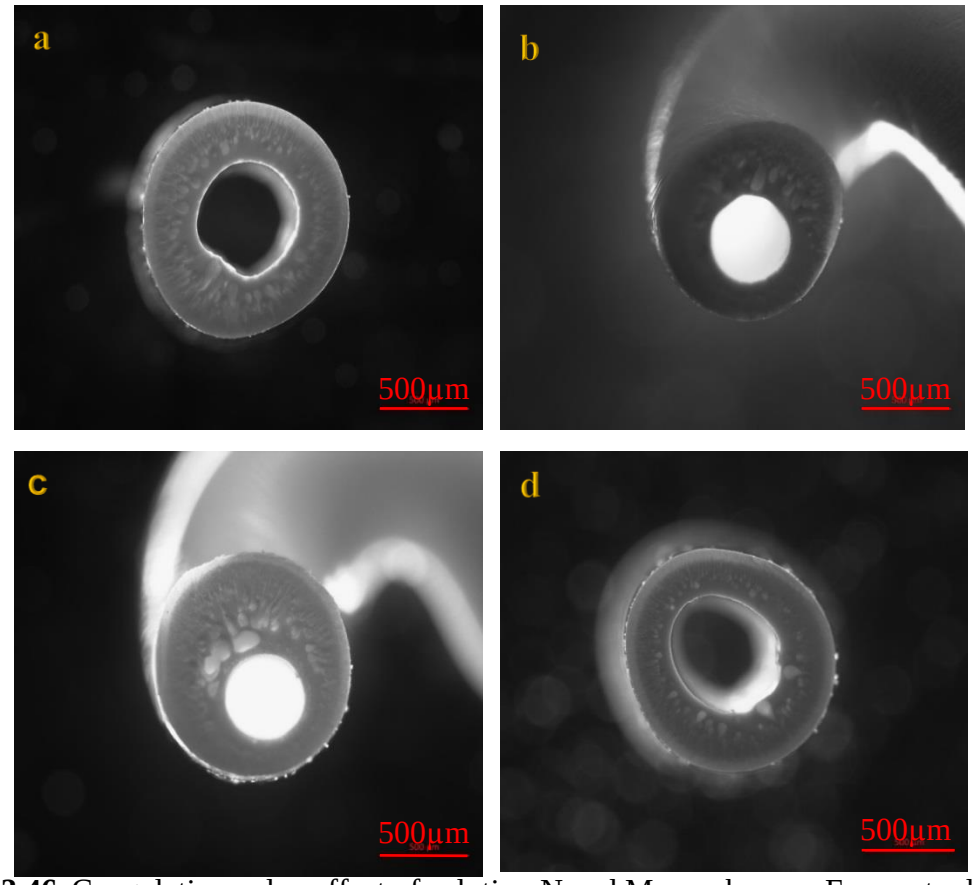

Figure 3.46. Coagulation value effect of solution N and M membranes. From a to d membranes H166, H172, H160 and H123 respectively.

On the other hand at the same PDFR (11.48 mL/min) and air gap (8 cm, 4 cm) produced membrane geometry was also different that can be shown in Table 3.40, Figure 3.47. At 8 cm membrane was produced that has an irregular helical form for solution M on the other hand with the same parameters for solution N, membrane could not produce because of the discontinuous flow. It was because of the solution N has higher content of water than solution M.

Table 3.40. Coagulation value effect of produced membranes at different parameters.

Membrane Code	PDFR (mL/min)	BLFR (mL/min)	Air Gap (cm)	Geometry
H163-(Sol N)	11.48	3.45	8	Disc.
H21-(Sol M)	11.48	3.45	8	Irr. H
H104-(Sol M)	11.48	3.45	4	S
H165-(Sol N)	11.48	3.45	4	Irr. S

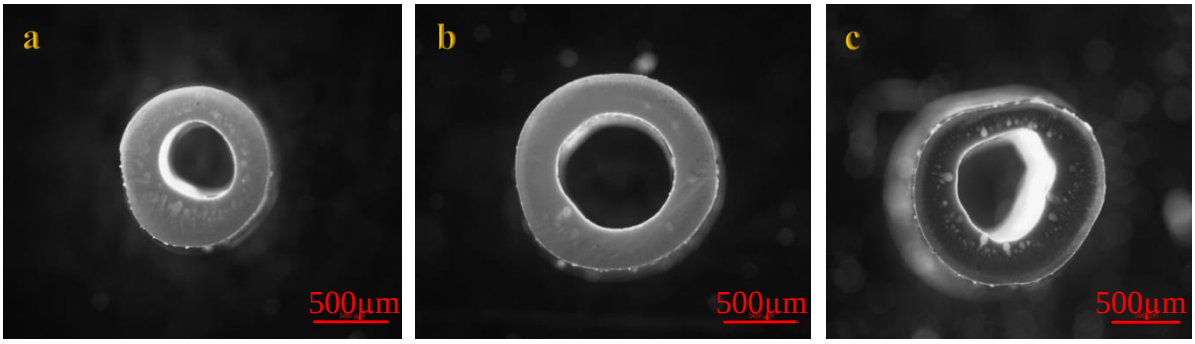

Figure 3.47. Coagulation value effect of solution N and M membranes. From a to c membranes H163, H165 and H104, respectively.

3.3.6. Comparison of Solution N versus O

Solution N and O different from each other by addition of pore forming agent PEG400. Membranes were produced with the same spinning parameters and their morphological difference investigated by SEM. Membrane H170 produced by using solution N and membrane H176 produced by solution O. They were fabricated at 8 cm and polymer dope flow rate for H170 was 18.18 mL/min and 17.23 mL/min for H176. Bore liquid flow rates and coagulation bath temperatures were the same and 5.18 mL/min and 50°C, respectively (Table 3.41, Fig 3.48).

Figure 3.49 shown SEM images of H170 and H176. They both have selective layer at the shell side. Cross section images shown that H170 has macrovoids, H176 has not. It was a result of PEG400 addition suppress the macrovoid formation in H176 (34-36).

Table 3.41. Comparison of solution N and O membranes.

Membrane Code	PDFR (mL/min)	BLFR (mL/min)	Air Gap (cm)	Geometry	D_i (µm)	D_o (µm)	D_{helix} (mm)	Pitch (mm)
H170 (Sol N)	18.18	5.18	8	Irr. H (nearly regular)	685	1203	-	-
H176 (Sol O)	17.23	5.18	8	H (mostly)	499	994	2.8	2.3
H171 (Sol N)	18.18	5.18	10	Irr. H (nearly regular)	750	1195	-	-
H185 (Sol O)	17.23	5.18	10	H (mostly)	514	908	2.3	2.8

Table 3.41 shows nearly the same PDFR was used and at different air gaps (8 cm, 10 cm) solution N and solution O membranes produced. Their geometry have a bit difference. They have the same coagulation value of %95 and the other parameters all fixed, but solution O includes 20% PEG400 and it may be the reason of this regular geometry.

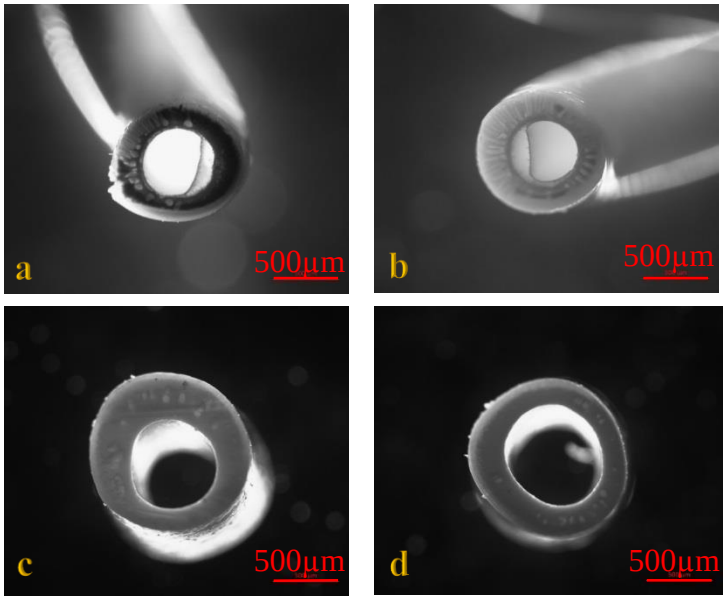

Figure 3.48. Optical microscope images of H185, H176, H170 and H171 from a to d.

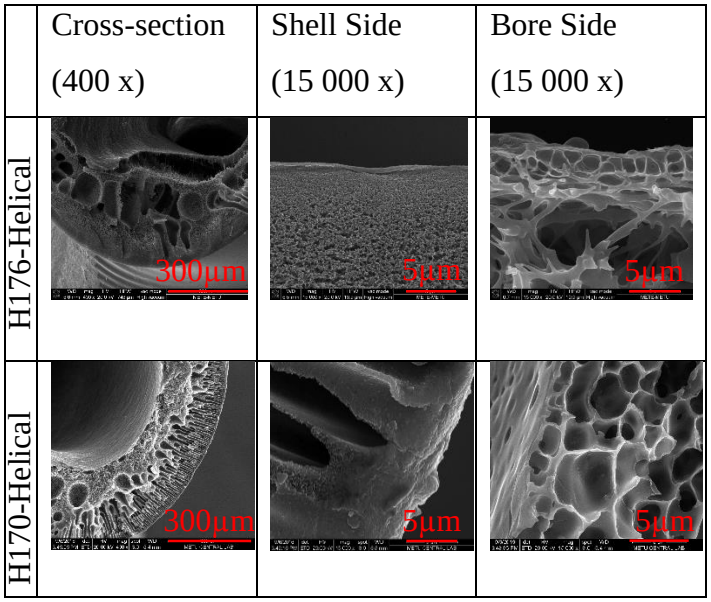

Figure 3.49. SEM images of the membranes H170 and H176.

3.3.7. Summary of Results From all Solutions

- When other parameters were fixed increasing polymer dope and bore liquid flow rates caused increased inner and outer diameter on the other hand increasing air gap caused decreased inner and outer diameter of the HFMs for all solutions. Polymer dope flow rate affected the membrane outer diameter whereas bore liquid flow rate affected the membrane inner diameter [12].
- For all solutions fabrication of HFMs in straight, helical forms can be achieved by changing the parameters. For solution D also the meander form can be achieved.
- Air in the air gap has a higher relative humidity so that phase inversion starts earlier. For using the same polymer dope (solution D or M) when other spinning parameters were fixed changing the coagulation bath temperature from room temperature to 50°C changed the membrane geometry from helical, meander and straight to just straight geometry for solution D. For solution M at certain air gaps geometry changed from regular straight to irregular helical form or irregular straight to helical form. When coagulation bath temperature was at room temperature solution M fibers inner and outer diameter was smaller than coagulation bath temperature was at 50°C. Before fiber enters to

the coagulation bath, increasing coagulation bath temperature starts phase inversion earlier because of the air in the air gap has a higher relative humidity. After fiber enters to the coagulation bath that have increased temperature (50°C) change the solvent and non-solvent diffusion rates so the fiber morphology affected.

- Increasing polymer dope flow rate and bore liquid flow rate ratio changes the membrane geometry from straight to helical for solution N and O. For solution M increasing PDFR-BLFR ratio at different air gaps change the membrane irregular geometry to regular geometry at PDFR 18.18 mL/min. When PDFR was 8.61 mL/min changing the PDFR-BLFR ratio did not change the membrane irregular geometry. Increasing the flow rate ratios not only increase the coiling tendency but also increase the fibers wall thickness.
- PEG400 addition of the polymer dope solution caused suppress the macrovoid formation for solution O. Also addition of PEG400 change the membrane irregular helical geometry to regular helical form.
- Solution D membranes geometries are more stable in wider range and regular meander shape was observed because of its viscosity much more higher than other solutions M, N and O, respectively.
- When we compare regular helical fibers for solution O at the same air gap increasing PDFR results in both helix and pitch diameter increase. At the same air gap increasing PDFR-BLFR ratio results in increasing the helix and decreasing pitch diameter of the fiber membrane. For solution M when PDFR was 8.61 mL/min increasing air gap decrease both helix diameter and pitch. When PDFR was 11.45 mL/min increasing air gap did not change helix diameter both decrease the pitch. At the highest flow rate, PDFR was 18.18 mL/min increasing the PDFR-BLFR ratio nearly not change both helix diameter and pitch (~0.1 mm).

3.4. Filtration Performance of the Membranes

As a performance tests pure water permeance (PWP), BSA rejection tests and dyed-yeast fouling tests were examined to fabricated membranes. After all spinnings H76

and H77 membranes were selected and their performance investigated with these experiments. Properties and spinning parameters of H76 and H77 are shown in Table 3.42. Also Figure 3.50 shows SEM images of these membranes.

Table 3.42. H76 an H77 membranes properties and spinning parameters.

Membrane Code	PDFR (mL/min)	BLFR (mL/min)	Air Gap (cm)	T (˚C)	Geo.	D_i (µm)	D_o (µm)	D_{helix} (mm)	Pitch (mm)
H76	8.61	2.59	6	27	H	519	948	2.0	1.9
H77			4	27	S	635	1307	-	-

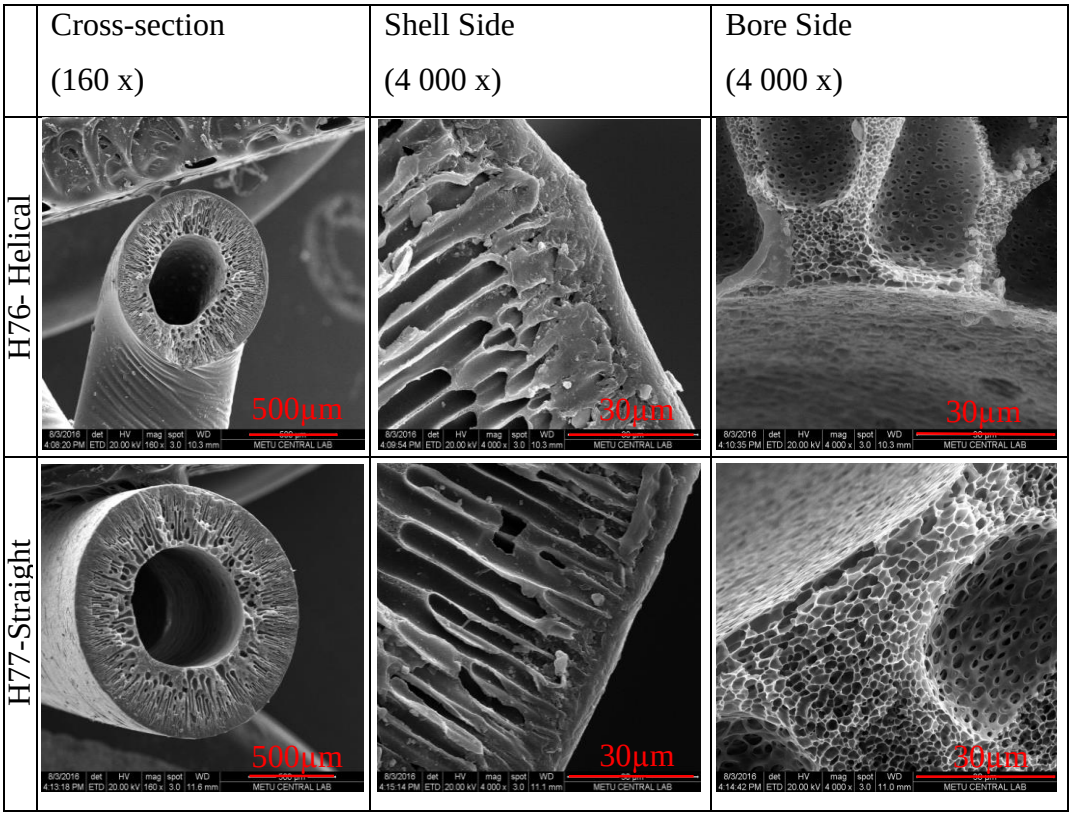

Figure 3.50. SEM images of H76 and H77 membranes.

Performance tests were done with two direction outside-in and inside-out and by cross-flow system. For inside out system, dyed-yeast fouling experiments Reynolds Number was at 400 and pressure was at 2 bar. For outside in system, dyed-yeast fouling experiments Reynolds Number was at 146 (for straight fiber), 125 (for helical fiber)

and pressure was at 2 bar. BSA rejection tests done at 1 bar and Reynolds Number was at 500. All experiments were repeated three times.

3.4.1. Outside-in Performance Tests (H76 versus H77)

Table 3.43 shows all performance tests were done outside-in direction. H77-Straight membrane pure water permeance was 130±40 L/hm^{2}bar and H76-Helical membrane pure water permeance was 227±27 L/hm^{2}bar. During dyed yeast fouling permeance for H77 and H76 were measured 47±4 L/hm^{2}bar and 142±14 L/hm^{2}bar, respectively. BSA retentions of the membranes were very close to each other for H76 and H77 BSA retentions were 95% and 98%, respectively.

Table 3.43. Membranes pure water permeances and permeances during fouling.

Memb.	**PWP (L/hm^{2}bar)**	**Permeance at the end of yeast fouling (L/hm^{2}bar)**	**Cross-flow rate (mL/min)**	**Cross-flow velocity (m/s)**	**BSA retention %R**
S-2o	170.18	52.06	32.5	$4.8*10^{-2}$	95
S-3o	90.71	43.47	32.5	$4.8*10^{-2}$	95
T-1o	203.22	128.8	24.6	$3.7*10^{-2}$	98
T-2o	252.08	156.81	24.6	$3.7*10^{-2}$	98

3.4.1.1. Yeast Fouling

Fouling with dyed-yeast test were examined ~2 hours for outside-in experiments. Straight membranes permeation were getting lower with time compare to helical membranes permeation as expected (Fig 3.51). So fouling resistance of the straight fibers were more than the helical ones (Fig 3.52).

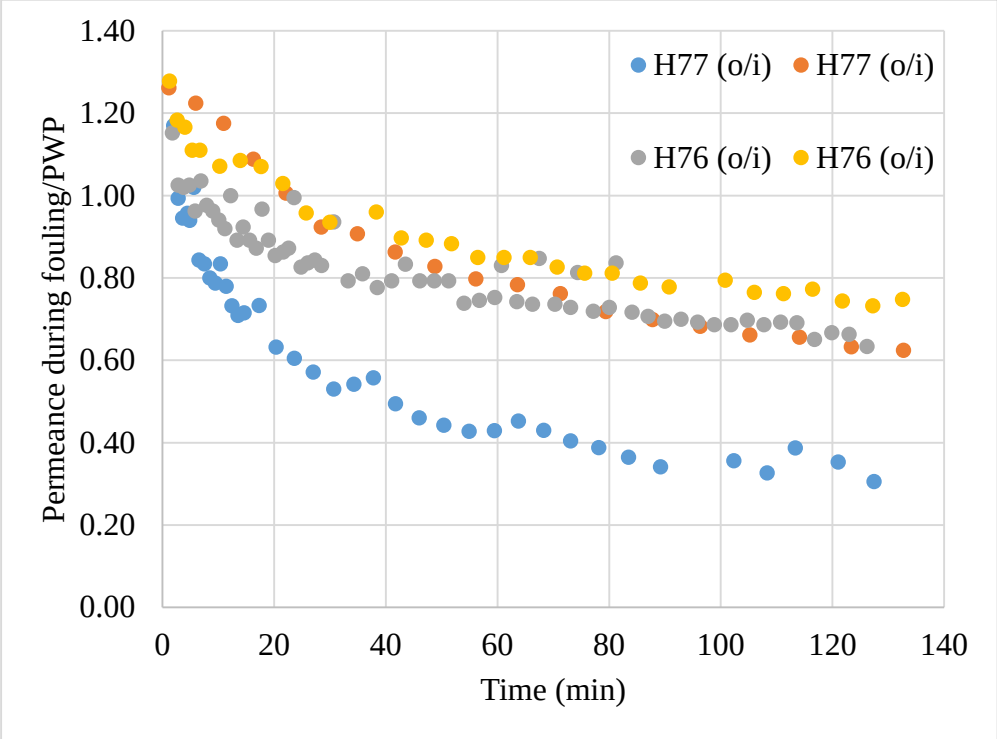

Figure 3.51. Outside-in permeances during fouling over PWP values of the membranes H76 and H77.

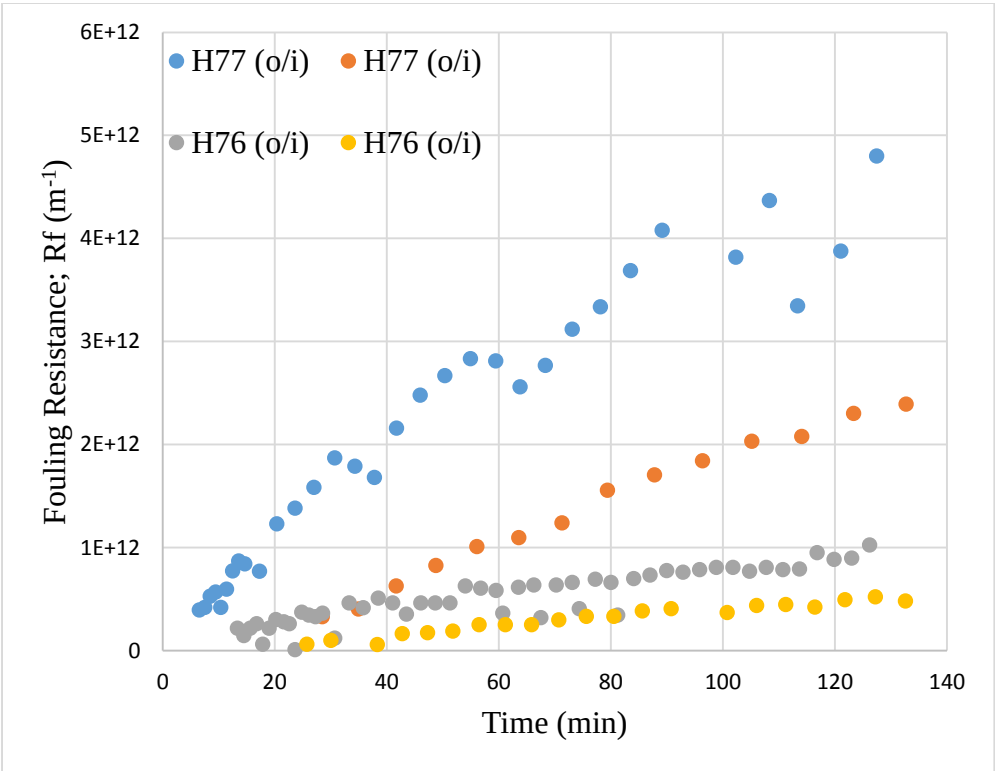

Figure 3.52. Outside-in fouling resistances of the membranes H76 and H77.

3.4.2. Inside-out Performance Tests (H76 versus H77)

Table 3.44 shows all performance tests done inside-out direction. H77-Straight membrane pure water permeance was 17±5 L/hm^{2}bar and H76-Helical membrane pure water permeance was 18±6 L/hm^{2}bar. During dyed yeast fouling permeance for H77 and H76 were measured 6±3 L/hm^{2}bar and 9±2 L/hm^{2}bar, respectively. Helical membrane (H76) fouling permeance higher than straight membrane (H77) because of the Dean vortex occur in the curvature of the membrane so fouling was lower ($De_{H76} = 190$).

Table 3.44. Membranes inside-out pure water permeances and permeances during fouling

Membranes	**PWP (L/hm^{2}bar)**	**Permeance at the end of yeast fouling (L/hm^{2}bar)**	**Cross-flow rate (mL/min)**	**Cross-flow velocity (m/s)**
S-2i (77-7)	21.35	8.07	10.68	0.56
S-1i (77-3)	12.17	3.35	10.68	0.56
T-1i (76-4)	12.19	8.2	8.7	0.69
T-2i (76-9)	23.35	11.87	8.7	0.69

3.4.2.1. Yeast Fouling

Fouling with dyed-yeast test were examined ~5 hours for inside-out experiments. Like the outside-in experiments for straight membranes permeation getting lower more than helical membranes (Fig 3.53). Fouling resistance of the straight fibers were more than the helical ones (Fig 3.54).

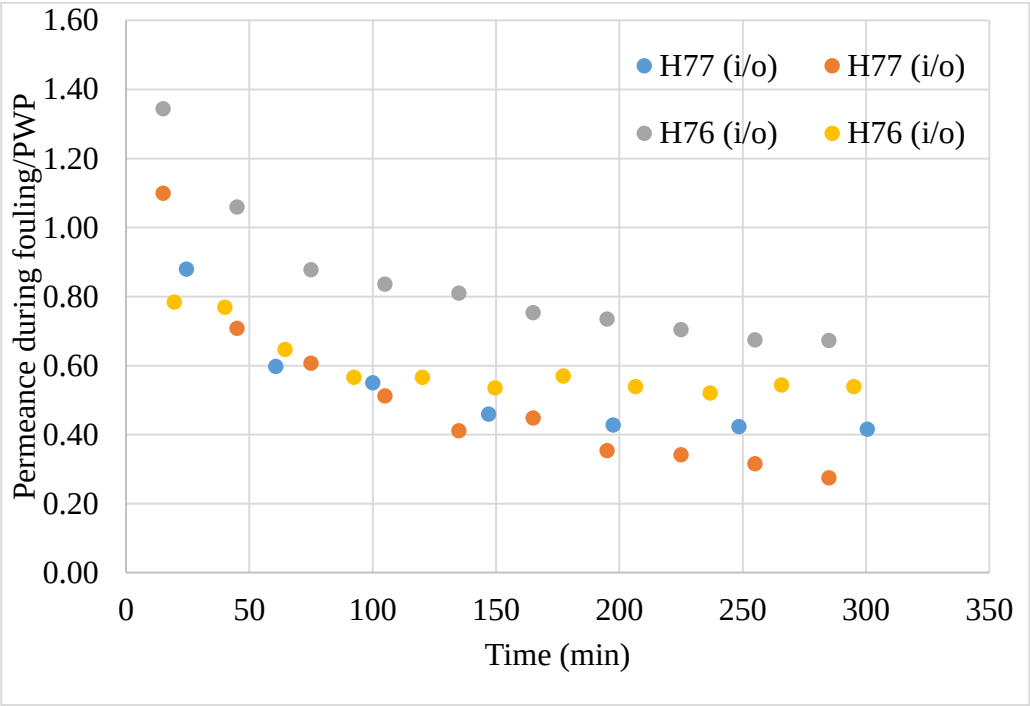

Figure 3.53. Inside-out permeances during fouling over PWP values of the membranes H76 and H77.

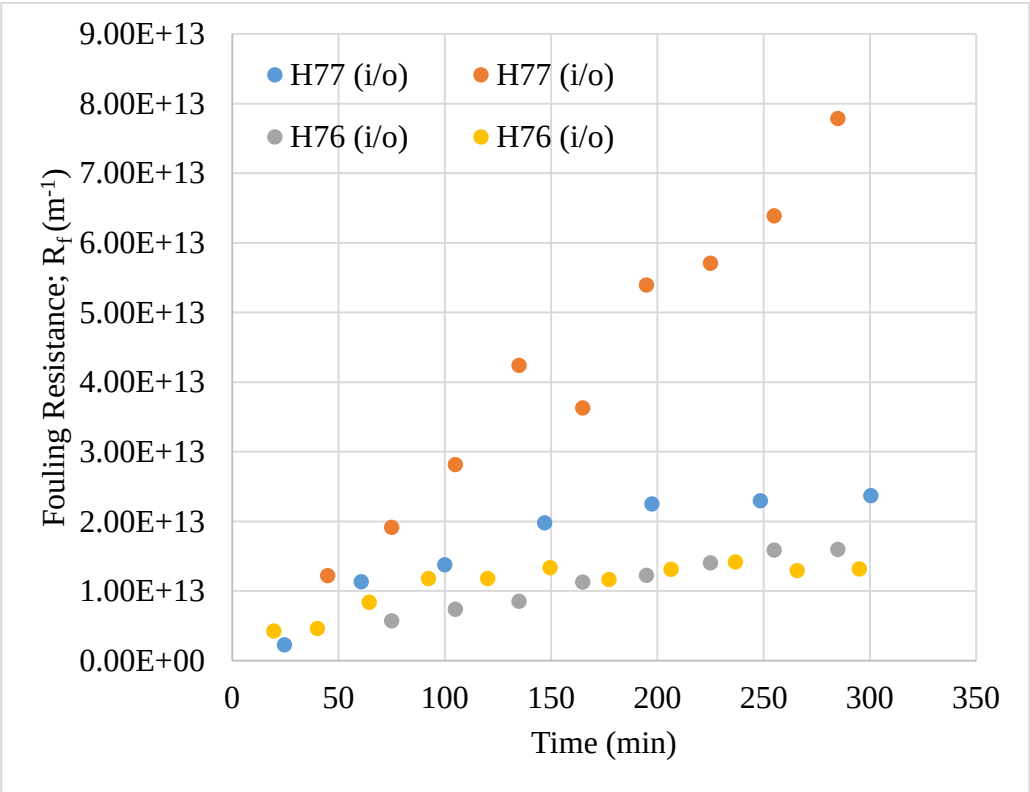

Figure 3.54. Inside-out fouling resistances of the membranes H76 and H77.

Pure water permeances (L/hm^{2}bar) and fouling resistances at the end of filtration (m^{-1}) of H76 and H77 membranes both inside-out and outside-in processes are drawn in Figures 3.55 and 3.56.

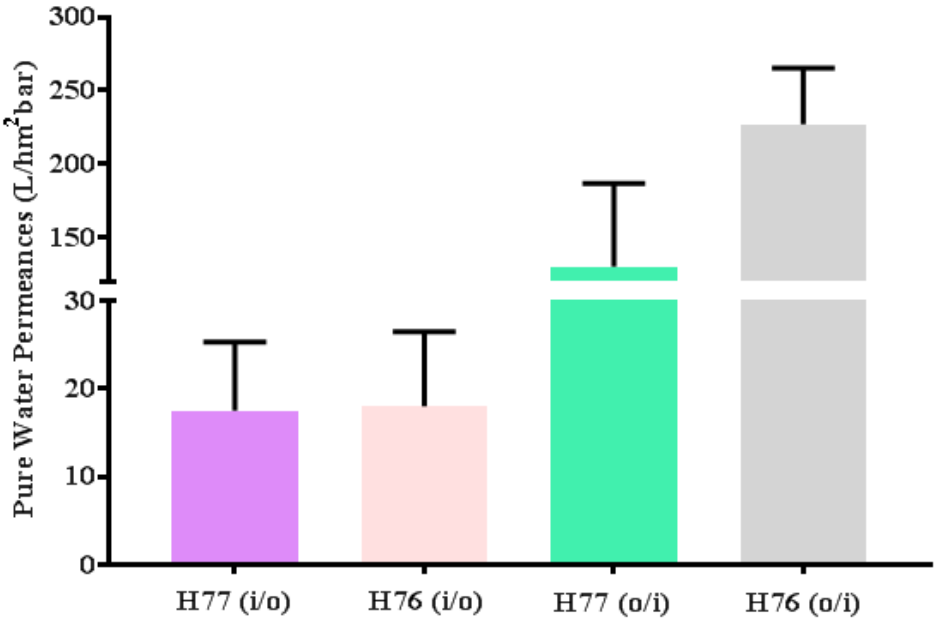

Figure 3.55. Pure water permeances of all membranes with error bars.

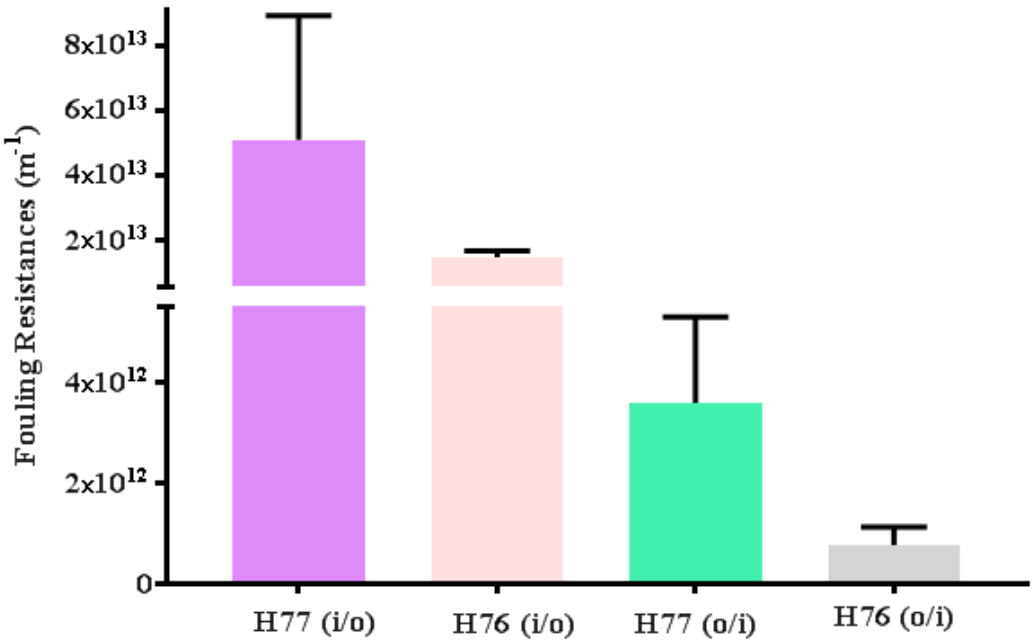

Figure 3.56. Fouling resistances of all membranes with error bars.

SEM images show that H76 and H77 fibers have macropores near the bore side of the membranes. Probably because of that, layer of the bore side was compressed with pressure during the inside-out PWP so that PWP differences occurred between inside-out and outside-in processes. For filtration there may be another possibility for permeance differences between inside-out process which is about the sizes of the yeast particles and bore side pores. Yeast particles are bigger than the bore side pores therefore they cannot plug into the membrane pores but they may interfere the pore entrances. Considering flux decline for both helical and straight fibers, it was less for helical fibers than straight fibers. Both inside-out and outside-in filtrations shows helical fibers more resistant to fouling then straight fibers.

With all four solutions D, M, N and O regular helical and straight membranes produced. As a performance test pure water permeance and yeast filtration done with selected solution M membranes which have regular straight and regular helical geometry. To decrease the concentration polarization these membranes are promising during membrane filtration by looking at the filtration test results.

CHAPTER 4

CONCLUSIONS

In this study fabrication of helical polyethersulfone hollow fiber membranes were done. After that fibers characterization and fouling behaviors were investigated.

Preliminary studies were done before the hollow fiber membranes (HFMs) fabrication. For the solutions including DMSO as a solvent, coagulation point determination were done. After that according to both coagulated in water and humid air membranes' pure water permeances, polymer dope composition was chosen as 20 wt. % PES, 40 wt. % PEG400, 40 wt. % DMSO to produce HFM. HFMs were fabricated by examining spinning parameters at two different coagulation bath temperatures; at 25°C (at room temperature) and at 50°C. By looking at membrane morphology, which was showing selective skin layer at shell side, other solutions were prepared with different coagulation values 95% and 50%. They both had just straight geometry and did not changed the skin layer side.

DMSO were reached cloud point combination with less water content compared to NMP solutions to see VIPS before the membrane coagulate and geometry was straight; new solution (Solution M) including NMP as a solvent was chosen to fabricate HFMs. Solution M composition was 15.3 %PES, 5.1 %Triton 100X, 72.3%NMP, 7.3%Upwater (75% of coagulation value). Also to see the effect on morphology 95% of coagulation value solution N, 15 %PES, 5 %Triton 100X, 70.7 %NMP, 9.3 %Upwater, was tested. HFMs from solution M and N were fabricated by examining spinning parameters at two different coagulation bath temperatures; at 25°C and at 50°C, as in the solution D. HFMs from solution M and N at 25°C and 50°C both have macrovoids and selective skin layer at the shell side. To suppress the macrovoid

formation PEG400 was used as an additive. Solution O, 15% PES, 5% Triton 100X, 20% PEG400, 52.4% NMP, 7.6% Upwater (95% of coagulation value) was prepared. HFMs were fabricated from solution O at 50°C have selective skin layer at the shell side and macrovoid formation was not observed. Also when compared to solution N fibers, addition of PEG400 changed the membrane irregular helical geometry to regular form when the other parameters all fixed.

Due to all helical fibers have selective skin layer at the shell side, HFMs both helical (H76) and straight (H77) geometry from solution N at 25°C were selected to examine performance tests of the membranes both inside out and outside in direction. BSA rejection tests for H76 and H77 were done and results were above 95%. Flux decline for helical membranes lower than straight membrane for inside out feed direction. It is considered due to the Dean vortex, that was calculated and higher than critical Dean number which was an indicator about Dean vortex occurrence. Also fouling resistance of straight fibers were higher than helical ones. When feed direction was outside in, results showed that fouling resistance of the straight fibers were more than helical fibers. The pressure drop along the fiber was at most 8 kPa per cm when the filtration was carried inside out with the helical fibers, while it was negligible in the straight fiber modules of 5 cm length and during outside-in filtrations [37].

At a general view, helical fibers have experienced less fouling and decrease the concentration polarization compare to the straight fibers due to their curvature structure when feed was both inside and outside of the membranes. Helical membranes have improved hydrodynamics and less fouling compared to straight ones.

REFERENCES

[1] Baker, R. W., Membrane Technology and Applications, WILEY, Second Edition, 2004, John Wiley and Sons.

[2] Mulder, M., Basic Principles of Membrane Technology, Kluwer Academic Publishers, Second Edition, 1997, Dordrecht.

[3] Cadotte J., Forester R., Kim M., Petersen R., Stocker T., Nanofiltration membranes broaden the use of membrane separation technology, Desalination 70 (1988) 77-88.

[4] Frank M., Bargeman G., Zwijnenburg A., Wessling M., Capillary hollow Fiber nanofiltration membranes, Separation and Purification Technology 22-23 (2001) 499-506.

[5] Machado, P.S.T., Habert, A.C., Borges, C.P., Membrane formation mechanism based on precipitation kinetics and membrane morphology: Flat and hollow fiber polysulfone membranes, Journal of Membrane Science, 155 (1999) 171-183.

[6] Strathmann H., Kock K., The formation mechanism of phase inversion membranes, Desalination 21 (1977) 241-255.

[7] Strathmann. H., Kock K., Amar P., The formation mechanism of asymmetric membranes, Desalination, 16 (2) (1975) 179-203.

[8] Winzeler, H.B., Belfort, G., Enhanced performance for pressure-driven membrane processes: the argument for fluid instabilities. Journal of Membrane Science 80 (1993) 35-47.

[9] Cheryan M., Ultrafiltration and Microfiltration Handbook, Technomic, 1998, University of Illinois.

[10] Luelf, T., Bremer, C., Wessling, M., Rope coiling spinning of curled and meandering hollow-fiber membranes. Journal of membrane science, 506 (2016) 86-94.

[11] Yang X., Wang R., Fane A.G., Tang C.Y., Wenten I.G., Membrane module design and dynamic shear-induced techniques to enhance liquid separation by hollow fiber modules: a review. Desalination and Water Treatment 51 (2013) 3604-3627.

[12] McKelvey S.A., Clausi D.T., Koros W.J., A guide to establishing hollow fiber macroscopic properties for membrane applications, Journal of Membrane Science 124 (1997) 223-232.

[13] Gupta V.B., Kothari V.K., Manufactured fibre technology, Springer Science, First Edition, 1998, Indian Institute of Technology.

[14] Matthiasson E., Sivik B., Concentration polarization and fouling, Desalination 35 (1980) 59-103.

[15] Jaffrin M.Y., Hydrodynamic techniques to enhance membrane filtration, Annual Review of Fluid Mechanics, 44 (2012) 77-96.

[16] Belfort G., Davis R.H., Zydney A.L., The behavior of suspensions and macromolecular solutions in crossflow microfiltration (Review), Journal of Membrane Science 96 (1994) 1-58.

[17] Aimar P., Meireles M., Bacchin P., Sanchez V., Fouling and concentration polarization in ultrafiltration and microfiltration, NATO ASI Series E, 272 (1994) 27-57.

[18] Kun C.Y., Brewster M.E., Belfort G., Dean Vortices with wall flux in a curved channel membrane system: 3. Concentration polarization in a spiral reverse osmosis slit, Journal of Chemical Engineering of Japan 31-5 (1998) 683-693.

[19] Chung K.Y., Lee M.S., Flux enhancement in a helical microfiltration module with gas injection, Separation Science and Technology 40 (2005) 2479-2495.

[20] Dean V.R., Fluid motion in a curved channel, Royal Society 121 (1928) 402-420.

[21] Kumar V., Aggarwal M., Nigam K.D.P., Mixing in curved tubes, Chemical Engineering Science 61 (2006) 5742-5753.

[22] Belfort G., Fluid mechanics in membrane filtration recent developments, Journal of membrane science 40 (1989) 123.

[23] Teoh M.M., Bonyadi S., Chung T.S., Investigation of different hollow fiber module designs for flux enhancement in the membrane distillation process, Journal of Membrane Science 311 (1-2) (1997) 17-29.

[24] Mallubhotla H., Nunes E., Belfort G., Microfiltration of yeast suspensions with self-cleaning spiral vortices: Possibilities for a new membrane module design, Biotechnology and Bioengineering 48 (1995) 375-385.

[25] Kaufhold D., Kopf F., Wolff C., Beutel S., Hilterhaus L., Hoffmann M., Scheper T., Schlüter M., Liese A., Generation of Dean vortices and enhancement of oxygen transfer rates in membrane contactors for different hollow fiber geometries, Journal of Membrane Science 423-424 (2012) 342-347.

[26] Ghogomu J.N., Guigi C., Rouch J.C., Clifton M.J., Apet P., Hollow-fibre membrane module design: comparison of different curved geometries with Dean vortices, Journal of Membrane Science 181 (2001) 71-80.

[27] Moulin P., Manno P., Rouch J.C., Serra C., Clifton M.J., Aptel P., Flux improvement by Dean vortices: ultrafiltration of colloidal suspensions and macromolecular solutions, Journal of Membrane Science 156 (1999) 109-130.

[28] Liu L., Li L., Ding Z., Ma R., Yang Z., Mass transfer enhancement in coiled hollow fiber membrane modules, Journal of Membrane Science 264 (2005) 113-121.

[29] Barnes G., Woodcook R., Liquid rope coil-effect, American Journal of Physiscs 26 (1958) 205-209.

[30] Jia, B., Yu, L., Fu, F., Li, L., Preparation of helical fibers from cellulose-cuprammonium solution based on liquid rope coiling. RSC Adv., 4 (2014) 9112.

[31] Çulfaz P.Z., Haddad M., Wessling M. and Lammertink R.G.H., Fouling behavior of microstructured hollow fibers in cross-flow filtrations: Critical flux determination and direct visual observation of particle deposition, Journal of Membrane Science 372 (2011) 210-218.

[32] Kaltalı G., Fabrication of Polyethersulfone Hollow Fibers For Ultrafiltration (Master Thesis, 2014), Middle East Technical University.

[33] Bolat K., Investigation of parameters affecting morphology of microfiltration and ultrafiltration membranes fabricated via Phase Separation Microfabrication (Master Thesis, 2017), Middle East Technical University.

[34] Torrestiana-Sanchez B., Ortiz-Basurto R.I., Brito-De La Fuente E., Effect of nonsolvents on properties of spinning solutions and polyethersulfone hollow fiber ultrafiltration membranes, Journal of Membrane Science 152 (1999) 19-28.

[35] Xu Z.L., Alsalhy Qusay F., Polyethersulfone (PES) hollow fiber ultrafiltration membranes prepared by PES/non-solvent/NMP solution, Journal of Membrane Science 233 (2004) 101-111.

[36] Liu Y., Strathmann. H., Henk Koops G., Characterization of morphology controlled polyethersulfone hollow fiber membranes by the addition of polyethylene glycol to the dope and bore liquid solution, Journal of membrane Science 223 (1) (2003) 187-199.

[37] H. Yucel, P. Z. Çulfaz Emecen, Helical hollow fibers via rope coiling: Effect of spinning conditions on geometry and membrane morphology, Journal of Membrane Science 559 (2018) 54-62.

APPENDIX A

OUTSIDE-IN PROCESS SAMPLE CALCULATIONS OF PWP AND FOULING

Straight Membrane

Straight-2o PWP (S-2o)

Pump Head: 7016-20

Calibration Eqn: y=0.7443x-0.3318

Volumetric Flow Rate Calculation

x=20 rpm;

$$y = 14.6\frac{\text{ml}}{\text{min}} = 14.6\ \frac{ml}{min}\left(\frac{1cm^3}{1\ ml}\right).\left(1 * 10^{-6}\frac{m^3}{cm^3}\right).\left(\frac{1\ min}{60\ s}\right) = 2.4 * 10^{-7}\frac{m^3}{s}$$

Membrane Effective Area Calculation

$$A = \pi D_0 L = \pi.(1307\mu m * 10^{-6}\ m/\mu m).(0.055\ m)$$

$$A = 2.26 * 10^{-4} m^2$$

Table A.1. PWP data and result for Straight-2o at 2 bar.

Δt (min)	ΔP (bar)	Δm (g)	Permeance (L/hm^2bar)	PWP Parameters
30	2	115.55	511.28	Membrane inner diameter: 635 µm Membrane outer diameter: 1307 µm Membrane Length: 5.5 cm Membrane Area: 2.26 $*10^{-4}$ m^2 Pump setting: 20 rpm (Q:14 ml/min) Pump Head: 7016-20 Dead end, outside-in
30	2	85.66	379.03	
30	2	72.9	322.57	
30	2	64.73	286.42	
30	2.05	53.01	228.84	
30	2.05	53.01	228.84	
30	2.05	48.94	211.27	
30	2.05	46.19	199.40	
30	2.05	43.38	187.27	
30	2.05	41.16	177.68	
30	2.05	39.26	169.48	
30	2.05	37.85	163.39	

Table A.2. PWP data and result for Straight-2o at 1 bar.

Δt (min)	ΔP (bar)	Δm (g)	Permeance (L/hm^2bar)	PWP Parameters
30	1.1	1.17	282.64	Membrane inner diameter: 635 µm Membrane outer diameter: 1307 µm Membrane Length: 5.5 cm Membrane Area: 2.26 $*10^{-4}$ m^2 Pump setting: 20 rpm (Q:14 ml/min) Pump Head: 7016-20 Cross-flow, outside-in
30	1.05	0.75	189.63	
30	1.05	0.71	180.36	
30	1.05	0.73	185.13	
30	1.05	0.72	183.14	
30	1.05	0.61	155.17	
30	1.05	0.70	177.93	
30	1.05	0.68	171.18	
30	1.05	0.66	167.21	
30	1.05	0.66	168.06	

Straight-2o Fouling (S-2o Fouling)

Pump Head: 7016-20

Calibration Eqn: y=0.7443x-0.3318

Volumetric Flow Rate Calculation

x=44.1 rpm;

$$\text{y} = 32.52\frac{\text{ml}}{min} = 32.52\ \frac{ml}{min}\left(\frac{1cm^3}{1\ ml}\right).\left(1*10^{-6}\frac{m^3}{cm^3}\right).\left(\frac{1\ min}{60\ s}\right)$$

$$\text{y} = 5.42*10^{-7}\frac{m^3}{s}$$

Module Hydraulic Diameter

$$D_H = \frac{4A_c}{P_w} = \frac{4\pi\left(\frac{{D_{tube}}^2 - {D_{o,fiber}}^2}{4}\right)}{\pi(D_t - D_o)} = D_t - D_o$$

$$D_H = 4000\mu m - 1307\mu m = 2693\mu m * 10^{-6}\frac{m}{\mu m}$$

$$D_H = 2.7*10^{-3}m$$

Reynolds Number Calculation

Sample calculation for x=44.1 rpm

$$\text{A}_c = \frac{V_f}{L_{tube}} = \frac{\frac{\pi {D_{tube}}^2}{4}L_{tube} - \frac{\pi {D_o}^2}{4}L_{fiber}}{L_{tube}}$$

$$L_{tube} = L_{fiber} \qquad for\ straight\ membrane$$

$$\text{A}_c = \frac{\pi\left({D_t}^2 - {D_O}^2\right)}{4} = \frac{\pi[(4000*10^{-6})^2 - (1307*10^{-6})^2]}{4} = 1.12*10^{-5}m^2$$

$$\text{Re} = \frac{Q.D_H}{\mathcal{V}.\text{A}_c} = \frac{\left(5.42\ *10^{-7}\frac{m^3}{s}\right)(2.7*10^{-3}m)}{\left(8.926*10^{-7}\frac{m^2}{s}\right)(1.12*10^{-5}m^2)}$$

$$\text{Re} = 146.4\ \ (\text{for 44.1 rpm})$$

Table A.3. Permeance during fouling data and result for Straight-2o

Δt (min)	ΔV (mL)	Permeance during fouling (L/hm^{2}bar)	Permeance during fouling/PWP	Fouling Resistance, R_f (m^{-1})	Fouling Parameters
2.00	3	199.12	1.17	-3.07407E+11	Pump model: 7016-20 P=2 bar outside-in, crossflow 200 gr (dye-upwater) 0.025 wt.% dye Re=146.4
1.57	2	169.10	0.99	13512784111	
1.65	2	160.90	0.95	1.21993E+11	
1.63	2	162.88	0.96	94872784111	
0.83	1	159.93	0.94	1.35553E+11	
1.53	2	173.52	1.02	-40727215889	
1.85	2	143.51	0.84	3.93193E+11	
1.87	2	141.97	0.83	4.20313E+11	
1.95	2	136.15	0.80	5.28793E+11	
1.98	2	134.08	0.79	5.69473E+11	
1.87	2	141.97	0.83	4.20313E+11	
2.00	2	132.74	0.78	5.96593E+11	
2.13	2	124.64	0.73	7.72873E+11	
2.20	2	120.68	0.71	8.67793E+11	
2.18	2	121.78	0.72	8.40673E+11	
5.32	5	124.76	0.73	7.70161E+11	
6.17	5	107.57	0.63	1.2312E+12	
6.45	5	102.90	0.60	1.38307E+12	
6.82	5	97.32	0.57	1.58376E+12	
7.35	5	90.30	0.53	1.87123E+12	
7.20	5	92.18	0.54	1.78987E+12	
7.00	5	94.82	0.56	1.68139E+12	
7.88	5	84.23	0.49	2.1587E+12	
8.47	5	78.36	0.46	2.47872E+12	
8.82	5	75.25	0.44	2.66856E+12	
9.12	5	72.78	0.43	2.83128E+12	
9.08	5	73.10	0.43	2.80958E+12	
8.62	5	77.00	0.45	2.56008E+12	
9.00	5	73.75	0.43	2.76619E+12	
9.65	5	68.78	0.40	3.11875E+12	
10.05	5	66.04	0.39	3.33571E+12	
10.70	5	62.03	0.36	3.68827E+12	
11.42	5	58.12	0.34	4.0788E+12	
26.25	12	60.68	0.36	3.81709E+12	
11.95	5	55.54	0.33	4.36627E+12	
10.07	5	65.91	0.39	3.34656E+12	

15.47	7	60.06	0.35	3.87811E+12	
12.75	5	52.06	0.31	4.80019E+12	

Helical Membrane

Helical-1o PWP (T-1o)

Pump Head: 7016-20

Calibration Eqn: y=0.7443x-0.3318

Volumetric Flow Rate Calculation

x=15 rpm; y=10.8 ml/min

$$y = 10.8\ \frac{ml}{min}\left(\frac{1cm^3}{1\ ml}\right).\left(1 * 10^{-6}\ \frac{m^3}{cm^3}\right).\left(\frac{1\ min}{60\ s}\right) = 1.8\ * 10^{-7}\ \frac{m^3}{s}$$

Membrane Effective Area Calculation

$$A = \pi D_0 L = \pi.(948\mu m * 10^{-6}\ m/\mu m).(0.1m) \qquad A = 2.98 * 10^{-4} m^2$$

Table A.4. PWP data and result for Helical-1o at 1.9 bar.

Δt (min)	ΔP (bar)	Δm (g)	Permeance (L/hm^{2}bar)	PWP Parameters
30	1.9	90.2	263.74	D_i: 519 µm D_o: 948 µm Membrane Length: 12 cm (corrected) Membrane Area: 3.6* 10^{-4} m^2 Pump setting: 15 rpm (Q:10.8 ml/min) Pump Head: 7016-20 Dead end, outside-in
30	1.9	82.61	241.55	
30	1.9	77.96	227.95	
30	1.9	75.42	220.53	
30	1.9	73.69	215.47	
30	1.9	72.11	210.85	
30	1.9	70.93	207.40	
30	1.9	69.59	203.48	
30	1.9	67.98	198.77	

Table A.5. PWP data and result for Helical-1o at 1.05 bar.

Δt (min)	ΔP (bar)	Δm (g)	Permeance (L/hm^{2}bar)	PWP Parameters
19	1.1	28.37	248.86	Membrane inner diameter: 519 µm Membrane outer diameter: 948 µm Membrane Length: 12 cm (corrected) Membrane Area: 3.6* 10^{-4} m^2 Pump setting: 15 rpm (Q:10.8 ml/min) Pump Head: 7016-20 Cross-flow, outside-in
30	1.05	43.63	230.85	
30	1.05	42.6	225.40	
30	1.05	41.92	221.80	
30	1.05	41.92	221.80	
35	1.05	48.6	220.41	
30	1.05	41.15	217.72	
30	1.05	40.96	216.72	

Helical-1o Fouling (T-1o Fouling)

Pump Head: 7016-20

Calibration Eqn: y=0.7443x-0.3318

<u>Volumetric Flow Rate Calculation</u>

x=33.5 rpm;

$$y = 24.6\ \frac{mL}{min} = 24.6\ \frac{mL}{min}\left(\frac{1\ cm^3}{1\ mL}\right)\left(\frac{1 * 10^{-6}\ m^3}{cm^3}\right)\left(\frac{1\ min}{60\ s}\right) = 4.1 * 10^{-7}\ m^3/s$$

<u>Membrane Effective Area Calculation</u>

$$A = \pi D_o L = \pi.(948\ \mu m * 10^{-6}\ m/\mu m).(0.1\ m) \qquad A = 2.97 * 10^{-4} m^2$$

<u>Module Hydraulic Diameter</u>

$$D_H = D_t - D_o$$

$$D_H = 4000\mu m - 948\mu m = 3052\mu m * 10^{-6}\frac{m}{\mu m}$$

$$D_H = 3.05 * 10^{-3} m$$

Reynolds Number Calculation

Sample calculation for x=12.13 rpm

$$A_c = \frac{V_f}{L_{tube}} = \frac{\frac{\pi {D_{tube}}^2}{4} L_{tube} - \frac{\pi {D_o}^2}{4} L_{fiber}}{L_{tube}}$$

$$2L_{tube} = L_{fiber} \qquad for\ helical\ membrane$$

$$A_c = \frac{\pi\left({D_t}^2 - 2{D_O}^2\right)}{4} = \frac{\pi[(4000 * 10^{-6})^2 - 2(948 * 10^{-6})^2]}{4} = 1.12 * 10^{-5} m^2$$

$$Re = \frac{Q.D_H}{\mathcal{V}.A_c} = \frac{\left(4.1 * 10^{-7}\frac{m^3}{s}\right)(3.05 * 10^{-3} m)}{\left(8.926 * 10^{-7}\frac{m^2}{s}\right)(1.12 * 10^{-5})}$$

Re=125.1

Table A.6. Permeance during fouling data and result for Helical-1o

Δt (min)	ΔV (mL)	Permeance during fouling (L/hm^{2}bar)	Permeance during fouling/PWP	Fouling Resistance, R_f (m^{-1})	Fouling Parameters
1.78	5	234.08	1.15	-2.33559E+11	Pump model: 7016-20
2.00	5	208.33	1.03	-43479185120	
2.01	5	207.30	1.02	-34839185120	
2.00	5	208.33	1.03	-43479185120	
2.13	5	195.62	0.96	68840814880	P=2 bar outside-in, crossflow
1.98	5	210.44	1.04	-60759185120	
2.10	5	198.41	0.98	42920814880	
2.13	5	195.62	0.96	68840814880	
2.18	5	191.13	0.94	1.12041E+11	200 gr (dye-upwater)
2.23	5	186.85	0.92	1.55241E+11	
2.05	5	203.25	1.00	-279185119.6	
2.30	5	181.16	0.89	2.15721E+11	
2.22	5	187.69	0.92	1.46601E+11	0.025 wt.% dye
2.30	5	181.16	0.89	2.15721E+11	
2.35	5	177.30	0.87	2.58921E+11	Re=125.1
2.12	5	196.54	0.97	60200814880	

2.30	5	181.16	0.89	2.15721E+11	
2.40	5	173.61	0.85	3.02121E+11	
2.85	6	175.44	0.86	2.80521E+11	
1.88	4	177.30	0.87	2.58921E+11	
2.06	5	202.27	1.00	8360814880	
2.48	5	168.01	0.83	3.71241E+11	
2.45	5	170.07	0.84	3.45321E+11	
2.43	5	171.47	0.84	3.28041E+11	
2.47	5	168.69	0.83	3.62601E+11	
4.38	10	190.26	0.94	1.20681E+11	
5.17	10	161.19	0.79	4.61961E+11	
5.06	10	164.69	0.81	4.14441E+11	
5.28	10	157.83	0.78	5.09481E+11	
5.17	10	161.19	0.79	4.61961E+11	
4.92	10	169.38	0.83	3.53961E+11	
5.17	10	161.19	0.79	4.61961E+11	
5.17	10	161.19	0.79	4.61961E+11	
5.17	10	161.19	0.79	4.61961E+11	
5.55	10	150.15	0.74	6.26121E+11	
5.50	10	151.52	0.75	6.04521E+11	
5.45	10	152.91	0.75	5.82921E+11	
2.47	5	168.69	0.83	3.62601E+11	
5.52	10	150.97	0.74	6.13161E+11	
5.57	10	149.61	0.74	6.34761E+11	
2.42	5	172.18	0.85	3.19401E+11	
5.57	10	149.61	0.74	6.34761E+11	
5.63	10	148.02	0.73	6.60681E+11	
2.52	5	165.34	0.81	4.05801E+11	
5.70	10	146.20	0.72	6.90921E+11	
5.63	10	148.02	0.73	6.60681E+11	
2.45	5	170.07	0.84	3.45321E+11	
5.72	10	145.69	0.72	6.99561E+11	
5.80	10	143.68	0.71	7.34121E+11	
5.90	10	141.24	0.70	7.77321E+11	
5.86	10	142.21	0.70	7.60041E+11	
5.92	10	140.77	0.69	7.85961E+11	
5.97	10	139.59	0.69	8.07561E+11	

5.97	10	139.59	0.69	8.07561E+11	
5.88	10	141.72	0.70	7.68681E+11	
5.97	10	139.59	0.69	8.07561E+11	
5.92	10	140.77	0.69	7.85961E+11	
5.93	10	140.53	0.69	7.90281E+11	
6.30	10	132.28	0.65	9.50121E+11	
6.15	10	135.50	0.67	8.85321E+11	
6.18	10	134.84	0.66	8.98281E+11	

APPENDIX B

INSIDE-OUT PROCESS SAMPLE CALCULATIONS OF PWP AND FOULING

Straight Membrane

Straight-1i PWP

Pump Head: 7016-20

Calibration Eqn: y=0.7443x-0.3318

Volumetric Flow Rate Calculation

x=6.73 rpm;

$$y = 4.68\ \frac{mL}{min} = 4.68\frac{mL}{min}\left(\frac{1\ cm^3}{1\ mL}\right)\left(\frac{1 * 10^{-6}\ m^3}{cm^3}\right)\left(\frac{1\ min}{60\ s}\right) = 0.78 * 10^{-7}\ m^3/s$$

Membrane Effective Area Calculation

$$A = \pi D_i L = \pi.(635\ \mu m * 10^{-6}\ m/\mu m).(0.065\ m) \qquad A = 1.3 * 10^{-4} m^2$$

Table B.1. PWP data and result for Straight-1i

Δt (min)	ΔP (bar)	Δm (g)	Permeance (L/hm^{2}bar)	PWP Parameters
30	2.1	66.37	247.23	Membrane inner diameter: 635 µm Membrane outer diameter: 1307 µm Membrane Length: 6.5 cm Membrane Area: 1.3 *10^{-4} m^2 Pump setting: 6.7 rpm (Q:4.6 ml/min) Pump Head: 7016-20 Dead-end, inside-out
30	2	19.5	150.00	
30	2	14.59	112.23	
45	2	11.2	86.15	
30	1.9	8.82	71.42	
30	1.9	6.73	54.49	
31	1.9	5.26	42.59	
30	1.9	3.08	24.94	
30	1.85	5.97	25.68	
30	1.85	2.53	19.13	
30	1.85	1.83	13.83	
30	1.85	1.6	12.10	
30	1.85	1.4	10.58	

Straight-1i Fouling

Pump Head: 7016-20

Calibration Eqn: y=0.7443x-0.3318

<u>Volumetric Flow Rate Calculation</u>

x=14.79 rpm;

$$y = 10.68\ \frac{mL}{min} = 10.68\frac{mL}{min}\left(\frac{1\ cm^3}{1\ mL}\right)\left(\frac{1 * 10^{-6}\ m^3}{cm^3}\right)\left(\frac{1\ min}{60\ s}\right) = 1.78 * 10^{-7}\ m^3/s$$

<u>Reynolds Number Calculation</u>

Sample calculation for x=14.79 rpm

$$A_c = \frac{\pi\left(D_i{}^2\right)}{4} = \frac{\pi(635 * 10^{-6})^2}{4} = 3.17 * 10^{-7} m^2$$

$$\mathrm{Re} = \frac{Q.D_i}{\mathcal{V}.\mathrm{A}_c} = \frac{\left(1.78 * 10^{-7}\,\frac{m^3}{s}\right)(6.35 * 10^{-4} m)}{\left(8.926 * 10^{-7}\,\frac{m^2}{s}\right)(3.17 * 10^{-7} m^2)} \qquad Re = 400$$

Table B.2. Permeance during fouling data and result for Straight-1i

Δt (min)	ΔP (bar)	Δm (g)	Permeance during fouling (L/hm^{2}bar)	Permeance during fouling/PWP	Fouling Resistance, R_f (m^{-1})	Fouling Parameters for H77
30	2	1.74	13.38	1.10	7.78817E+13	D_i: 635 µm D_o: 1307 µm Memb. Length: 6.5 cm Memb. Area: 1.3 *10^{-4} m^2 Pump setting: 14.8 rpm (Q:10.7 ml/min) Pump Head: 7016-20 Cross-flow, inside-out Re=400
30	2	1.12	8.62	0.71	1.22048E+13	
30	2	0.96	7.38	0.61	1.91691E+13	
30	2	0.81	6.23	0.51	2.81968E+13	
30	2	0.65	5.00	0.41	4.24191E+13	
30	2	0.71	5.46	0.45	3.63346E+13	
30	2	0.56	4.31	0.35	5.39905E+13	
30	2	0.54	4.15	0.34	5.70857E+13	
30	2	0.5	3.85	0.32	6.39256E+13	
30	2	0.435	3.35	0.27	7.78817E+13	

<u>Helical Membrane</u>

Helical-1i PWP

Pump Head: 7016-20

Calibration Eqn: y=0.7443x-0.3318

<u>Volumetric Flow Rate Calculation</u>

x=5.52 rpm;

$$y = 3.78\,\frac{mL}{min} = 3.78\frac{mL}{min}\left(\frac{1\,cm^3}{1\,mL}\right)\left(\frac{1 * 10^{-6}\,m^3}{cm^3}\right)\left(\frac{1\,min}{60\,s}\right) = 0.63 * 10^{-7}\,m^3/s$$

Membrane Effective Area Calculation

$A = \pi D_i L = \pi.(519\ \mu m * 10^{-6}\ m/\mu m).(0.1\ m)$ $A = 1.63 * 10^{-4} m^2$

Table B.3. PWP data and result for Helical-1i at 1.9 bar.

Δt (min)	P_{feed} (bar)	$P_{retentate}$ (bar)	ΔP (bar)	Δm (g)	Permeance (L/hm^2bar)	PWP Parameters
30	2	1.7	1.85	33.03	219.07	D_i: 519 µm D_o: 948 µm Memb. Length: 5 cm (corrected 10 cm) Memb. Area: 1.63 *10^{-4} m^2 Pump setting: 5.52 rpm (Q:3.78 ml/min) Pump Head: 7016-20 Dead-end, inside-out
30	2	1.7	1.85	18.69	123.96	
30	2	1.8	1.9	14.43	93.19	
30	2	1.8	1.9	11.34	73.23	
30	2	1.85	1.93	8.86	56.47	
30	2	1.85	1.93	7	44.62	
30	1.95	1.95	1.95	5.64	35.49	
30	1.95	1.95	1.95	4.73	29.76	
30	1.95	1.95	1.95	3.96	24.92	
30	1.95	1.95	1.95	3.29	20.70	
30	1.95	1.95	1.95	2.72	17.11	
32	1.95	1.95	1.95	2.4	14.16	
30	1.9	1.9	1.9	1.88	12.14	
30	1.9	1.9	1.9	1.59	10.27	

Table B.4. PWP data and result for Helical-1i at 1 bar.

Δt (min)	P_{feed} (bar)	$P_{retentate}$ (bar)	ΔP (bar)	Δm (g)	Permeance (L/hm^2bar)	PWP Parameters
30	1.25	0.85	1.05	2.22	25.94	D_i: 519 µm
30	1.25	0.8	1.025	2.04	24.42	D_o: 948 µm
30	1.25	0.8	1.025	1.81	21.67	Memb. Length: 5 cm
30	1.25	0.85	1.05	1.69	19.75	(corrected 10 cm)
30	1.25	0.85	1.05	1.64	19.16	Membrane Area:
30	1.15	0.75	0.95	1.26	16.27	$1.63 * 10^{-4}$ m^2
30	1.2	0.8	1	1.31	16.07	Pump setting:
30	1.2	0.8	1	1.25	15.34	5.52 rpm
30	1.25	0.8	1.025	1.24	14.84	(Q:3.78 ml/min)
30	1.25	0.8	1.025	1.24	14.84	Pump Head: 7016-20
30	1.25	0.8	1.025	1.17	14.01	Cross-flow
30	1.25	0.8	1.025	1.11	13.29	inside-out

Helical-1i Fouling

Pump Head: 7016-20

Calibration Eqn: y=0.7443x-0.3318

<u>Volumetric Flow Rate Calculation</u>

x=12.13 rpm;

$$y = 8.7\ \frac{mL}{min} = 8.7\ \frac{mL}{min}\left(\frac{1\ cm^3}{1\ mL}\right)\left(\frac{1 * 10^{-6}\ m^3}{cm^3}\right)\left(\frac{1\ min}{60\ s}\right) = 1.45 * 10^{-7}\ m^3/s$$

<u>Reynolds Number Calculation</u>

Sample calculation for x=12.13 rpm

$$\mathrm{A}_c = \frac{\pi\left(D_i{}^2\right)}{4} = \frac{\pi(519 * 10^{-6})^2}{4} = 2.11 * 10^{-7} m^2$$

$$\mathrm{Re} = \frac{Q.D_i}{\mathcal{V}.\mathrm{A}_c} = \frac{\left(1.45 * 10^{-7}\frac{m^3}{s}\right)(5.19 * 10^{-4} m)}{\left(8.926 * 10^{-7}\frac{m^2}{s}\right)(2.11 * 10^{-7} m^2)} \qquad Re = 400$$

Table B.5. Permeance during fouling data and result for Helical-1i

Δt (min)	P_{feed} (bar)	$P_{retentate}$ (bar)	ΔP (bar)	Δm (g)	Permeance during fouling (L/hm^2bar)	Permeance during fouling /PWP	Fouling Resistance, R_f (m^{-1})	Fouling Parameters for H76
30	2	~1.6	1.8	2.41	16.39	1.34	-5.9477E+12	D_i: 519 µm D_o: 948 µm Length: 10 cm (corrected) Area: $1.63*10^{-4}m^2$ Pump : 12.1 rpm (Q:8.7 ml/min) Pump Head: 7016-20 Cross-flow, inside-out Re=400
30	2	~1.8	1.9	2	12.92	1.06	-3.3977E+10	
30	2	1.9	1.95	1.7	10.70	0.88	5.74773E+12	
30	1.95	1.95	1.95	1.62	10.19	0.84	7.40969E+12	
30	1.95	1.95	1.95	1.57	9.88	0.81	8.53442E+12	
30	1.95	1.95	1.95	1.46	9.19	0.75	1.128E+13	
30	1.9	1.9	1.9	1.39	8.96	0.74	1.22558E+13	
30	1.9	1.9	1.9	1.33	8.58	0.70	1.40388E+13	
30	1.9	1.9	1.9	1.27	8.22	0.67	1.58841E+13	
30	1.9	1.9	1.9	1.27	8.20	0.67	1.59875E+13	